

APPLICATION OF A BOUNDING SURFACE PLASTICITY LAW
TO THE PREDICTION OF PRESSUREMETER TESTS

By

DEVO SEEREERAM

A THESIS PRESENTED TO THE GRADUATE SCHOOL
OF THE UNIVERSITY OF FLORIDA IN
PARTIAL FULFILLMENT OF THE REQUIREMENTS
FOR THE DEGREE OF MASTER OF ENGINEERING

UNIVERSITY OF FLORIDA

1983

ACKNOWLEDGEMENTS

The author would like to express his sincere appreciation to his graduate advisor, Dr. Michael McVay, who generously dedicated the major portion of his working hours during the Summer semester of 1983 to ensure the completion of this project. His tasks, which were by no means simple, included personally instructing the writer on the subjects of plasticity theory, efficiency in computer programming, both basic and complex concepts in soil mechanics, continuum mechanics, and finite element analysis.

Along with Dr. McVay, the two other members of the soil mechanics faculty at the University of Florida rendered invaluable assistance in this research effort; I would like to thank Dr. Frank Townsend, Chairman of the geotechnical group, for devoting an entire day to supervise the author through the rigor of triaxial testing, and also making available to the writer his technical literature on the Reid-Beford sand. The help of Dr. John Davidson in securing information on the self-boring pressuremeter and the tests in the calibration chamber was also crucial in understanding a) the operation, b) the present methods of data analysis, c) the laboratory study in the calibration chamber, and d)

the merits of this insitu instrument; his assistance in this regard is sincerely appreciated.

This acknowledgement would not be complete without mentioning the love and support I received from my family and friends which were essential in maintaining my perspective on life through this, at times, frustrating, but mentally fulfilling assignment. Particularly, I would like to thank Charmaine, my fiance and friend for the last six years, for her understanding and patience during the long hours spent at work, and, my mother, who put my education above everything else, and my father, who gave me the financial freedom and motivation to do whatever I chose. Special thanks also go to my typist, Meredith, for her superb handling of this manuscript.

Again I would like to conclude by thanking Dr. McVay, without whom this thesis would not have been possible.

TABLE OF CONTENTS

	<u>PAGE</u>
ACKNOWLEDGEMENTS.....	ii
LIST OF TABLES.....	vi
LIST OF FIGURES.....	vii
ABSTRACT.....	ix
 CHAPTER	
1 INTRODUCTION	
1.1 General.....	1
1.2 Purpose.....	3
1.3 Scope.....	4
2 REVIEW OF SOIL CONSTITUTIVE MODELS	
2.1 Introduction.....	7
2.2 Statistical Methods.....	8
2.3 Non-Linear Elastic Approach.....	8
2.4 Failure Criteria.....	10
2.5 Classical Plasticity Theories	12
2.6 Critical State Soil Mechanics.....	13
2.7 Lade's Elasto-plastic Soil Constitutive Model.....	16
2.8 Chang's Particulate Mechanics Soil Model.....	27
3 BOUNDING SURFACE PLASTICITY FORMULATION FOR SAND	
3.1 Introduction.....	39
3.2 Theory.....	41
3.3 Important Aspects of B.S. Formulation.....	57
3.4 Calibration of Model Parameters.....	59
4 SELF BORING PRESSUREMETER TESTS	
4.1 Introduction.....	63
4.2 Equipment and Field Testing Procedure.....	65
4.2.1 Equipment.....	65
4.2.1.1 Introduction.....	65
4.2.1.2 The probe.....	66
4.2.2.3 SBPM rig.....	69
4.2.1.4 Control unit.....	69
4.2.2 Typical field testing procedure.....	71

<u>CHAPTER</u>	<u>PAGE</u>
4.2.3 Advantages and disadvantages of SPBM.....	75
4.3 Laboratory Study of Pressuremeter Test.....	76
4.3.1 Soil description.....	77
4.3.2 Test chamber.....	77
5 PRESSUREMETER ANALYSIS BY THE FINITE ELEMENT METHOD	
5.1 Introduction.....	83
5.2 Theory.....	84
5.2.1 Element Characteristics.....	86
5.2.1.1 Displacement function.....	86
5.2.1.2 Strains.....	90
5.2.1.3 Element stiffness matrix.....	91
5.2.2 Generalization to the Whole Region.....	96
5.2.3 Boundary Conditions.....	99
5.2.4 Quadrilateral Element.....	100
5.3 Computer Procedure.....	102
5.3.1 Introduction.....	102
5.3.2 Preliminary Information.....	102
5.3.3 General Procedure.....	103
5.4 Conclusion.....	104
6 DISCUSSION AND PRESENTATION OF RESULTS	
6.1 Introduction.....	110
6.2 Determination of Model Parameters.....	114
6.3 Coefficient of Lateral Earth Pressure.....	123
6.4 Simulation of pressuremeter test.....	129
6.4.1 Boundary conditions.....	133
6.4.2 Actual vs. predicted SBPM results.....	136
6.4.3 Stress paths.....	140
6.4.4 Variation of principal stresses.....	145
6.4.5 Stress distribution from PMT axis.....	147
7 CONCLUSIONS AND RECOMMENDATIONS.....	148
LIST OF REFERENCES.....	158
APPENDIX	
A TRIAXIAL TEST DATA.....	163
B SOURCE LISTING OF COMPUTER PROGRAM.....	169
BIOGRAPHICAL SKETCH.....	206

LIST OF TABLES

TABLE		PAGE
3.1	SUMMARY OF HOW B.S. MODEL PARAMETERS ARE DERIVED.....	62
6.1	MODEL PARAMETERS FROM CTC TESTS.....	117
6.2	SUMMARY OF MODEL PARAMETERS FOR DENSE REID BEDFORD SAND.....	131

LIST OF FIGURES

FIGURE		PAGE
2.1	Schematic Illustrations of Strain Components and Yield Surfaces for Lade's Model.....	17
2.2	Schematic Diagram (Lade) of Yielding Process with Plastic Strain Components Superimposed in Triaxial Space	21
2.3	Lade's Proposed Failure Surface in Principal Stress Space.....	25
2.4	Mechanics of Particulate Approach.....	31
3.1	Bounding Surface in Stress Invariant Space.....	43
4.1	Cambridge Self Boring Pressuremeter Probe.....	67
4.2	Photograph of SBPM Probe.....	68
4.3	Photograph of SBPM Control Unit.....	68
4.4	Photograph of SBPM Rig.....	70
4.5	Flow Chart Showing Data Processing of SBPM Model.....	73
4.6	Grain Size Distribution Curve of Reid Bedford Sand.....	78
4.7	Calibration Chamber Situation During SBPM test.....	80
4.8	Sample Results of SBPM Tests in Chamber.....	82
5.1	Strains & Stresses in Analysis of Axisymmetric Solids.....	87
5.2	Triangular Element.....	94
5.3	Assembly Process.....	94

FIGURE	PAGE
5.4	Quadrilateral Element.....94
5.5	Elements of the Matrix $[g]^T [CL] [g]$97
5.6	Flowchart of General Computational Procedure.....106
5.7	Flowchart of SUBROUTINE SAND.....107
5.8	Flowchart of SUBROUTINE STRESS.....108
6.1	Finite Element Used for Simulation of CTC Test.....112
6.2	F.E.M. vs. Closed-form Solution for Isotropic Comp. Test.....113
6.3	Photograph of Triaxial Testing Apparatus.....115
6.4	Actual vs. Predicted Triaxial Test Results.....118
6.5	Actual vs. Predicted Volume Strain (CTC Test)..121
6.6	Actual vs. Predicted Isotropic Compression Test Data.....123
6.7	K_o Consolidation Simulation With B.S. Law.....125
6.8	Relationship Between K_o and Relative Density.....126
6.9	Finite Element Mesh Used for B.C. #1.....133
6.10	Finite Element Mesh Used for B.C. #2.....133
6.11	Actual vs. Predicted SBPM Test for B.C. #1.....135
6.12	Actual vs. Predicted SBPM Test for B.C. #3.....135
6.13	Stress Paths for SBPM Test for B.C. #1 and #3.....139
6.14	Predicted Principal Stresses as a Function of Cavity Pressure for Tresca and Mises Material.....143
6.15	Predicted Principal Stresses as a Function of Cavity Pressure for B.S. Material.....143
6.16	Typical Distribution of Principal Stresses with Distance from SBPM Axis, @ B.C. #1.....147

Abstract of Thesis Presented to the Graduate School
of the University of Florida in Partial Fulfillment of the
Requirements for the Degree of Master of Engineering

APPLICATION OF A BOUNDING SURFACE PLASTICITY LAW
TO THE PREDICTION OF PRESSUREMETER TESTS

By

Devo Seereeram

December, 1983

Chairman: Dr. M.C. McVay
Major Department: Civil Engineering

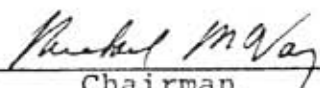
In this thesis, the performance of a bounding surface plasticity constitutive relationship, successfully implemented in previous research efforts to model the triaxial test and the moving wheel stress path, is examined for consistency and reliability under generalized loading conditions.

Concurrent with the development of this bounding surface (B.S.) theory during the first half of 1983, another unrelated research project at the University of Florida's geotechnical testing laboratory focused on gathering and analyzing data on cast-in-place self-boring pressuremeter tests under controlled conditions (i.e., a calibration chamber). These tests served as the principal source of "generalized loading path" experimental data which was used

for comparison to predictions generated by the constitutive model.

As research progressed with the aid of a modified finite element program, some deficiencies were noted in the original bounding surface theory which made it necessary to reformulate the model, and the version presented herein (Fall, 1983) includes all modifications, but should by no means be considered as its final form.

Results of this study indicate that the boundary conditions play a major role in the solution to the pressuremeter expansion problem. Of the two cyclic pressuremeter tests investigated, one of the predictions may be adjudged as being very good while the other is only moderately so. The author has serious reservations in interpreting the K_0 consolidation simulation, and it is clearly obvious that further research is needed to address the problem or problems which are restricting the prediction of realistic results along this stress path. Nevertheless, the bounding surface plasticity formulation is indeed a novel approach to modeling cyclic elasto-plastic stress-strain behavior of soil, and it is quite possible that the fundamentals of this plasticity approach may serve as the precursor to the future attempts by engineers to mathematically model soil response.


Chairman

CHAPTER 1 INTRODUCTION

1.1 General

The theoretical formulation of rational constitutive relationships to predict the load-deformation response of soil media subject to complex static and cyclic excitations must account for a stress-strain phenomena which is known to be non-linear, inelastic, compressive and/or dilatative, anisotropic, hysteretic, stress history- and time-dependent. Such an all-encompassing mathematical model, or even one that is only applicable over specified regions of interest, will present the geotechnical practitioner with a potent research and design tool to solve increasingly sophisticated problems which are usually not amenable to analysis by traditional approaches based on empirical methods correlated to field tests or elementary soil constitutive models.

In response to the need for more accurate predictions of the performance of soils under load, several recently developed methods of analysis and models of soil behavior have appeared in published literature, particularly, the proceedings of the NSF/NSERC (National Science Foundation/National Science & Engineering Research Council, Canada) and ASCE (American Society of Civil Engineers)

sponsored workshops on limit equilibrium, plasticity and generalized stress-strain in geotechnical engineering. Even with this vastly improved capability to predict soil deformation and stability, opinions still differ as to which models provide the most accurate and reliable predictions, and as to whether or not it is in fact possible to realistically model actual soil behavior over the entire range of stress-strain performance for most typical soils.

The root of the current dilemma presently faced by many users in selecting the "most appropriate" soil rheological model can be traced to the basic methodology used in proposing most of these yield/failure theories and constitutive relationships. This fundamental approach involves hypotheses based on data obtained from extensive laboratory studies on certain well documented soils, and as Yong and Ko (p. 49, 1980) succinctly state "the relationships developed therefrom have been obviously conditioned to respond to the soils tested as well as for the particular test system constraints, and therefore the parameters used and material properties sensed have been chosen to fit the test circumstance. Extension and projection into a more general framework for wider use do not appear to be sufficiently well-founded." John Christian (p. 61, 1980), senior consulting engineer at Stone & Webster, puts forward yet another pertinent point of view on the current status of constitutive models in geotechnical engineering: ". . . it should be the objective of every developer of a constitutive

model to make the model understandable to potential users. The temptation to express the model in complicated mathematical notation and arcane terminology is almost overwhelming . . . failure to describe new constitutive models in terms that are sufficiently simple, clear, and unambiguous is probably the greatest single barrier to the application of such models to practical problems."

Having identified the potential problem areas that exist in constitutive soil modeling, it is now necessary to outline a means of probing the performance and hence the ultimate usefulness of any particular constitutive relationship; this scheme should at least include a study of the following (from Ansal et al., 1980): (a) the versatility of the theory to characterize experimental data obtained from a variety of tests, (b) the ability of the resulting relationship to predict behavior for conditions other than those which were used to calibrate the model, and (c) the ease with which the formulation can be adopted to the solution of practical boundary value problems.

1.2 Purpose

Rate independent bounding surface plasticity constitutive modeling has been at the focus of recent research efforts at the University of Florida, and the facility of this model to predict the triaxial test stress path and the moving wheel stress path has been ascertained in previous research (Taesiri, McVay & Townsend, 1983). It is the purpose of this thesis to investigate the

applicability of this model in simulating stress-strain response under generalized loading paths. The "general stress path" load-deformation data chosen for analysis is a series of pressuremeter test results extracted from another research project (Davidson, 1983) which concentrated on a) developing techniques for performing self-boring pressuremeter (SBPM) tests in a large-scale sand chamber, and b) the evaluation of currently available techniques of interpreting the results of SBPM tests.

Two secondary objectives were accomplished as a direct consequence of the primary goal of this thesis: 1) a computer program capable of modeling axi-symmetric loading conditions was modified such that it now has the capacity to execute elasto-plastic incremental analysis; in its contemporary form, it is feasible to accommodate most of the common elasto-plastic constitutive equations, but for the purpose of this study, it was only necessary to incorporate the bounding surface model into the computer code; and 2) valuable academic information on the stress paths and the stress distribution of an undisturbed soil mass stressed by an expanding cylindrical cavity was gleaned from the finite element analysis.

1.3 Scope

There were a few apparent shortcomings in the version of the bounding surface model developed at the University of Florida (Taesiri et al., 1983) which required some modifications before it could be applied in the simulation

of the pressuremeter test. Although these refinements are included herein, the Taesiri et al. (1983) reference should be consulted for a more complete description of the bounding surface model since certain unused aspects of his model were not included in this thesis because of space restrictions and the protracted nature of these equations. Also, this bounding surface constitutive model was developed specifically for dense sands so all predictions presented in this report were for the sequence of pressuremeter tests in dense sand samples.

An important limitation of the finite element program is its inability to deal with a constant stress boundary conditions, and hence it was necessary to approximate the idealized situation in the calibration chamber by making some justifiable adjustments to the finite element meshes.

This report consists of seven chapters. A brief review of constitutive equations used in soil mechanics is presented in chapter 2 with particular emphasis on Lade's elasto-plastic model and the particulate approach of Chang (1983). Chapter 3 is devoted entirely to a description of the theory and calibration procedure of the bounding surface plasticity model used in the simulation of the pressuremeter tests which are then in turn explained in chapter 4. The numerical technique and the computer procedure used in modelling the pressuremeter tests and other loading conditions are described in chapter 5, and chapter 6 presents and discusses the results of this numerical

analysis. Finally, in chapter 7, conclusions and recommendations are made on the performance of the constitutive model and the finite element computer program.

CHAPTER 2 REVIEW OF SOIL CONSTITUTIVE LAWS

2.1 Introduction

As detailed in the first chapter, the stress-strain relation of soil is non-linear and much more complex than the response generated by classical linear elastic theory. Recognition of this phenomena has led to four different methods of formulating the constitutive laws of geologic media: 1) curve fitting, 2) non-linear elastic theories, 3) plasticity theories (including viscous behavior), and 4) endochronic theories. In this chapter, a summary of some of the more popular soil models are reviewed with particular emphasis on two examples of plastic stress-strain relationships based on both a continuum and a particulate mechanics field theory. The chapter that follows provides a detailed description of what is perhaps the most innovative attempt to model the elasto-plastic cyclic loading of soils: a bounding surface plasticity model. The bounding surface model is the constitutive relation chosen in this report to simulate the pressuremeter test in cohesionless soil.

2.2 Statistical Methods

There are several curve-fitting procedures which were developed to reproduce typical stress-strain curves for non-linear material. The bilinear model consists essentially of defining both an initial and an ultimate value of the Young's modulus which are interchanged when the yield stress has been attained. With a constant Poisson's ratio, this model suffers from the disadvantage of effectively decreasing the bulk modulus the same order of magnitude as the shear modulus; this results in reasonable predictions of the shear distortion but unrealistically large simulation of volumetric compression at failure. This problem may be remedied by holding the bulk modulus constant while the shear modulus is reduced. Further refinements led to the piecewise linear models which defined straight line portions of the stress-strain curve for different stress levels. Data for these multi-linear models consisted of tabulated stress-strain points which were used to compute the tangent modulus between two points,

$$E_t = \frac{\sigma_i - \sigma_{i-1}}{\epsilon_i - \epsilon_{i-1}} \quad (2.2.1)$$

2.3 Non-linear Elastic Approach

Clough and Woodward (1967) were among the first to employ non-linear modeling of soil in a finite element idealization; they studied incremental construction analysis by revising the values of the elastic constants by an

interpolation scheme. Under the assumption of plane strain, two elastic parameters were used: the bulk modulus, M_b , and the distortional modulus, M_d , defined as

$$M_b = \frac{E}{2(1 + \nu)(1 - 2\nu)} \quad (2.3.1)$$

$$M_d = \frac{E}{2(1 + \nu)} \quad (2.3.2)$$

Initial values of the moduli above were determined from the elastic modulus computed at the origin of the stress-strain curve and an assumed value of Poisson's ratio. At the end of analysis for the first construction step, the state of stress in each finite element was determined and the slope ($E = M_t$) of the triaxial test curve was approximated from a series of typical triaxial test data for the soil under investigation. Based on the new value of M_t , the following equation for the Poisson's ratio was then solved:

$$\nu = \frac{-1 + \sqrt{1 - 8 \left(\frac{M_t}{M_b} - 1 \right)}}{4} \quad (2.3.3)$$

With this revised value of Poisson's ratio, a new distortional modulus is computed from equation 2.3.2 while the bulk modulus remains unchanged throughout the analysis.

A hyperbolic equation was found to represent a plot of deviatoric stress versus axial strain in triaxial compression (Kondner, 1963). The utility of such an

amenable mathematical relation was embodied by Duncan (Duncan & Chang, 1970) in the development of sophisticated non-linear elastic equations to aid in the study of soil-structure interaction by numerical methods. This method does however possess certain disadvantages (Desai & Christian, 1977): a) it is valid for stress below the peak of the stress-strain curve, b) when anisotropy or other complications appear, the simplicity of the relation begins to disappear under correction factors, c) dilatant materials cannot be treated since they require a Poisson's ratio of greater than 0.5 which can create potentially severe problems (such as lack of uniqueness) in numerical solutions, d) the relationship is based directly on experimental observation with very little physical justification, and e) they work well so long as the stresses and strains are similar to those under which the experimental observations were made.

2.4 Failure Criteria

Most analyses in geotechnical engineering are presently based on deriving a factor of safety after a limit equilibrium solution to the problem is obtained. Although a failure criterion does not prescribe the constitutive nature of a soil per se, it does play a significant role in defining the ultimate strength of the material and an approximation to the yield surface used in plasticity theory. Perhaps the simplest and most utilized failure

criterion is that proposed by Coulomb in 1776; the failure state of a frictional material can be represented by what is commonly termed the Mohr-Coulomb failure principle:

$$\tau - \tan\phi - c = 0 \quad (2.4.1)$$

where c and ϕ denote the cohesion and angle of internal friction respectively.

Although it has been widely used in the past, this criterion does have its restrictions: a) the influence of the intermediate principal stress on shear strength is neglected; and 2) the failure surface exhibits corners or singularities in three dimensional stress space (Mizuno & Chen, 1980). A three dimensional approximation to the Mohr-Coulomb criterion, which has instead the shape of a circle in the octahedral plane, was introduced to overcome the limitations mentioned previously (Drucker & Prager, 1952). This surface is established in terms of the invariants of stress:

$$F = \alpha I_1 + \sqrt{J_2} - k = 0 \quad (2.4.2)$$

where I = 1st invariant of stress tensor

J_2 = 2nd invariant of deviator stress tensor

and k and α are material constants which can be expressed in terms of ϕ and c :

$$\alpha = \frac{2 \sin\phi}{3(3 - \sin\phi)} \quad (2.4.3)$$

$$k = \frac{6 c \cos \phi}{3(3 - \sin \phi)} \quad (2.4.4)$$

Two additional failure criteria are introduced in the next paragraph; although each will be discussed in the context of serving as a yield conditions (Tresca and von-Mises), it must be noted that these functions can similarly be used to identify failure states.

2.5 Classical Plasticity Theories

The elastic theories described previously express stress directly in terms of strain by a tangent modulus; however, plasticity theory is formulated on an incremental stress-strain basis so it is imperative to specify the loading path in order to compute the constitutive equation. For a perfectly plastic material, a yield function, F , can be defined in terms of stress or any other "plastic state variable" as separating stress states below which the response of the material is elastic and above which the response is plastic. The theory of plasticity in its early development focused on modeling the constitutive behavior of polycrystalline metals; two classical yield criteria unfolded as researchers attempted to distinguish the elastic range from the stress states in which plastic flow occurs. The Tresca yield criterion is based on a maximum shear stress, k , and in terms of the stresses for plane strain, the criterion may be stated as

$$F(\sigma) = \left(\frac{\sigma_{xx} - \sigma_{yy}}{2} \right)^2 + \sigma_{xy}^2 - k^2 = 0 \quad (2.5.1)$$

The other classical yield function is known as the Von-Mises yield condition, and this postulated function is based on the theory of maximum energy of distortion - it is expressed here in terms of principal stresses.

$$F(\sigma) = (\sigma_1 - \sigma_2)^2 + (\sigma_2 - \sigma_3)^2 + (\sigma_3 - \sigma_1)^2 + 2k^2 \quad (2.5.2)$$

Now that the stress combinations which permit inelastic response have been defined, the post yield behavior - i.e. relationship between plastic deformation increments and stress components, and the change in the yield condition with work hardening - must be characterized. One of the basic concepts of plasticity theory is the plastic potential and the associated flow rule; this states that when a material undergoes plastic flow, the direction of the incremental plastic strain tensor is in a direction normal to the yield criterion (this relationship is also known as the normality rule):

$$d\epsilon_{ij}^p = \lambda \frac{\partial F}{\partial \sigma_{ij}} \quad (2.5.3)$$

where λ is a scalar,

This relationship follows from the principles of thermodynamics and its application in deriving the constitutive laws of soils is not discussed further here since it has been extensively treated in many texts (example: Jain, 1980).

2.6 Critical State Soil Mechanics

The next concept that is introduced is that of critical state soil mechanics (Schofield & Wroth, 1968) and its

physical significance in modeling the response of soil. The strength of a material is not only governed by the effective normal stress across the failure plane but also by the number of particles per unit volume (i.e. its relative density). Also, the shear-volumetric behavior of a sand is a function of its void ratio (or its relative density); "loose" specimens compress when subjected to shear stresses while "dense" samples undergo an initial compaction followed by dilation. At large strains, both "loose" and "dense" cohesionless soils approach a constant void ratio which indicates that there is no further volume change. This void ratio is known as the critical void ratio and defines the boundary between the dense and loose states of a granular material. Since the strength is related to the void ratio and the effective normal traction, the strength of the sand - usually referred to as the ultimate or residual strength - is constant once the material has achieved this critical state. Two equations are used to characterize this well defined critical state which causes the soil or other granular material to flow as a frictional fluid if continuously distorted:

$$q = Mp \quad (2.6.1)$$

$$\Gamma = v + \lambda \ln(p) \quad (2.6.2)$$

where M , Γ , and λ are basic soil properties and

p = effective pressure

q = deviator stress

v = specific volume

The first equation determines the magnitude of the deviator stress required to keep the soil flowing continuously as a product of a frictional constant M with the effective pressure. The well-known relationship between void ratio and normal effective stress (e vs. $\log p$) is expressed in the second equation. The significance of the critical state hypothesis will become more apparent after the presentation of the bounding surface plasticity model in which this concept is an integral part in the simulation of the shear-dilation properties of dense or over-consolidated soils.

An attempt is made in this chapter to critique some of the available formulations for investigating soil rheology; the discussion presented here is by no means exhaustive, many credible plasticity models were not mentioned owing to space limitations. For further reference, the author recommends any of the speciality conference journals on limit equilibrium and plasticity in geotechnical engineering listed in the bibliography. The rest of this chapter is devoted to a moderately detailed description of two plasticity models: Lade's elasto-plastic model (Lade, 1980), and the particulate approach as presented by Chang (1983).

2.7 Lade's Elasto-Plastic Soil Constitutive Model

2.7.1 Introduction

This fourteen-parameter model (Lade, 1980) is used to simulate several aspects of the stress-strain behavior and strength of soils; these phenomena include non-linearity, strain softening, stress-path dependency, K_0 - loading conditions, influence of both minor and intermediate principal stresses, shear-dilatancy behavior (as a function of confining pressure), and pore pressure development with resulting effective stress paths. The model does, however, suffer from the inability to simulate: a) soil response during large stress reversals, b) cyclic loading, and c) the behavior of soils which are initially anisotropic.

2.7.2 Mathematical Development of Theory

The total incremental strain tensor is attributed to three types of deformations: an elastic component, plastic expansive strains, and plastic collapse strains,

$$d\epsilon_{ij} = d\epsilon_{ij}^e + d\epsilon_{ij}^p + d\epsilon_{ij}^c \quad (2.7.1)$$

Figure 2.1(a) shows the relative contribution of each strain component for a drained triaxial compression test. Elastic strains are computed from Hooke's Law while both plastic strains are calculated using plasticity theory based on a continuum mechanics approach. The theory and computational procedure for each component of the incremental strain is treated separately.

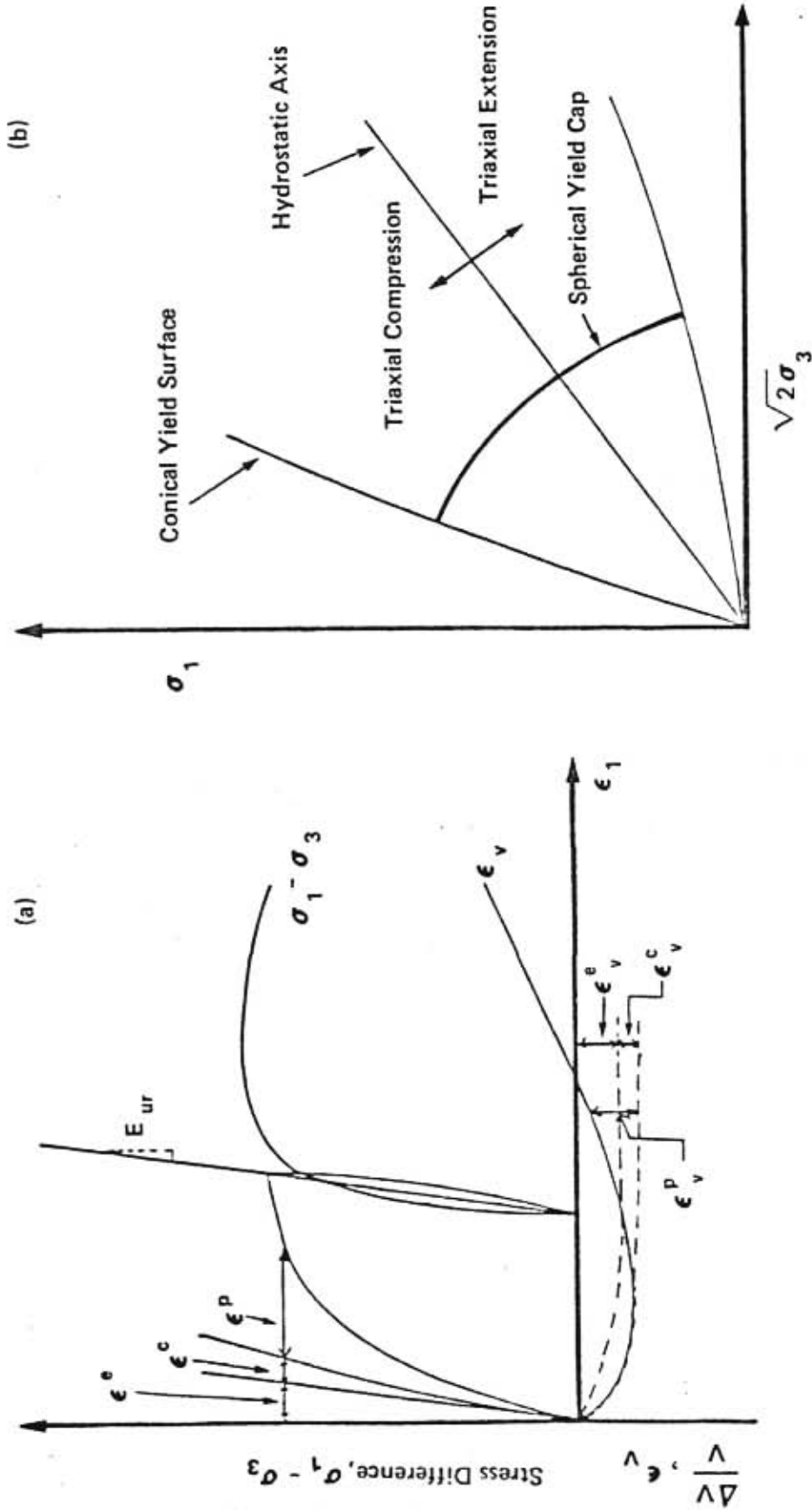


Figure 2.1 Schematic Illustrations of (a) Elastic, Plastic Collapse and Plastic Expansive Strain Components in Drained Triaxial Compression Test, (b) Conical and Spherical Cap Yield Surfaces in Triaxial Plane

(After Lade, 1980)

2.7.3 Elastic Behavior

The recoverable (elastic) strains are computed using the unload-reload elastic modulus (depicted in figure 2.1a) which is defined as follows:

$$E_{ur} = K_{ur} \cdot P_a \cdot \left(\frac{\sigma_3}{P_a}\right)^n \quad (2.7.2)$$

where E_{ur} = unload-reload Young's modulus

P_a = atmospheric pressure (same units as E_{ur})

K_{ur} = dimensionless constant known as modulus number

n = exponent (also a dimensionless constant)

Both parameters K_{ur} and n may be determined from unload-reload cycles in triaxial compression tests. A log-log plot of (E_{ur}/P_a) vs. (σ_3/P_a) yields the value of n and K_{ur} while the Poisson's ratio is usually assumed to be 0.2 (Lade, 1980). In summary, three parameters are used to describe the elastic response of the soil; this differs from classical elasticity in that the elastic modulus is assumed to be a function of the confining pressure.

2.7.4 Plastic Compressive Behavior

These strains are based on the application of plasticity theory to a spherical yield surface with its center at the origin of principal stress space. Any yielding which results from an outward movement of this cap does not lead to eventual failure. The rationality of this concept manifests itself in the quantitative modeling of

plastic behavior during an isotropic compression test in which, of course, it is impossible to fail a specimen of soil.

In terms of the first and second invariants of stress, the yield criteria (spherical yield cap in figure 2.1b), f_c , has the following form:

$$f_c = I_1^2 + 2I_2 \quad (2.7.3)$$

$$\text{where } I_1 = \sigma_1 + \sigma_2 + \sigma_3$$

$$I_2 = -(\sigma_1\sigma_2 + \sigma_2\sigma_3 + \sigma_3\sigma_1) \text{ in terms of principal stresses}$$

Since an associative flow rule is postulated for this yield criteria, the plastic potential function is coincident with the yield function (i.e. $g_c = f_c$). From the normality rule, the relationship between the plastic strain and the yield surface, F , is expressed in general form:

$$d\varepsilon_{ij} = \lambda \frac{\partial F}{\partial \sigma_{ij}} \quad (2.7.4)$$

where λ is a constant of proportionality

For the case of the collapse (or compressive) strains,

$$d\varepsilon_{ij}^c = \lambda_c \frac{\partial f_c}{\partial \sigma_{ij}} \quad (2.7.5)$$

or in its final form,

$$d\varepsilon_{ij}^c = \frac{dW_c}{f_c} \sigma_{ij} \quad (2.7.6)$$

where dW_c is an increment of work per unit volume for a given value of f_c and a given increment of df_c .

The plastic collapse work can be computed from:

$$W_c = \int \sigma_{ij}^T d\epsilon_{ij}^C \quad (2.7.7)$$

During isotropic consolidation,

$$W_c = \int \sigma_{11} \cdot d\epsilon_{11}^C + \int \sigma_{22} \cdot d\epsilon_{22}^C + \int \sigma_{33} \cdot d\epsilon_{33}^C$$

but

$$\begin{aligned} \sigma_{11} &= \sigma_{22} = \sigma_{33} \\ \text{and } d\epsilon_{11}^C + d\epsilon_{22}^C + d\epsilon_{33}^C &= d\epsilon_v^C \end{aligned}$$

therefore,

$$W_c = \int \sigma_{33} \cdot d\epsilon_v^C \quad (2.7.8)$$

$$\text{also, } f_c = I_1^2 + 2I_2$$

$$= (\sigma_{11} + \sigma_{22} + \sigma_{33})^2 - 2(\sigma_{11} \cdot \sigma_{22} + \sigma_{22} \cdot \sigma_{33} + \sigma_{33} \cdot \sigma_{11})$$

$$= 3(\sigma_{33})^2 - 2(3\sigma_{33}^2)$$

$$= 3\sigma_{33}^2 \quad (2.7.9)$$

The relationship between W_c and f_c is represented as

$$W_c = C \cdot p_a \left(\frac{f_c}{p_a} \right)^p \quad (2.7.10)$$

where C = collapse modulus

p = collapse exponent

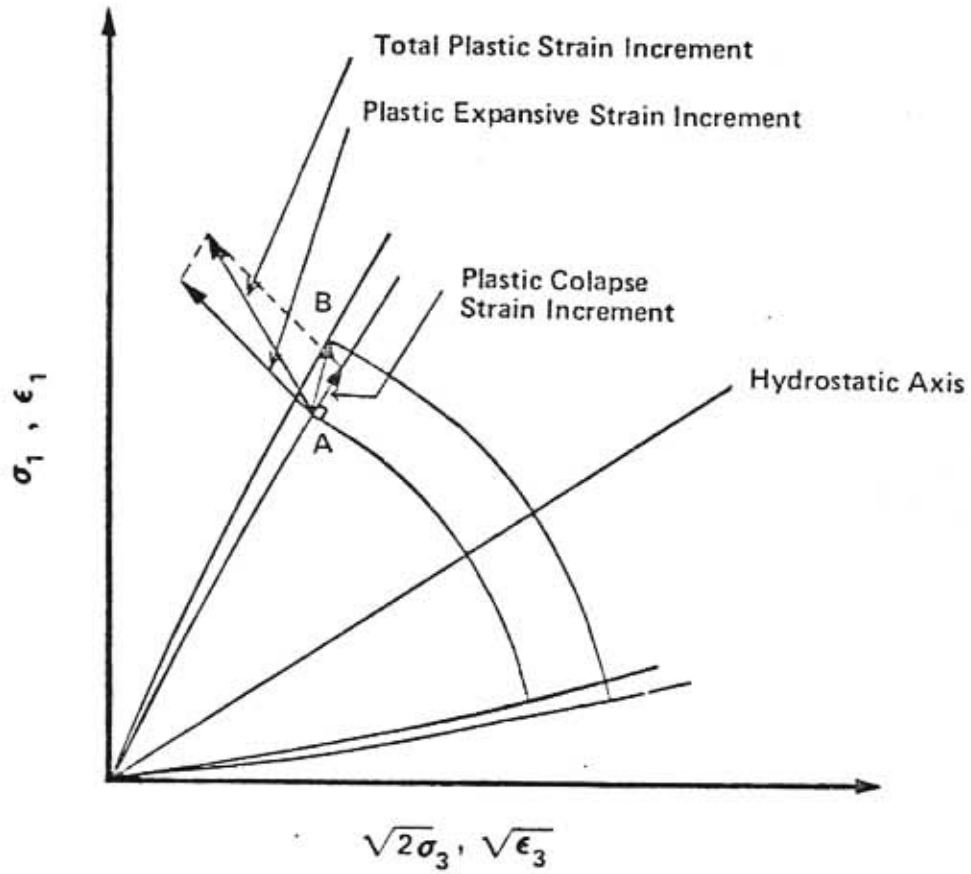


Figure 2.2 Schematic Diagram of Yielding Process with Plastic Strain Components Superimposed in Triaxial Plane

(After Lade, 1980)

Parameters p and c can be determined from a log-log plot of (W_c/P_a) vs. (f_c/P_a^2) from which the slope is equal to p and the intercept of the (W_c/P_a) axis at $(f_c/P_a^2) = 1$ is equal to C . The plastic collapse work is subsequently determined from the following equation:

$$dW_c = C \cdot p \cdot P_a \cdot (P_a^2/f_c)^{1-p} \cdot d(f_c/P_a^2) \quad (2.7.11)$$

The value of dW_c (from eqn. 2.7.11) is used for computing the plastic collapse strains in equation (2.7.6).

2.7.5. Plastic Expansive Behavior

The equation of the curved conical yield surface (in terms of the 1st and 3rd invariants of stress) used in plastic analysis of the expansion strains is expressed as

$$f_p = \left(\frac{I_1^3}{I_3} - 27 \right) \cdot \left(\frac{I_1}{P_a} \right)^m$$

$$f_p = \eta_1 \quad \text{at failure} \quad (2.7.12)$$

where $I_3 = \sigma_{11} \cdot \sigma_{22} \cdot \sigma_{33}$ (in terms of principal stresses) and η_1 and m are material parameters for sand at a given density.

The value of η_1 controls the apex angle of the failure surface. Both these parameters are determined from a log-log plot of $(I_1^3/I_3 - 27)$ vs. (P_a/I_1) at failure. Unlike the yield criteria used for the collapse strains, Lade implements a non-associative flow rule for this plastic strain component. The plastic potential function, g_p , is written as follows:

$$g_p = I_1^3 - (27 + \eta_2 \cdot (P_a/I_1)^m) \cdot I_3 \quad (2.7.13)$$

In this expression, a new constant, η_2 , is introduced; its value depends on f_p and the minor principal stress, σ_{33} . A conventional triaxial compression test is used to determine η_2 from the following expression:

$$\eta_2 = \frac{3(1 + \nu^P) \cdot I_1^2 - 27 \cdot \sigma_3 \cdot (\sigma_1 + \nu^P \cdot \sigma_3)}{(P_a/I_1)^m \cdot [\sigma_3(\sigma_1 + \nu^P \cdot \sigma_3) - I_3/I_1 \cdot m(1 + \nu^P)]} \quad (2.7.14)$$

where $\nu^P = -d\epsilon_3^P/d\epsilon_1^P$ is the plastic expansive conjugate of the elastic Poisson's ratio, ν . Note that these plastic incremental strains do not include the elastic or plastic collapse components. The expression above for η_2 can be simplified for computational purposes to this form:

$$\eta_2 = S \cdot f_p + R \cdot \sqrt{\sigma_3/P_a} + t \quad (2.7.15)$$

which yields three additional constants (R, S, & t) to describe the plastic potential function. These model parameters are derived from a plot of η_2 vs. f_p ; the slope gives the constant S while the intercept is equal to parameter t. An indication of the variation of S and t with confining pressure (σ_{33}) is mathematically represented by the value of R.

The next step in the development is the hardening of the conical surface based on plastic expansive work which can be calculated from:

$$W_p = \int \sigma : d\epsilon^P \quad (2.7.16)$$

The relationship between f_p (eq. 2.7.12) and W_p is approximated by the following exponential function:

$$f_p = a \cdot e^{-b W_p} (W_p/P_a)^{1/q} \quad \text{for } q > 0 \quad (2.7.17)$$

where a, b, & c are constants at a specified value of

σ_3 .

With data given at a particular confining pressure, the constant q can be determined from the following equation:

$$q = \frac{\log \left(\frac{W_{p.\text{peak}}/W_{p.60}}{1 - W_{p.60}/W_{p.\text{peak}}} \right) \cdot .434}{\log (\eta_1/f_{p60})} \quad (2.7.18)$$

where .434 = logarithm of base for natural logarithm, e

$W_{p.\text{peak}}$ = peak plastic work corresponding to

$$f_p = \eta_1 \quad (\text{i.e. failure})$$

$W_{p.60}$ = plastic expansive work at a stress level

$$\text{of } f_p = 0.60 \times \eta_1$$

As previously mentioned, the value of q computed in equation 2.7.18 is based on a triaxial test at a specific confining pressure; it is therefore necessary to model the change in q with confining pressure, σ_3 , by this expression:

$$q = \alpha + \beta (\sigma_3/P_a) \quad (2.7.19)$$

The model parameters α and β for this proposed linear relationship are obtained by performing a linear regression of q vs (σ_3/P_a) .

The constants a and b are computed according to:

$$a = \eta_1 (e \cdot P_a / W_{p.\text{peak}})^{1/q} \quad (2.7.20)$$

and

$$b = \frac{1}{q \cdot W_{p.\text{peak}}} \quad (2.7.21)$$

where e = base of natural logarithm

and q is computed from equation (2.7.19)

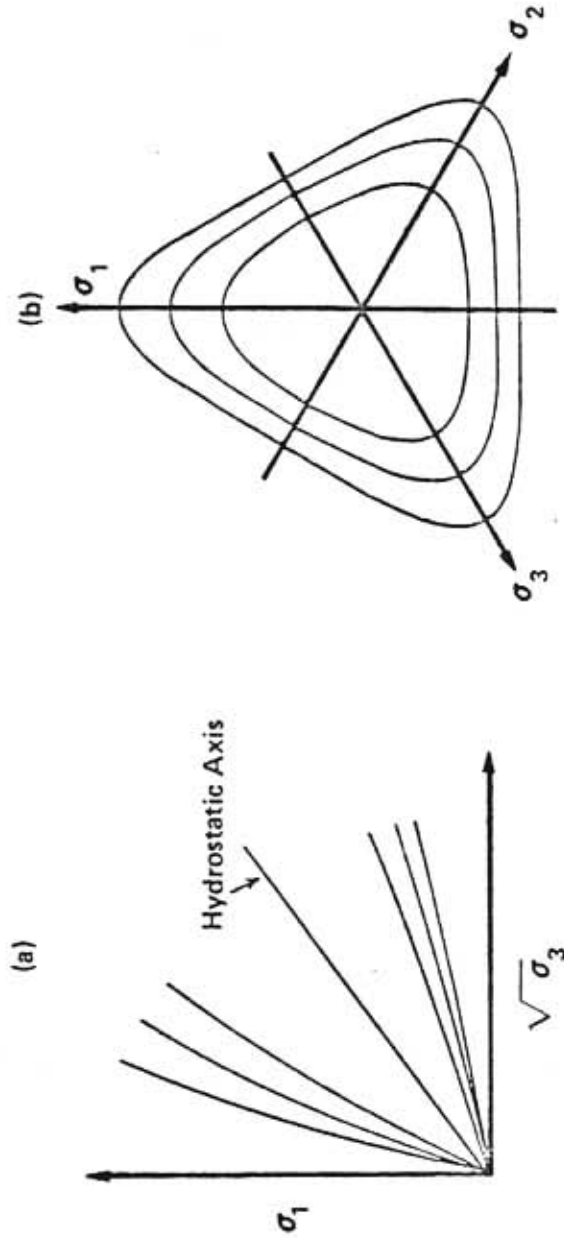


Figure 2.3 Characteristics of Proposed Failure and Yield Surfaces Shown in Principal Stress Space. (a) Traces of Failure and Yield Surfaces in Triaxial Plane. (b) Traces of Failure and Yield Surfaces in Octahedral Plane

(After Lade, 1980)

Lade assumes the relationship between the maximum plastic expansive work and the confining pressure can be patterned by this power function:

$$W_{p \cdot \text{peak}} = P \cdot P_a (\sigma_3/P_a)^l \quad (2.7.22)$$

where P and l are determined from a plot of $(W_{p \cdot \text{peak}}/P_a)$ vs. (σ_3/P_a) . P is the intercept at $\sigma_3/P_a = 1$ and l is the slope of the straight line.

From the normality rule, the incremental plastic strains are determined from:

$$d\varepsilon_{ij}^p = d\lambda_p \frac{\partial g_p}{\partial \sigma_{ij}} \quad (2.7.23)$$

The derivative of g_p with respect to the principal stresses which are to be used in equation (2.7.23) are presented below:

$$\frac{\partial g_p}{\partial \sigma_{11}} = 3I_1^2 - (27 + \eta_2 \cdot (P_a/I_1)^m) \cdot (\sigma_{22} \cdot \sigma_{33} - \sigma_{23}^2) + I_3/I_1 \cdot m \cdot \eta_2 \cdot (P_a/I_1)^m \quad (2.7.24)$$

and similarly for the shear stress component.

$$\frac{\partial g_p}{\partial \sigma_{23}} = (27 + \eta_2 \cdot (P_a/I_1)^m) \cdot (\sigma_{11} \cdot \sigma_{23} - \sigma_{12} \cdot \sigma_{31}) \quad (2.7.25)$$

The expression for the other derivatives can be obtained by simply interchanging the indices. With the values of the derivatives known, the final step for computing the incremental plastic strain tensor from equation (2.7.23) involves the determination of the proportionality constant, $\Delta\lambda_p$; the expression for computing $\Delta\lambda_p$ is stated as

$$\Delta\lambda_p = \frac{dW_p}{3 \cdot g_p + m \cdot \eta_2 \cdot (P_a/I_1)^m \cdot I_3} \quad (2.7.26)$$

where g_p is the plastic potential function and dW_p is the increment in plastic expansive work due to a change in stress df_p :

$$dW_p = \frac{df_p}{f_p} \cdot \frac{1}{(1/q \cdot W_p - b)} \quad (2.7.27)$$

where f_p = current value of the stress level.

2.8 Particulate Mechanics Approach For Modeling The Behavior of Sand

2.8.1 Introduction

The theory used to predict the behavior of a material may be based on one of several field theories which include: quantum mechanics, wave mechanics, particulate mechanics, rigid body mechanics and continuum mechanics. The distinguishing feature of each of these approaches is the level of observation; i.e. the theories listed (from quantum to continuum) increase in the phenomenological scale of material behavior (microscopic vs. gross) necessary for theory formulation. Plasticity theory in soil mechanics is founded on the principles of continuum mechanics of which a fundamental assumption is that the material has no holes or voids. Such a premise makes available the powerful methods of calculus for the interpretation and quantitative predictions of material response over a wide range of conditions. Chang (1983), however, disputes the acceptance of the continuum mechanics approach by stating that "modeling the complex mechanical behavior of granular soil by continuum mechanics usually requires excessively

complicated yielding and potential functions which engineers have difficulties using and implementing in numerical analysis". Without endorsing this statement, the writer finds it appropriate to present a particulate mechanics model (Chang, 1983) that has been successfully applied to monotonic loading conditions.

This model is based on the law of equilibrium between particles and the concept that the direction of sliding changes as the the stress state varies. The sliding mechanism is used as a basis to develop the constitutive law by incorporating: a. the effect of material structure on sliding deformation, b. volume change induced by sliding, and c. stress-induced anisotropy. Particles are idealized as being rigid, convex, simply connected, unbreakable, and of finite curvature.

When an assembly of particles is subjected to surface tractions, its strains may be due to any combination of these three components: 1) Sliding and rotation between particles, 2) elastic compression of particles, and 3) crushing of particles. Studies have shown that the elastic and rotational strains are negligible in comparison to the sliding deformations while the strain component due to particle crushing are also insignificant at ordinary stress levels. Therefore, it may be assumed that the total deformation within the granular assemblage can be solely attributed to the sliding mechanism.

2.8.2 Theoretical development*

Consider a unit cube of sand particles in which the contact points may slide or remain stable when subjected to a boundary load. Obviously, the sliding contacts are the only ones which contribute to the deformation of the mass so the strain along a length of the unit cube may be represented by

$$\epsilon_x = \sum_{j=1}^{n_x} u_j \quad (2.8.1.a)$$

where u_j = vertical component (x - direction) of the sliding deformation at contact point j.
 n_x = number of sliding contacts along this vertical column.

Strains in the other two coordinate directions may then be similarly expressed as

$$\epsilon_y = \sum_{j=1}^{n_y} v_j \quad (2.8.1.b)$$

and

$$\epsilon_z = \sum_{j=1}^{n_z} w_j \quad (2.8.1.c)$$

Given this representation of strains in the principal directions, the next sequence of the discussion will be to formulate the computational procedure for stress-history dependent incremental strains due to increments of external stress.

* Based on principal stresses.

Coulomb's law of friction governs the sliding mechanism of a two-particle configuration as shown in figure 2.4 A. At the contact point i , there are two equal but opposite interparticle forces, F_i . This force (F_i) can be decomposed into its normal component, N_i , and shear component, T_i . According to Coulomb's law, $T_i = N_i \tan \alpha$, or $\alpha = \tan^{-1}(T_i/N_i)$. If the value of the angle is less than its limiting value, ϕ_u , relative sliding of the particles is not initiated; on the other hand, a stress change may increase the value of α to the ultimate angle of internal friction, ϕ_u , with the result that the contact point i will now be classified as a sliding contact. The direction of the particle sliding will be in a direction opposite to that of the contact shear force and can be computed as a unit sliding vector in the following form:

$$\bar{S}_i = \bar{F}_i \sin \phi_u - \cos \phi_u \bar{t}_i \quad (2.8.2)$$

where \bar{F}_i and \bar{t}_i are the unit vectors of the contact interparticle force and contact shear force respectively.

A statistical approach is employed to analyse a column of the assembly of particles. The cone depicted in the upper portion of figure 2.4B represents contact points whose contact forces are all pointing in the same direction. Note that for the threshold contact points, the normal force, N_i , is the side of the cone which lies at an angle ϕ_u from \bar{F}_i . Say these particles (depicted by the cone) are now subjected to an external load, it is expected that some of the contact forces will remain stable while the others will slide due to

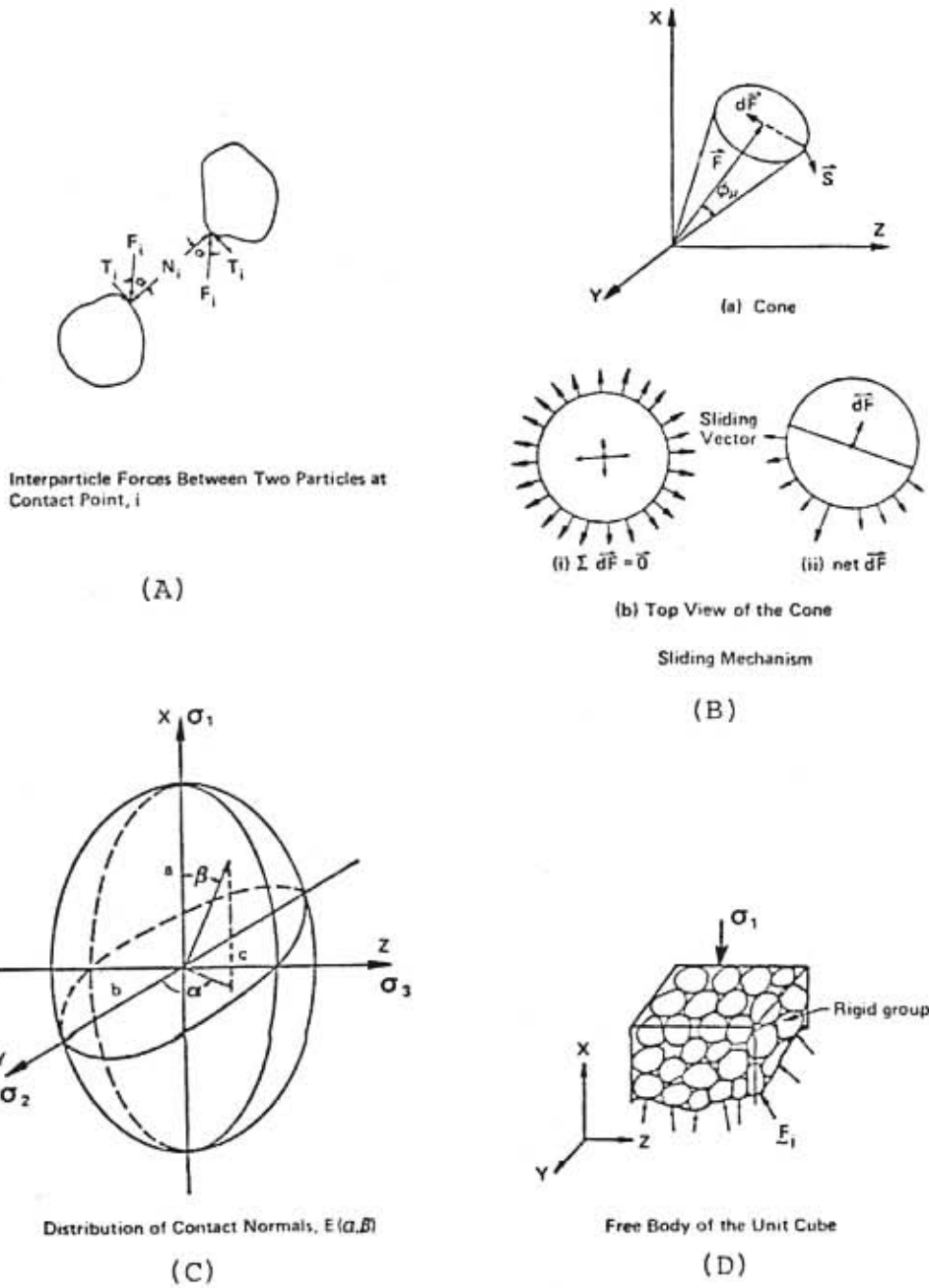


Figure 2.4 Mechanics of Particulate Approach (After Chang, 1983)

an increase in angle between \underline{F} and \underline{N} . Owing to the random nature of the particle packing, some of the contact forces will undoubtedly re-orient themselves as shown by dF in the upper part of figure 2.4 B. In order to facilitate computation of the sliding vector for the particles represented by this cone, the summation of dF for the particle set is treated as two components: the first (as shown in figure 2.4B b(i)) is such that $\sum dF = 0$, and thus the unit sliding vector, \bar{S}_c , (or collapse deformation) is pointed in the direction \underline{F} . The second part (see figure 2.4B b(ii)) considers the net dF which acts opposite to \underline{F} ; this conjugate of the collapse deformation sliding vector is termed the shear deformation vector, \bar{S}_s . The total sliding vector is then simply the sum of the compression (or collapse) and expansion (or shear) deformation:

$$\begin{aligned}\bar{S} &= \bar{S}_s + \bar{S}_c \\ &= (\bar{F}_i \sin\phi_u - \cos\phi_u \cdot d\bar{f}_i) + C_1 (\bar{F}_i)\end{aligned}\quad (2.8.3)$$

where C_1 is a weighting parameter which indicates the percentage of collapsing deformation and shear deformation.

Given the direction of sliding, the strains along a particle column can now be computed if the number of particle contacts and the mean sliding distance are known. The following equation mathematically represents the straining of a unit cube of granular material.

$$\epsilon_x = N_x \bar{L} [(\bar{F}_x \sin\phi_u - \cos\phi_u \cdot d\bar{f}_x) + C_1 \bar{F}_x] \quad (2.8.4)$$

where N_x = number of sliding contacts/column in x -
direction

\bar{f}_x = component of mean unit force vector, \bar{f} , in
x-direction

$d\bar{f}_x$ = increment of \bar{f}_x

\bar{L} = mean magnitude of sliding deformation
between 2 contact particles.

Similarly, ϵ_x and ϵ_y may be obtained from equation 2.8.4 by using the appropriate indices. Note that strains are related to mean interparticle force in equation 2.8.4 so it is still necessary to link force, \bar{f} , to stress in order to establish the constitutive relationship between stress and strain.

One of the more potent aspects of this model is its ability to incorporate the influence of stress-induced anisotropy. The density function, $E(\alpha, \beta)$, is represented by an ellipsoid as shown in figure 2.4C. The equation for this surface takes the following form:

$$E(\alpha, \beta) = \frac{abc}{[a \sin^2\beta(c \cos^2\alpha + b \sin^2\alpha) + bc \cos^2\beta]} \quad (2.8.5)$$

where α and β are used to describe a contact normal, and a, b, c , are the maximum, intermediate, and minimum principal radii which are at any time proportional to the principal stresses:

$$\frac{a}{\sigma_1^2} = \frac{b}{\sigma_2^2} = \frac{c}{\sigma_3^2} \quad (2.8.6)$$

Based on this density function, an anisotropy index can be derived as follows:

$$\begin{aligned}
 A_{13} &= \frac{\# \text{ of particles along the } \sigma_1 \text{ direction}}{\# \text{ of particles along the } \sigma_3 \text{ direction}} \\
 &= R_{13}^{(1-B)} [\log R_{13}/R_{13} - 1]^{(1-2B)} \quad (2.8.7)
 \end{aligned}$$

$$\begin{aligned}
 A_{23} &= \frac{\# \text{ of particles along the } \sigma_2 \text{ direction}}{\# \text{ of particles along the } \sigma_3 \text{ direction}} \\
 &= [R_{23} - 1/\log R_{23}] \quad (2.8.8)
 \end{aligned}$$

$$A_{12} = \frac{\# \text{ of particles along the } \sigma_2 \text{ direction}}{\# \text{ of particles along the } \sigma_3 \text{ direction}} = \frac{A_{13}}{A_{23}} \quad (2.8.9)$$

where $R_{13} = \sigma_1/\sigma_3$; $R_{23} = \sigma_2/\sigma_3$; and

$$B = (\sigma_2 - \sigma_3)/(\sigma_1 - \sigma_3)$$

As mentioned previously, the relationship in equation 2.8.4 expresses strains in terms of inter-particle contact force so it is now necessary to present the method by which external stresses are converted into contact forces. Figure 2.4D is a free body diagram of a unit cube of sand particles. From static equilibrium, the mean vertical component of the interparticle force can be approximated as

$$\bar{F}_x = \sigma_1/N_y \cdot N_z \quad (2.8.10)$$

where $N_y \times N_z = \#$ of contacts points subject to σ_1 .

Similarly,

$$F_y = \sigma_2/N_x \cdot N_z \quad \text{and} \quad F_z = \sigma_3/N_x \cdot N_z \quad (2.8.11)$$

where $N_i =$ total $\#$ of particles along column i .

The direction cosines of the mean interparticle force vector, \underline{F} , are

$$\begin{aligned}\bar{f}_x &= \frac{\bar{F}_x}{|\bar{F}|} = \frac{\sigma_1}{[\sigma_1^2 + (A_{12}\sigma_2)^2 + (A_{13}\sigma_3)^2]^{1/2}} \\ \bar{f}_y &= \frac{\bar{F}_y}{|\bar{F}|} = \frac{A_{12}\sigma_2}{[\sigma_1^2 + (A_{12}\sigma_2)^2 + (A_{13}\sigma_3)^2]^{1/2}} \\ \bar{f}_z &= \frac{\bar{F}_z}{|\bar{F}|} = \frac{A_{13}\sigma_3}{[\sigma_1^2 + (A_{12}\sigma_2)^2 + (A_{13}\sigma_3)^2]^{1/2}}\end{aligned}$$

Differentiation of equation 2.8.12 gives the change in direction cosine of the mean interparticle force vector, \bar{f} , due to increments of external stress;

$$d\bar{f}_x = X[(A_{12}^2\sigma_2^2 + A_{13}^2\sigma_3^2)d\sigma_1 - A_{13}^2\sigma_1\sigma_3d\sigma_3 - A_{12}^2\sigma_1\sigma_2d\sigma_2]$$

$$d\bar{f}_y = X[(\sigma_1^2 + A_{13}^2\sigma_3^2)A_{12}d\sigma_2 - A_{12}A_{13}^2\sigma_2\sigma_3d\sigma_3 - A_{12}\sigma_1\sigma_2d\sigma_1]$$

$$d\bar{f}_z = X[(\sigma_1^2 + A_{12}^2\sigma_2^2)A_{13}d\sigma_3 - A_{13}\sigma_1\sigma_3d\sigma_1 - A_{13}A_{12}^2\sigma_2\sigma_3d\sigma_2]$$

$$\text{where } X = (\sigma_1^2 + A_{12}^2\sigma_2^2 + A_{13}^2\sigma_3^2)^{-3/2} \quad (2.8.13)$$

Combining equations 2.8.4, 2.8.12, and 2.8.13, it is now possible to establish the stress-strain relationship. With the further assumption that the number of sliding particles is directly proportional to the total number of particles in each column (ratio = C), the expressions for incremental strains are as follows:

$$d\epsilon_x = (CN_x \bar{L}) \bar{u} = H \bar{u}$$

$$d\epsilon_y = (CN_y \bar{L}) \bar{v} = A_{xy} H \bar{v}$$

$$d\epsilon_z = (CN_z \bar{L}) \bar{w} = A_{xz} H \bar{w} \quad (2.8.14)$$

$$\text{where } A_{xy} = N_y/N_z; \quad A_{xz} = N_x/N_z$$

H = hardening parameter defining the magnitude of strains due to external stresses.

\bar{u} , \bar{v} , \bar{w} can be determined from eq 2.8.4, to be:

$$\begin{aligned} \bar{u} &= (\bar{f}_x \sin\phi_u - \cos\phi_u d\bar{f}_x) + C_1 \bar{f}_x \\ \bar{v} &= (\bar{f}_y \sin\phi_u - \cos\phi_u d\bar{f}_y) + C_1 \bar{f}_y \\ \bar{w} &= (\bar{f}_z \sin\phi_u - \cos\phi_u d\bar{f}_z) + C_1 \bar{f}_z \end{aligned} \quad (2.8.15)$$

The hardening parameter, H, is characterized by the following fundamentals: a) $d\epsilon_1$ increases as the stress ratio increases and becomes infinite at failure, b) $d\epsilon_1$ decreases as confining pressure increases, and c) the influence of the intermediate principal stress is also incorporated. The failure criteria is the same as that presented for the Lade elasto-plastic model (Lade, 1980), i.e.

$$M = (I_{1f}^3 / I_{3f} - 27) (I_{1f} / P_a)^m \quad (2.8.16)$$

where I_{1f} = 1st invariant of stress at failure

I_{3f} = 3rd invariant of stress at failure

P_a = atmospheric pressure

M, m = material constants

The quantity η is represented by the same equation for M (eq., 2.8.16) except for one difference: the invariants of stress are for any stress state below the limiting value, i.e.

$$\eta = (I_1^3/I_3 - 27) (I_1/P_a)^m \quad (2.8.17)$$

Another quantity, the stress ratio λ , is defined to be an indicator of proximity to failure,

$$\lambda = \frac{M - n}{M} \quad (2.8.18)$$

The hardening parameter, H , is represented by the following equation,

$$H = \frac{\lambda^{1/2}}{a \left(\frac{\sigma_3}{\sigma_m}\right)^b \left(\frac{3}{P_a}\right)^c} \frac{ds}{\left(\frac{3\sigma_m}{3} - 1\right) (1 + B)} \quad (2.8.19)$$

where a , b , and c = material constants

$$B = \frac{\sigma_2 - \sigma_3}{\sigma_1 - \sigma_3}$$

and

$$ds = (d\sigma_1^2 + d\sigma_2^2 + d\sigma_3^2)^{1/2}$$

Also, it is assumed that the fraction of sliding contacts subject to collapsing deformation is equal to 0% for stress paths that have an increase in σ_1 and a decreasing or constant σ_3 . It is found that stress paths which have both an increase in σ_1 and σ_3 do not result in negligible collapse deformations, therefore the following formula for C_1 is assumed:

$$C_1 = \frac{dI_3}{d\sigma_1^3 - dI_3} \quad (2.8.20)$$

In summary, six parameters are required to calibrate this constitutive model - M , m , a , b , and c - which can be obtained from conventional triaxial testing. General monotonic loading conditions can be simulated to include these phenomena: shear sliding induced compressive or expansive volume change, and also volume change due to collapsing sliding deformation.

CHAPTER 3
BOUNDING SURFACE PLASTICITY FORMULATION FOR SAND

3.1 Introduction

Most constitutive laws in soil mechanics have been formulated for very specific loading conditions, but, in many instances, the analysis of earth structures involves complex and varying loading conditions. Although it is dubious that a genuinely general constitutive model will ever be developed, it is important that the model be able to simulate undrained and drained response as well as the effect of interchangeable loadings on a normally or over-consolidated soil. Classical plasticity theory does provide the anatomy for modeling these very important aspects of soil behavior except for one major deficiency: plastic irreversible deformation cannot occur within the yield surface, which defines a purely elastic range of the material response, contrary to observed behavior. This short-coming led to the concept of the bounding surface which was originally introduced by Dafalias and Popov (1976) and independently by Krieg (1975) to model both the monotonic and cyclic loading of metals within the same theoretical framework. The kernel of this idea is that for any stress state within (or residing on) the bounding surface, a corresponding "image" point on the surface is

specified by an appropriate mapping rule which becomes the identity mapping if the stress state is on the surface (Dafalias, Hermann & DeNatale, 1980). This salient and novel feature permits plastic deformations within the surface by rendering the plastic modulus an increasing function of the Euclidean distance between the actual stress point and the "image" stress point on the bounding surface. The "image" stress point on the bounding surface serves the dual role of determining the magnitude and the direction of the plastic strain rate; the plastic modulus, as mentioned above, controls the magnitude while the direction of loading and that of the plastic strain rate are defined by the unit normal to the bounding surface at points properly defined by the given stress state and the stress rate direction.

To the author's knowledge, Aboim and Roth (1982) were the first investigators to apply the bounding surface theory to cohesionless soils. When this model was later implemented (Taesiri, McVay, & Townsend, 1983) to imitate the cyclic stress-strain behavior along the moving wheel stress path, certain deficiencies in the hardening rule were noted and therein modified. In this thesis, further refinements are made to the model and each will be summarized at the end of the presentation of the theory. Several features of the model which were not used in the simulation of the pressuremeter tests or any other tests in this report are not included. For instance, only associative flow is considered so the plastic potential and

the bounding surface become coincident; this significantly reduces the number of equations that need to be presented. More detailed discussion on the general aspects of the model can be found in the Taesiri et al. (1983) reference.

3.2 Theory

The mathematical development of this model necessitates the introduction of and definition of some of the more frequently used symbols. $\underline{\sigma}$ is used for the effective stress tensor and \underline{S} for the deviator stress tensor. The invariants of stress are defined as follows:

$$I = \text{tr}(\underline{\sigma}) = \underline{\sigma} : \underline{\delta} = \sigma_{ij} \delta_{ij} = \sigma_{kk} \quad (3.1)$$

$$J = \frac{1}{2} \underline{S} : \underline{S} = \frac{1}{2} S_{ij} S_{ij} \quad (3.2)$$

where the indexed symbols refer to the components of the tensors. The double contraction, represented by the double dots (:), is defined by using the summation convention over repeated indices (Malvern, 1969). δ is the Kronecker delta. The strain rate tensor is decomposed into its elastic and plastic parts through a mathematical relation such as:

$$\dot{\underline{\epsilon}} = \dot{\underline{\epsilon}}^e + \dot{\underline{\epsilon}}^p \quad (3.3)$$

The elastic incremental constitutive relations are given by (Little, 1973):

$$\dot{\underline{\sigma}} = D : \dot{\underline{\epsilon}}^e$$

with

$$D_{ijkl} = (K - \frac{2}{3}G) \delta_{ij} \delta_{kl} + G(\delta_{ik} \delta_{jl} + \delta_{il} \delta_{jk}) \quad (3.4)$$

where K and G are the elastic bulk & shear modulus, respectively:

The plastic constitutive relation requires the definitions of the direction of plastic loading $n:\dot{\underline{\sigma}}$ and of the plastic modulus, K_p , which in turn determine the loading function L as:

$$L = \frac{\underline{n}:\dot{\underline{\sigma}}}{K_p} \quad (3.5)$$

where \underline{n} is a second order tensor such that $\underline{n}:\underline{n} = 1$ and K_p is the generalized plastic modulus. The constitutive equation for the plastic strain rates is assumed to have the following form:

$$\dot{\underline{\epsilon}}^p_{ij} = \langle L \rangle n_{ij} \quad (3.6)$$

where $\langle \rangle$ are the Macauley brackets which define the operation $L = \langle L \rangle H(L)$, with H being Heaviside's step function, which is zero for $L < 0$ and unity for $L > 0$.

The final pre-requisite to the description of the bounding surface is the explanation of the role of critical state soil mechanics in this formulation. During a conventional triaxial compression test on a dense sand, the specimen will be observed to compress initially and then dilate until "failure". It is hypothesized that the start of the dilation phase of the volumetric behavior can be predicted if the state of stress in the soil is known. In stress invariant space, a straight line, passing through the origin, can be visualized as differentiating stress states above and below which dilation can occur (figure 3.1). It

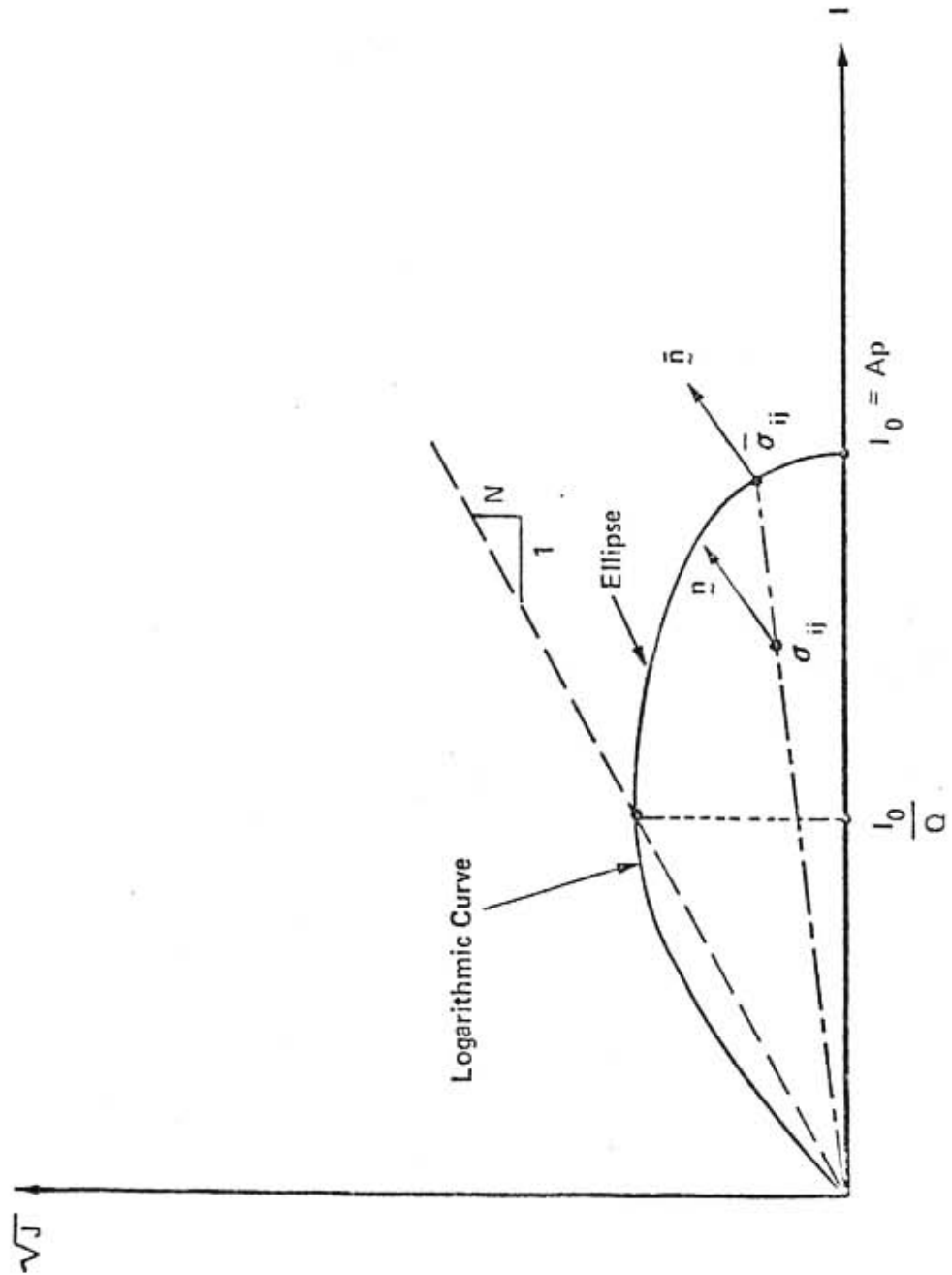


Figure 3.1 The Bounding Surface in Stress Invariant Space
(After Taesiri et al., 1983)

is postulated that the slope of this straight line, aptly known as the critical state line, is both unique and constant for a sand at a given relative density. Our attention is therefore brought to the introduction of the first model parameter, N , which is the slope of the critical state line (henceforth abbreviated to "CSL").

In principal stress space, the shape of the bounding surface is assumed to be logarithmic between the origin and the CSL, and then undergoes a continuous transition into an ellipse which forms somewhat of a bullet-shaped cap axially symmetric about the hydrostatic axis. Defining $\theta = \sqrt{J} / I$, the proposed bounding surfaces can be expressed as follows:

$$F = \bar{I}^2 + \frac{(Q - 1)^2 \bar{J}}{N} - \frac{2\bar{I}I_0}{Q} + \frac{(2 - Q)I_0^2}{Q} = 0 \quad (3.7)$$

for $0 \leq \theta \leq N$
and

$$F = \sqrt{J} + N(e - 1) \left[\frac{e}{e-1} \frac{I_0}{Q} - \bar{I} \right] \ln \left[1 - \frac{(e - 1)Q\bar{I}}{eI_0} \right] = 0 \quad (3.8.a)$$

for $N \leq \theta \leq \infty$

By letting $x = ep / Q(e - 1)$ in eq 3.8a, the equation becomes more tractable in later derivations,

$$F = \sqrt{J} + N(e - 1)(xA - \bar{I}) \ln(1 - \bar{I}/xA) = 0 \quad (3.8.b)$$

where Q is a "trial and error" model parameter which partly governs the ratio of the major to minor axes of the elliptic surface (i.e. $(Q - 1)/N$), e is the base of the natural logarithm. I_0 is the vertex of the ellipse (i.e. intersection of the ellipse with the hydrostatic axis) and the bars over the stress invariants indicate that they apply

to the bounding surface. The quantity I_0 (in units of stress) is employed in monitoring the hardening parameter defined as:

$$A = I_0/p \quad (3.9)$$

where p = atmospheric pressure in units of I_0 . Note that only a single constant, A , is sufficient in recording the position of the surface in stress space since the shape of the surface does not change. Later it will be shown that A is a function of "plastic internal variables" - such as the history of the plastic strain rate tensor - which are a manifestation of the plastic state of the material at any instant.

The mapping rule used in this thesis is the regular mapping rule of Dafalias which relates σ_{ij} to a unique "image" point, $\bar{\sigma}_{ij}$ on $F=0$ by a straight line passing through the origin of stress space and σ_{ij} . This can be mathematically expressed in terms of the stress invariants as:

$$\bar{I} = \beta I \quad (3.10)$$

$$\bar{J} = \beta^2 J \quad (3.11)$$

where β = radial factor (greater than or equal 1)

$\beta = 1$ attests that the actual stress point and its "image" are concomitant

Once the "image" stress point on the bounding surface has been located, it is possible to compute the unit second order normal to the bounding surface, \underline{n} , by:

$$\underline{n} = \frac{\nabla F}{\|\nabla F\|} \quad (3.12)$$

where ∇F = gradient of F and

$$\|\nabla F\| = \text{norm of } F$$

Three different loading conditions are possible: virgin loading, reloading or unloading. Each loading situation generates varying amounts of plastic strain so it is imperative to specify an appropriate quantity for the plastic modulus, K_p , based on its relative position to the bounding surface (β) and the phase of the loading cycle. The proposed conditions are as follows:

a) Virgin Loading - $\dot{\underline{q}}:\underline{n} > 0$ with $\beta = 1$,

$$K_p = \bar{K}_p \quad \text{where } \underline{n} = \bar{\underline{n}} \quad (3.13)$$

b) Unloading - $\dot{\underline{q}}:\underline{n} < 0$ with $\beta > 1$,

$$K_p = \beta H_u / (\beta - 1) \quad \text{where } \underline{n} = -\bar{\underline{n}} \quad (3.14)$$

and $\dot{\underline{q}}$ pointing inward from F

c) Reloading - $\dot{\underline{q}}:\underline{n} < 0$ with $\beta > 1$,

$$K_p = K_p + (\beta - 1)H_r/\beta, \quad \text{where } \underline{n} = \bar{\underline{n}} \quad \text{and} \\ \dot{\underline{q}} \text{ pointing outward from } F \quad (3.15)$$

where H_u and H_r are model parameters estimated from curve fitting and K_p is obtained from the consistency condition (discussed later).

In order to compute the normals to the bounding surface, the partial derivatives of equations 3.1, 3.2, 3.7, and 3.8b are required; the solution of n_{ij} on both surfaces is written out in long form below:

For $0 \leq \theta \leq N$ i.e. Elliptic surface

$$\frac{\partial F}{\partial I} = 2(\bar{I} - I_0/Q)$$

$$\frac{\partial F}{\partial J} = \frac{(Q-1)^2}{N}$$

$$\frac{\partial \bar{I}}{\partial \sigma_{ij}} = \delta_{ij} \quad \text{and} \quad \frac{\partial \bar{J}}{\partial \sigma_{ij}} = \bar{S}_{ij}$$

$$(\nabla F)_{ij} = \frac{\partial F}{\partial \sigma_{ij}} = \frac{\partial F}{\partial I} \cdot \frac{\partial \bar{I}}{\partial \sigma_{ij}} + \frac{\partial F}{\partial J} \cdot \frac{\partial \bar{J}}{\partial \sigma_{ij}}$$

$$\begin{aligned} \|\nabla F\| &= 2(\bar{I} - I_0/Q)\delta_{ij} + (Q-1/N)^2\bar{S}_{ij} \\ \|\nabla F\| &= \sqrt{12(\bar{I} - I_0/Q)^2 + 2(Q-1/N)^4\bar{J}} \end{aligned} \quad (3.16)$$

$$\text{from equation 3.9, } \bar{n} = \frac{\nabla F}{\|\nabla F\|}$$

therefore

$$n_{ij} = \frac{2(\bar{I} - I_0/Q)\delta_{ij} + (Q-1/N)^2\bar{S}_{ij}}{\sqrt{12(\bar{I} - I_0/Q)^2 + 2(Q-1/N)^4\bar{J}}} \quad (3.17)$$

For $N \leq \theta \leq \infty$ i.e. logarithmic surface

$$\frac{\partial F}{\partial I} = -N(e-1)[1 + \ln(1 - \bar{I}/xA)]$$

$$\frac{\partial F}{\partial J} = \frac{1}{2\sqrt{J}}$$

$$(\nabla F)_{ij} = \frac{\partial F}{\partial \sigma_{ij}} = -N(e-1)[1 + \ln(1 - \bar{I}/xA)]\delta_{ij} + \frac{1}{2\sqrt{J}}\bar{S}_{ij}$$

$$\|\nabla F\| = \sqrt{3N^2(e-1)^2[1 + \ln(1 - \bar{I}/xA)]^2 + \frac{1}{4}} \quad (3.18)$$

$$n_{ij} = -\frac{N(e-1)[1 + \ln(1 - \bar{I}/xA)]\delta_{ij} + 1/2\sqrt{J}(\bar{S}_{ij})}{\sqrt{3N^2(e-1)^2[1 + \ln(1 - \bar{I}/xA)]^2 + \frac{1}{4}}} \quad (3.19)$$

The location of the bounding surface in stress space is a function of the state of stress and the plastic state variables (q_n). i.e.

$$F = f(\sigma_{ij}, q_n) \quad \text{where } f(x,y) \text{ signifies} \quad (3.20)$$

a function of x & y

In this plasticity model, there are two plastic state variables: (a) the plastic equivalent shear strain, η , and (b) the plastic volumetric strain, ξ . These components of the plastic strain rate tensor are defined as:

$$\dot{\eta} = \sqrt{\frac{1}{2} \dot{e}^P : \dot{e}^P} \quad \text{and} \quad \dot{\xi} = \dot{e}_{kk}^P \quad (3.21)$$

where \dot{e}^P is the plastic deviatoric strain rate tensor with components

$$\dot{e}_{ij}^P = \dot{e}_{ij}^P - 1/3 \dot{e}_{kk}^P \delta_{ij} \quad (3.22)$$

$\dot{\eta}$ and $\dot{\xi}$ can be written in terms of $\dot{\eta}$ by using equation 3.6,

$$\dot{\eta} = \sqrt{\frac{1}{2} \dot{e}^P : \dot{e}^P} = \langle L \rangle \sqrt{\frac{1}{2} n_{ij}^d n_{ij}^d} \quad (3.23)$$

$$\text{where } n_{ij}^d = n_{ij} - 1/3 n_{kk} \delta_{ij}$$

Therefore, $\dot{\eta}$ and $\dot{\xi}$ can be restated as

$$\dot{\eta} = \langle L \rangle \sqrt{\frac{1}{2} - (1/6) n_{kk}^2} \quad (3.24)$$

$$\dot{\xi} = \langle L \rangle n_{kk} \quad (3.25)$$

By invoking the consistency condition (Prager, 1949), the general equation for the plastic modulus, K_p , may be computed as follows:

Consistency condition,

$$\dot{F} = \frac{\partial F}{\partial \bar{\sigma}_{ij}} \dot{\sigma}_{ij} + \frac{\partial F}{\partial \eta} \dot{\eta} + \frac{\partial F}{\partial \xi} \dot{\xi} = 0 \quad (3.26)$$

$$\text{Rearranging eqn 3.12, } \frac{\partial F}{\partial \bar{\sigma}_{ij}} = \nabla F = ||\nabla F|| \bar{v}$$

Therefore

$$\frac{\partial F}{\partial \sigma_{ij}} \dot{\sigma}_{ij} = \|\nabla F\| \frac{\bar{n} : \dot{\sigma}}{\bar{n} : \sigma} \quad (3.27)$$

The plastic constitutive relation, equation 3.5, is now incorporated in equation 3.27:

$$\frac{\partial F}{\partial \sigma_{ij}} \dot{\sigma}_{ij} = \|\nabla F\| \frac{\bar{n} : \dot{\sigma}}{\bar{n} : \sigma} = \bar{K}_p \|\nabla F\| \frac{\bar{n} : \dot{\sigma}}{\bar{K}_p}$$

$$\text{but } L = \frac{\bar{n} : \dot{\sigma}}{\bar{K}_p} \text{ from equation 3.5,}$$

$$\text{Therefore } \frac{\partial F}{\partial \sigma_{ij}} \dot{\sigma}_{ij} = \bar{K}_p \|\nabla F\| \langle L \rangle \quad (3.28)$$

Substituting equations 3.24, 3.25 and 3.28 in the consistency condition (eqn 3.26) results in

$$\bar{K}_p \|\nabla F\| \langle L \rangle + \frac{\partial F}{\partial \eta} \langle L \rangle \sqrt{\frac{1}{2} - (1/6)n^2_{kk}} + \frac{\partial F}{\partial \xi} \langle L \rangle n_{kk}$$

from which \bar{K}_p can be solved as

$$\bar{K}_p = - \frac{1}{\|\nabla F\|} \left[\frac{\partial F}{\partial \eta} \sqrt{\frac{1}{2} - (1/6)n^2_{kk}} + \frac{\partial F}{\partial \xi} n_{kk} \right] \quad (3.29)$$

The next task at hand is the explanation of how the quantities $\partial F/\partial \eta$ and $\partial F/\partial \xi$ are computed and the methodology by which the position of the surface is updated by using the hardening parameter, A. Consider now that the hardening parameter A represents the combined effect of η and ξ on the bounding surface F; this can be expressed mathematically as:

$$A = f(\eta, \xi)$$

but $F = f(\sigma_{ij}, \eta, \xi)$ which is only an explicit statement of equation 3.20

therefore $F = f(\sigma_{ij}, A)$

So this means that the consistency condition (eqn. 3.26) can now be restated as:

$$\dot{F} = \frac{\partial F}{\partial \sigma_{ij}} \cdot \dot{\sigma}_{ij} + \left(\frac{\partial F}{\partial A} \cdot \frac{\partial A}{\partial \eta} \right) \dot{\eta} + \left(\frac{\partial F}{\partial A} \cdot \frac{\partial A}{\partial \xi} \right) \dot{\xi} = 0. \quad (3.30)$$

Remembering that $I_0 = Ap$, the derivatives $\partial F/\partial A$ and $\partial F/\partial XA$, which are to be used in eqn. 3.30, follows from equations 3.7 and 3.8b respectively:

$$\frac{\partial F}{\partial A} = - \frac{2}{Q^p} \bar{I} + 2 \frac{(2 - Q)}{Q} p^2 A \quad \text{for } 0 \leq \theta \leq N \quad (3.31)$$

and

$$\frac{\partial F}{\partial XA} = (e - 1) \left[\ln \left(1 - \frac{\bar{I}}{XA} \right) + \frac{\bar{I}}{XA} \right] \quad \text{for } N \leq \theta \leq \infty \quad (3.32)$$

The partial derivatives, $\partial A/\partial \eta$ and $\partial A/\partial \xi$, are calibrated along stress paths which dictate that only one of the partials - $\partial F/\partial \eta$ or $\partial F/\partial \xi$ - is a non-zero term along that particular stress path. The stress paths chosen are the standard triaxial stress path and the isotropic consolidation stress path.

Let us consider first the hardening along the standard triaxial stress path; this path can be represented in general stress space as follows:

$$I = \sqrt{3J} + 3 \sigma_m \quad (3.33)$$

where σ_m is the effective confining pressure before the specimen is sheared or generally, the minor principal stress

It is postulated that a hyperbolic relationship exists between the deviator stress, \sqrt{J} , and the plastic equivalent shear strain, η :

$$g = f(\eta) = \frac{\eta}{R + S\eta} = \frac{\sqrt{J}}{\sigma_m} \quad (3.34)$$

where R and S are model parameters depicting the hyperbolic function g.

Associating equations 3.33 and 3.34 leads to the following expression for the triaxial stress path:

$$I = (\sqrt{3} + \sqrt{3}/g)g\sigma_m \quad (3.35)$$

Although the discussion of the derivation of $\frac{\partial A}{\partial \eta}$ in this paper may seem somewhat superfluous, it is considered appropriate since it is the procedure adopted in numerical analysis. The computational technique is depicted compactly by this equation:

$$\frac{\partial A}{\partial \eta} = \frac{|\partial F / \partial \eta|_{tx}}{|\partial F / \partial A|_{tx}} \quad (3.36)$$

where the subscript tx refers to the triaxial stress path.

$|\partial F / \partial A|_{tx}$ is simply reckoned by substituting equation 3.35 into equations 3.31 or 3.32 depending on the surface that is relevant. Along a conventional triaxial compression (CTC) stress path, $\frac{\partial F}{\partial \xi} = 0$, so the consistency condition (equation 3.26) condenses to

$$\frac{\partial F}{\partial \sigma_{ij}} \hat{\sigma}_{ij} + \frac{\partial F}{\partial \eta} \dot{\eta} = 0 \quad (3.37)$$

From equation 3.16, $\partial F / \partial \sigma_{ij}$ can be replaced in eq 3.37 to result in the new expression:

$$[2(I - I_o/Q) \delta_{ij} + (Q - 1/N)^2 \bar{S}_{ij}] \hat{\sigma}_{ij} + \frac{\partial F}{\partial \eta} \dot{\eta} = 0$$

which further simplifies to

$$2(\bar{I} - I_0/Q)I + ((Q - 1)/N)^2 2\sqrt{J}\dot{\sqrt{J}} + \frac{\partial F}{\partial \eta} \dot{\eta} = 0 \quad (3.38)$$

for $0 \leq \theta \leq N$

Recalling equation 3.35 and taking the derivatives \bar{I} and $\dot{\sqrt{J}}$, as shown below, for eventual insertion in equation 3.38,

$$\bar{I} = \sqrt{3}g\sigma_m + 3\sigma_m \quad (3.39)$$

$$\dot{\bar{I}} = \sqrt{3}\sigma_m g' \dot{\eta}$$

and

$$\sqrt{J} = g\sigma_m$$

$$\dot{\sqrt{J}} = g' \sigma_m \dot{\eta} \text{ where } g' = \partial g / \partial \eta \quad (3.40)$$

results in this final form of the equation.

$$\left. \frac{\partial F}{\partial \eta} \right|_{tx} = -2\sigma_m g' \{ [\sqrt{3}[\sigma_m(\sqrt{3}g + 3) - Ap/Q] + g\sigma_m((Q - 1)/N)^2] \}$$

for $0 \leq \theta \leq N$ (3.41)

The corresponding equation for $\left. \frac{\partial F}{\partial \eta} \right|_{tx}$ on the log surface is

$$\left. \frac{\partial F}{\partial \eta} \right|_{tx} = \sigma_m g' \left\{ N(e - 1) \left[1 + \ln \left(1 - \frac{\sqrt{3}g\sigma_m + 3\sigma_m}{XA} \right) \right] \sqrt{3} - 1 \right\} \quad (3.42)$$

After this lengthy derivation, it is instructive to remind the reader that equation 3.41 and 3.42 are only to be used in conjunction with equations 3.31 or 3.32 in the definition of $\frac{\partial A}{\partial \eta}$ as exhibited in equation 3.36.

Having completed the outline of the derivation of $\frac{\partial A}{\partial \eta}$, it remains now to describe its conjugate: $\frac{\partial A}{\partial \xi}$. This component of the hardening is calibrated along the isotropic consolidation path from which it is easily shown that

deviatoric component of the plastic strain rate is zero, i.e. $\dot{\eta} = 0$. The consistency condition (eqn. 3.26) reduces in this instance to:

$$\frac{\partial F}{\partial \bar{\sigma}_{ij}} \dot{\bar{\sigma}}_{ij} + \frac{\partial F}{\partial \xi} \dot{\xi} = 0 \quad (3.43)$$

Another empirical relationship (Baladi and Sandler, 1980) similar to the hyperbolic function used to model shear stress vs. shear strain, is proposed to depict the bulk stress vs plastic volumetric strain:

$$\sigma_{kk} = - 1/D \ln(1 - \xi/W) \quad (3.44)$$

where D and W are model parameters

This exponential function (eq 3.44) can be conveniently manipulated to yield the expression for $\frac{\partial A}{\partial \xi}$:

$$\begin{aligned} \sigma_{kk} &= - 1/D \ln(1 - \xi/W) \\ A_p &= - 1/D \ln(1 - \xi/W) \\ A &= - 1/D_p \ln(1 - \xi/W) \\ |\partial A / \partial \xi|_{\text{isotrop}} &= 1/D_p (W - \xi) \end{aligned} \quad (3.45)$$

where the subscript isotrop indicates the isotropic consolidation stress path

Note that the parameters D and W have some physical significance in that W represents the maximum plastic volumetric strain on a plot of σ_{kk} vs. ϵ_{kk}^p while D signifies the rate at which the plastic volumetric strain approaches its limit.

On the log surface, the derivative may be similarly derived to be:

$$\frac{\partial xA}{\partial \xi} = \frac{e}{(e - 1)Q} \frac{1}{D(W - \xi)} \quad (3.46)$$

It was found that the hardening along the CTC stress path was adequately simulated by the hardening law originally proposed by Aboim and Roth (1982). Therefore for a general stress path, it is judicious to decouple the influence of $\frac{\partial A}{\partial \xi}$ on the hardening. Taesiri et al. (1983) tendered that the value of $\frac{\partial A}{\partial \xi} = 0$ along the CTC stress path so the following hardening in general stress space was proposed:

$$\frac{\partial A}{\partial \xi} = \left| \frac{\partial A}{\partial \xi} \right|_{\text{isotrop}} \left\langle 1 - \frac{\sqrt{3J}}{I-3\sigma_m} \right\rangle \quad (3.47)$$

where $\langle \rangle$ is the Heaviside step function similarly,

$$\frac{\partial xA}{\partial \xi} = \left| \frac{\partial xA}{\partial \xi} \right|_{\text{isotrop}} \left\langle 1 - \frac{\sqrt{3J}}{I-3\sigma_m} \right\rangle \quad (3.48)$$

We are now furnished with all the equations to compute the general plastic modulus, \bar{K}_p , from equation 3.29. The final requirement in the discussion of the theory is the presentation of the elasto plastic incremental constitutive equation. Combining equations 3.3 and 3.4 produces the following:

$$\dot{\sigma}_{ij} = D_{ijkl} (\dot{\epsilon}_{kl} - \dot{\epsilon}_{kl}^p) \quad (3.49)$$

and introducing equation 3.5 into equation 3.49 results in

$$\dot{\sigma}_{ij} = D_{ijkl} \dot{\epsilon}_{kl} - \left\langle \frac{n_{pq} \dot{\sigma}_{pq}}{K_p} \right\rangle D_{ijkl} n_{kl} \quad (3.50)$$

Taking the inner product of equation 3.50 with n_{ij} and solving for

$$\frac{n_{ij} \dot{\sigma}_{ij}}{K_p} \quad \text{affords}$$

$$\frac{n_{ij} \dot{\sigma}_{ij}}{K_p} = \frac{n_{ij} D_{ijkl} \dot{\epsilon}_{kl}}{K_p + n_{pq} D_{pqrs} n_{rs}} \quad (3.51)$$

Entering equation 3.51 into equation 3.50 gives the rate independent elasto plastic constitutive relation for controlled strain:

$$\dot{\sigma}_{ij} = D_{ijkl} \dot{\epsilon}_{kl} - \left\langle \frac{n_{ab} D_{abcd} \dot{\epsilon}_{cd}}{K_p + n_{pq} D_{pqrs} n_{rs}} \right\rangle D_{ijkl} n_{kl} \quad (3.52a)$$

or in matrix notation

$$\begin{Bmatrix} \dot{\sigma} \\ \dot{\sigma} \end{Bmatrix}_{6 \times 1} = \begin{bmatrix} C & L \end{bmatrix}_{6 \times 6} \begin{Bmatrix} \dot{\epsilon} \\ \dot{\epsilon} \end{Bmatrix}_{6 \times 1} \quad (3.52b)$$

In long form, the elements of the non-symmetric [CL] matrix are:

Preliminary definitions,

$$\psi = - \frac{1}{K_p + n_{ab} D_{abcd} n_{cd}}$$

$$u = G = \frac{E}{2(1 + \nu)}$$

$$\lambda = K - 2/3 G = \frac{E}{(1 + \nu)(1 - 2\nu)}$$

where E = modulus of Elasticity

ν = Poisson's Ratio.

$$\begin{aligned} CL_{11} &= \lambda + (2u + [\psi(2un_{11} + \lambda n_{kk})^2]) \\ CL_{12} &= \lambda + [(2u\psi n_{22} + \lambda\psi n_{kk})(\lambda n_{kk} + 2un_{11})] \\ CL_{13} &= \lambda + [(2u\psi n_{33} + \lambda\psi n_{kk})(\lambda n_{kk} + 2un_{11})] \\ CL_{14} &= 4u\psi n_{12} (\lambda n_{kk} + 2un_{11}) \\ CL_{15} &= 4u\psi n_{13} (\lambda n_{kk} + 2un_{11}) \\ CL_{16} &= 4u\psi n_{23} (\lambda n_{kk} + 2un_{11}) \end{aligned}$$

$$\begin{aligned}
CL_{21} &= \lambda + [(2 u \psi n_{11} + \lambda \psi n_{kk}) (n_{kk} + 2 u n_{22})] \\
CL_{22} &= \lambda + 2 u + [(2 u \psi n_{22} + n_{kk}) (\lambda n_{kk} + 2 u n_{22})] \\
CL_{23} &= \lambda + [(2 u \psi n_{33} + \lambda \psi n_{kk}) (\lambda n_{kk} + 2 u n_{22})] \\
CL_{24} &= 4 u \psi n_{12} (\lambda n_{kk} + 2 u n_{22}) \\
CL_{25} &= 4 u \psi n_{13} (\lambda n_{kk} + 2 u n_{22}) \\
CL_{26} &= 4 u \psi n_{23} (\lambda n_{kk} + 2 u n_{22})
\end{aligned}$$

$$\begin{aligned}
CL_{31} &= \lambda + [(2 u \psi n_{11} + \lambda \psi n_{kk}) (\lambda n_{kk} + 2 u n_{33})] \\
CL_{32} &= \lambda + [(2 u \psi n_{33} + \lambda \psi n_{kk}) (\lambda n_{kk} + 2 u n_{33})] \\
CL_{33} &= \lambda + 2 u + [(2 u \psi n_{33} + \lambda \psi n_{kk}) (\lambda n_{kk} + 2 u n_{33})] \\
CL_{34} &= 4 u \psi n_{12} (\lambda n_{kk} + 2 u n_{33}) \\
CL_{35} &= 4 u \psi n_{13} (\lambda n_{kk} + 2 u n_{33}) \\
CL_{36} &= 4 u \psi n_{23} (\lambda n_{kk} + 2 u n_{33})
\end{aligned}$$

$$\begin{aligned}
CL_{41} &= 2 u n_{12} (2 u \psi n_{11} + \lambda \psi n_{kk}) \\
CL_{42} &= 2 u n_{12} (2 u \psi n_{22} + \lambda \psi n_{kk}) \\
CL_{43} &= 2 u n_{12} (2 u \psi n_{33} + \lambda \psi n_{kk}) \\
CL_{44} &= 2 u + 8 \psi u^2 n_{12}^2 \\
CL_{45} &= 8 \psi u^2 n_{12} n_{13} \\
CL_{46} &= 8 \psi u^2 n_{12} n_{23}
\end{aligned}$$

$$\begin{aligned}
CL_{51} &= 2 u n_{13} (2 u \psi n_{11} + \lambda \psi n_{kk}) \\
CL_{52} &= 2 u n_{13} (2 u \psi n_{33} + \lambda \psi n_{kk}) \\
CL_{53} &= 2 u n_{13} (2 u \psi n_{33} + \lambda \psi n_{kk}) \\
CL_{54} &= 8 \psi u^2 n_{13} n_{12} \\
CL_{55} &= 2 u + 8 \psi u^2 n_{13}^2 \\
CL_{56} &= 8 \psi u^2 n_{13} n_{23}
\end{aligned}$$

$$\begin{aligned}
 CL_{61} &= 2 u n_{23} (2 u \psi n_{11} + \lambda \psi n_{kk}) \\
 CL_{62} &= 2 u n_{23} (2 u \psi n_{33} + \lambda \psi n_{kk}) \\
 CL_{63} &= 2 u n_{23} (2 u \psi n_{33} + \lambda \psi n_{kk}) \\
 CL_{64} &= 8 \psi u^2 n_{23} n_{12} \\
 CL_{65} &= 8 \psi u^2 n_{23} n_{13} \\
 CL_{66} &= 2 u + 8 \psi u^2 n_{23}^2
 \end{aligned}$$

3.3 Some Important Aspects of the Bounding Surface

Formulation

Whereas the original concept of the bounding surface in plasticity analysis is attributed to Dafalias and Popov (1976) and Krieg (1975), its application to modeling the elastoplastic response of sand was first introduced by Aboim and Roth (1982). Taesiri, McVay and Townsend (1983) further modified Aboim and Roth's original model and it is this altered model which serves as the superlative reference for the theoretical presentation in this thesis. However, further important modifications to the Taesiri model have been presented herein and some aspects have been omitted altogether; it is therefore instructive to summarize these distinctions:

1. The parameters T and U which were used in the prior version of this plasticity model have been excluded. These model parameters relate the plastic equivalent shear strain to the plastic volumetric strain by a transformed hyperbolic relationship; their significance was inconsequential in comparison to the parameters R and S which associate the

deviatoric stress to the plastic shear strain. However, when T and U were included in the formulation, the predictions of the stress-strain response were very sensitive to the assigned values of these parameters. The entire model has herein been re-formulated based on the exclusion of both the parameters T and U .

2. Accomodations have been made by Taesiri et al. (1983) for a non-associative flow rule for this plasticity model. All of the predictions in this thesis are based on associative flow so it was not necessary to include the protracted equations which are used in the description of the non-associative flow theory.

3. The mapping rule is the simple mapping rule of Dafalias and does not consider any value other than zero for the "back" isotropic stress. The simplification permits the elimination of yet another parameter (λ) from Taesiri's 14-parameter model.

4. The second major modification to the reference model embraces the hardening relationship along the hydrostatic axis. Originally, a straight line was proposed linking plastic volumetric strain to the bulk stress; however, this empirical simulation proved to be inadequate along stress paths which generated little or no shear strains such as the K_0 consolidation stress path. An exponential function, similar to the one employed by Baladi and Sandler (1980), has been selected to replace the less realistic straight line relationship.

3.4. Calibration of Model Parameters

There are two elastic constants and eight parameters used in developing the incremental plastic constitutive law which need to be estimated in order to characterize the elasto-plastic stress-strain response of a granular soil. The elastic constants are the bulk modulus, K , and the shear modulus, G , which are computed by first calculating the elastic modulus and using an assumed value of Poisson's ratio. The modulus of elasticity is derived from the unload cycle of a cyclic conventional triaxial compression test or equivalent.

The parameters R and S depict the proposed hyperbolic relationship between deviatoric stress ($J^{\frac{1}{2}}$ in terms of the stress invariants) and plastic equivalent shear strain (η). For the conventional triaxial compression test, both these components of the stress and strain tensor are simply evaluated by the following equations:

$$\eta = \frac{\epsilon_1^p - \epsilon_3^p}{\sqrt{3}} \quad (3.4.1)$$

$$\sqrt{J} = \frac{\sigma_1 - \sigma_3}{\sqrt{3}} \quad (3.4.2)$$

Aboim and Roth (1982) state that the total principal strain can be used instead of the plastic principal strains in equation 3.4.1 since the elastic component is numerically insignificant in comparison to its plastic conjugate. Since data reduction procedures utilized in this research were facilitated by a microprocessor, it was not considered

laborious to remove the elastic strains before analysis. Also, unless a radial strain measuring device such as an LVDT (linear variable differential transformer) clamp is used, the radial strain ($\epsilon_2 = \epsilon_3$) of the specimen will have to be computed indirectly from the recorded volumetric strain and the axial strain (ϵ_1), i.e.

$$\epsilon_3^P = \frac{\epsilon_{kk}^P - \epsilon_1^P}{2} \quad (3.4.3)$$

The slope of a plot of $\sigma_m \eta / J^{1/2}$ vs. η is equal to the parameter S while the intercept on the $\sigma_m \eta / J^{1/2}$ axis is equal to the value of R. These model parameters do bear some physical significance to a triaxial stress-strain curve; the inverse of S is indicative of the "strength" of the sand since it mathematically depicts the horizontal asymptote at the "failure" deviatoric stress. Alternatively, R governs the initial slope of the deviator stress vs axial strain curve.

The parameter N is also appraised from the triaxial test, and it is the ratio \sqrt{J}/I at which volumetric behavior evinces the start of dilation; this information can be easily extracted by noting the deviatoric stress corresponding to the peak of the positive volume strain (i.e. compression) vs axial strain plot. Knowing the magnitude of this deviatoric stress and the confining pressure, N can be obtained as follows:

$$N = \frac{\sqrt{J}}{I} = \frac{\sigma_d}{\sqrt{3}[\sigma_d + 3\sigma_m]} \quad (3.4.4)$$

where σ_d = deviatoric stress at which dilation begins

and σ_m = confining pressure

The model parameters, D and W, used in characterizing the hardening along the hydrostatic axis is routinely obtained from an isotropic consolidation test. The test data may be conveniently obtained from the consolidation phase of the triaxial test before the specimen is subjected to shear stresses. Parameters D and W are then estimated from the plot of plastic volumetric strain vs bulk stress. Here again the parameters do manifest some physical significance; W is representative of the maximum plastic volumetric strain for the stresses under consideration while D suggests the rate at which this limiting value of plastic volume strain is achieved.

No empirical basis has been established for determining the following parameters: the unload modulus, H_u , the reload modulus, H_r , and the constant which controls the shape of the elliptic bounding surface, Q. These parameters are therefore evaluated from trial and error methods.

The table below summarizes the procedures for obtaining the model parameters:

TABLE 3.3.1

SUMMARY OF HOW B.S. MODEL PARAMETERS ARE DERIVED

MODEL PARAMETER	DERIVED FROM
R	Hyperbolic stress-strain curve
S	Hyperbolic stress-strain curve
D	Isotropic consolidation test
W	Isotropic consolidation test
K	Bulk Modulus, triaxial or consolidation test
G	Shear Modulus, triaxial test
H _r	Trial and Error
H _u	Trial and Error
Q	Trial and Error
N	Triaxial test

CHAPTER 4
SELF-BORING PRESSUREMETER TESTS

4.1 Introduction

The Cambridge Self Boring Pressuremeter is perhaps the most advanced insitu geotechnical testing device in the world today. Although much used in European countries, this device can be found at only four locations in the United States - the University of Florida, Stanford University, California Department of Transportation, and the Federal Highway Administration in Washington D.C. As its name implies, this combination boring-pressuremeter instrument inserts a pressuremeter probe into the ground by a self-tunnelling technique which minimizes the disturbance of the insitu soil, and then performs a test at the desired *depth by expanding a rubber membrane into the soil by gas pressure*. The importance of reducing soil disturbance is crucial since the theoretically derived correlations, between the soil parameters and the cavity pressure-displacement curve, are based on the assumption that the soil surrounding the probe is undisplaced. On the other hand, where the insertion technique may differ, such as in a Mennard pressuremeter test in a pre-drilled borehole, it is necessary to determine the soil properties

from empirical formulas because of the disturbance introduced by stress relief.

The principle of self boring was first applied at the San Briec Laboratory at the Ponts et Chaussees in 1967 where difficulties had arisen while trying to interpret the results of certain Mennard pressuremeter tests (Baguelin, Jezequel & Shields, 1978). Research and development followed at Cambridge University which initially focused on utilizing this self-boring technique to measure in-place total stresses. After fabricating the machine that permitted only minimal disturbance, the notion of incorporating such a system with a pressuremeter became palpable; Dr. Wroth, then at Cambridge University, along with a succession of research students - Hughes, Windle, Clarke, and Fahey - started investigating and developing the self boring pressuremeter (henceforward abridged to "SBPM") in 1970. The apparatus is now manufactured for the commercial market by the "Cambridge Insitu" company which was licensed in 1974. Although mostly research organizations were originally interested in the device, its potential and applications were being realized, and in 1978, the machine became commercially available. Even so, only an elite group of research engineers were experienced enough to realistically analyze test results and this led to the formation of the consulting firm "P.M. Insitu Techniques Ltd" in 1978 (Wroth, 1983).

4.2 Equipment & Field Testing Procedure

4.2.1 Equipment

4.2.1.1 Introduction

The key to self boring is the ability to penetrate the ground without displacing it. In order to achieve such an effective drilling operation, some of the soil disturbance factors that would need to be eliminated are as follows: the cutting action of the drilling tools, borehole yielding, water content changes due, for example, to the fluid which is used to wash out the hole or to the drainage of ground water into the hole, and finally, the disturbance due to the introduction of the probe.

Four principal components comprise the self boring pressuremeter: a) the probe which includes the self-tunnelling mechanism, b) the control unit which is located at the ground surface, c) the tubings which connect the probe to the control unit, and d) the drill rig.

Three simultaneous actions are propagated by the drilling apparatus -

- 1) the application of static force to overcome the small resistance of a cutting edge and the relatively large skin friction due to the surface area of the probe.
- 2) rotation of the grinder
and
- 3) Injection of fluid for washing.

4.2.1.2 The Probe

The probe itself consists of a cylindrical rubber membrane (as depicted in figure 4.1 & figure 4.2) which has three electrical strain gauges attached circumferentially around its midplane. There are two pore stones at either side of the cylindrical membrane fitted with transducers for measuring the pore water pressure. A pressure transducer is also mounted in the cavity to measure its internal applied pressure. Each of these electronic instruments are calibrated to measure the desired change in length or stress. The membrane is protected while the instrument is being inserted into stiff or abrasive soil by a series of narrow flexible stainless steel strips running longitudinally down it and looking much like a Chinese lantern. This protective shell adds very little to the radial stiffness of the instrument and whatever errors it introduces can be rationally eliminated since its stiffness is a known constant. Fitting flush at the front of the measurement module is a thin walled "sampler" with a rotating blade at its mouth for grounding up the soil core that enters it as the sampler probes through the ground. It is noteworthy that the cutting edge of the "sampler" slopes towards the interior which is contrary to the structure of typical sampling tubes where alteration of the soil's stress state on the periphery of the sampler is not of major importance. A controlled flow of water is injected onto the "cuttings" at the mouth in order to provide a dynamic medium

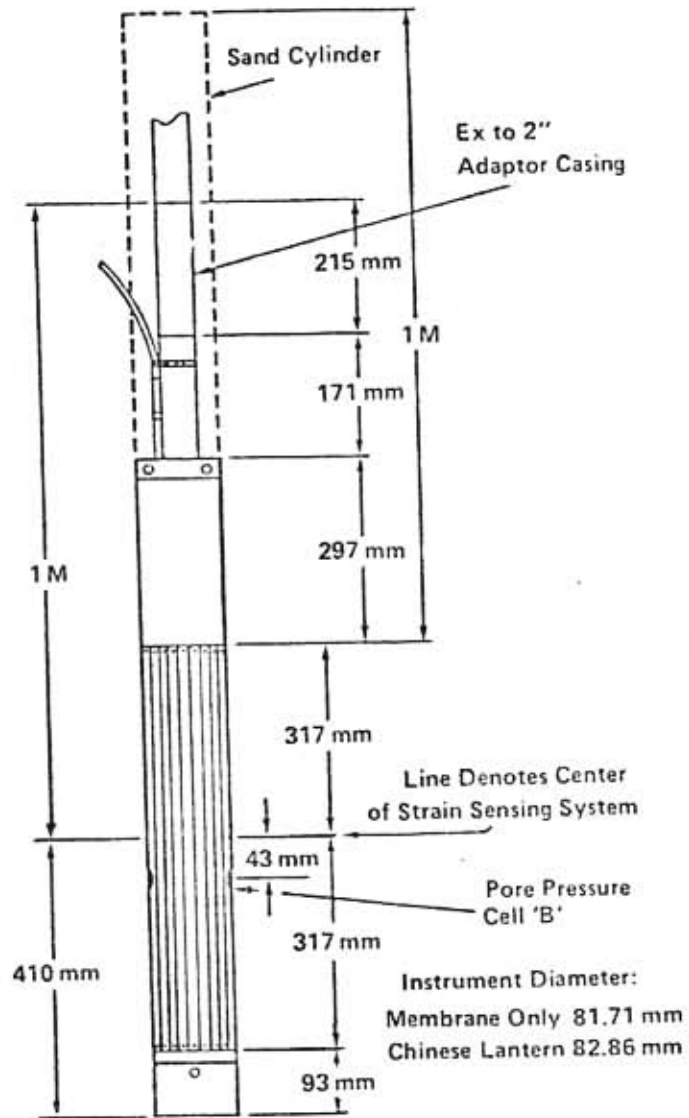


Figure 4.1 The Cambridge Self-Boring Pressuremeter Probe (After Davidson et al., 1983)



Figure 4.2 Photograph of SBPM Probe

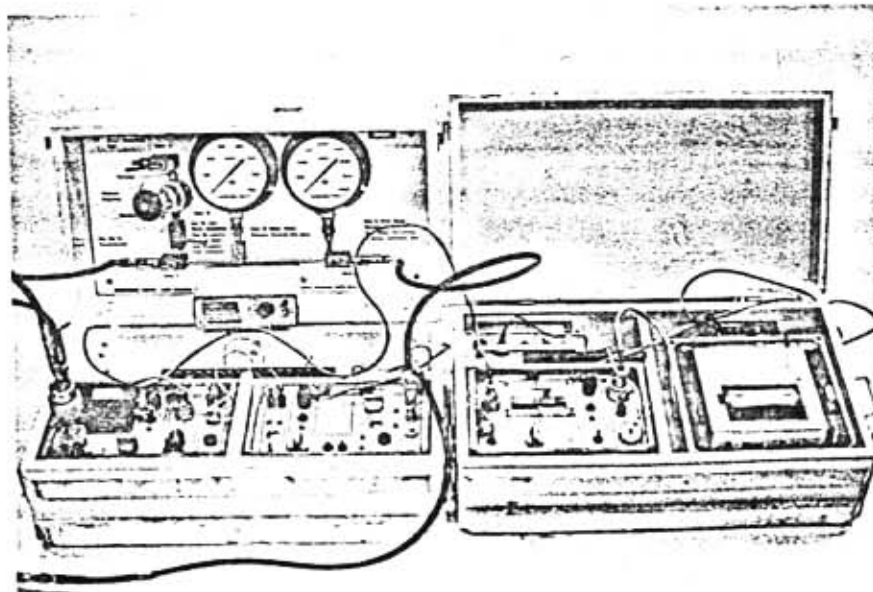


Figure 4.3 Photograph of SBPM Control Unit

for the transportation of displaced soil to the ground surface.

As mentioned previously, three actions are required to maintain the self-boring process and the mechanisms used in effecting these operations are as follows: 1) static force on the rods is supplied by a hydraulic system at the surface, 2) the torque for the rotation of the cutter is transmitted by inner rods coupled along the axis of the cylindrical shell, and 3) the wash water is flushed down the center of these rotating rods while the suspension of "cuttings" in water returns to the surface up a concentric outer tube coupled along the axis of the cylindrical shell.

4.2.1.3 SBPM rig

The self-boring pressuremeter trailer (as shown in figure 4.4) has a 10-hp gasoline engine which powers both a water pump and a hydraulic pump. Interconnected baffled water tanks on the rear of the rig are used to clarify the recycled water. Gauges are provided to monitor the pressure of the hydraulic fluid so the operator can control the thrust on the cutting shoe as materials of varying stiffness are encountered during boring.

4.2.1.4 The control unit

A single cable carries both the electrical wires and the gas pressure from the control units (depicted in figure 4.3) at ground elevation to the measuring cell. At the surface, this cable links into the control unit to measure the gas pressure; in addition, the control unit performs a

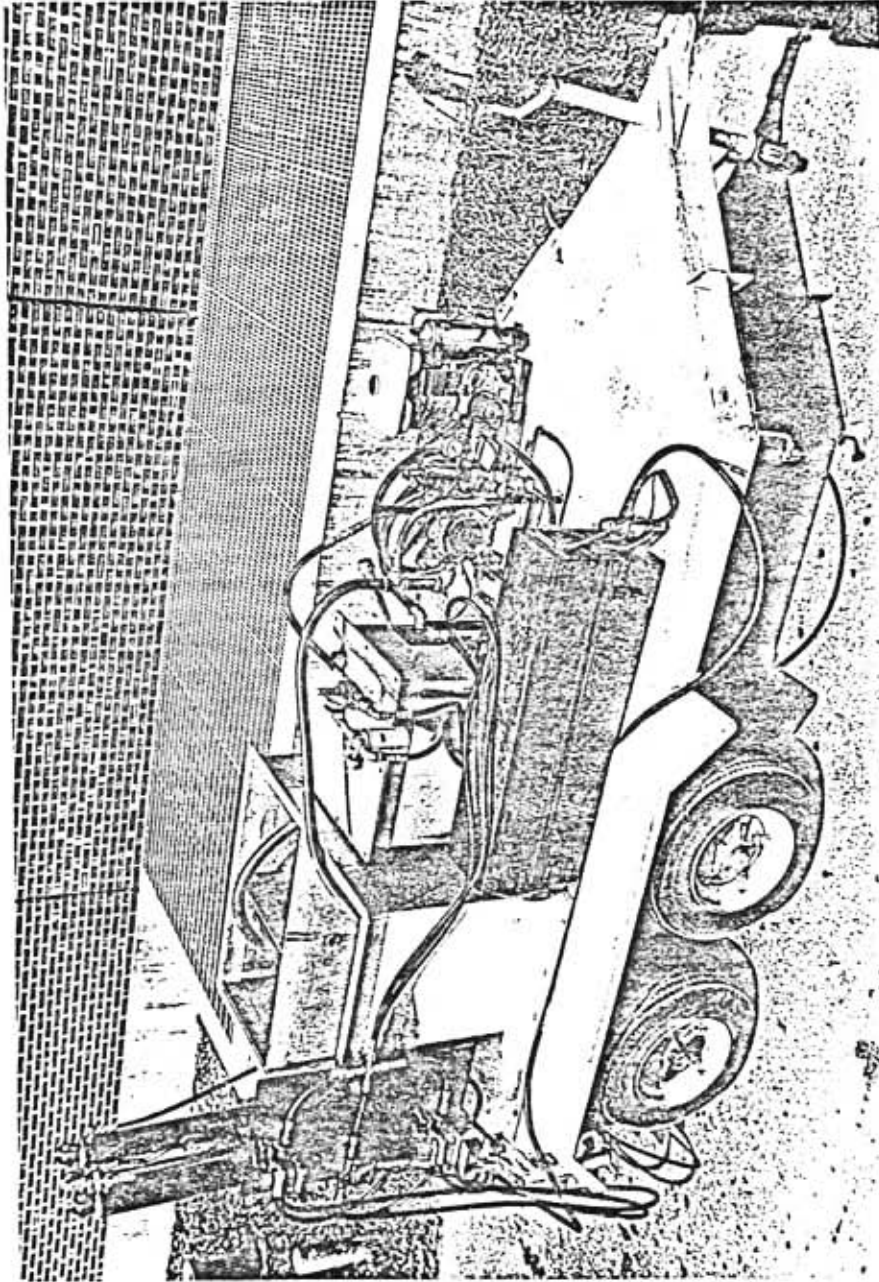


Figure 4.4 Photograph of SBPM Rig

number of other functions which include: constant rate of strain testing, automatic data retrieval on an electrostatic printer, adjustment of print intervals during data recording, self-test switches, etc.

4.2.2 Typical field testing procedure

Field testing consists of two basic operations: a) the probe is first implanted in the ground at the desired depth by the self-tunnelling technique, and b) this is then ensued by a cavity expansion test under supposedly undisturbed conditions. The adjective "undisturbed", although not literally descriptive, is justified when one considers the capabilities of other present-day insitu investigative devices; researchers at Cambridge University have reported a maximum lateral movement of the soil in the immediate vicinity of the probe to be less than 0.5% of its diameter (Hughes, 1973).

After the surficial soil has been manually grubbed from the intended point of probe penetration, two pistons mounted on a frame are used to thrust the probe into the ground. The rotating cutter, situated at the mouth of the hollow probe, operates simultaneously while pulverizing and removing the soil that lies in the probe's path. A stream of recycled water, flowing down the rods to the cutter, impinges horizontally on the "cuttings" to aid in the transportation of the soil to the surface sedimentation tanks. Fluid flow is optimized to maintain effective removal of solids while avoiding the other extremity where

the wash boring flow disturbs the insitu soil. The location of the cutter with respect to the probe's entrance port must also be adjusted such that the cutting operation is efficient but yet does not cause undue soil disturbance outside the probe.

At the desired depth, the rubber membrane, with its accessory measuring devices, is inflated by introducing gas (nitrogen) pressure. Whereas the insertion of the probe was the responsibility of the hydraulic system on the drill rig, the monitoring and control of a constant rate of strain test (and to a lesser extent the regulated pressure test) is entrusted to some of the more sophisticated electronic equipment (i.e. the control unit) currently used in insitu soil studies. Eight variables are registered and output in digitized form: gas pressure in the membrane, 3 radial deformations of the membrane at mid-height, the total radial deformation, pore water pressure readings at the two transducers, and the sum of both pore water pressure readings. Figure 4.5 illustrates the data processing system used in the presentation of pressuremeter test results. (Note that in this figure as well as the rest of this chapter, strain is defined as the radial displacement divided by the initial displacement i.e. circumferential strain at the cavity wall).

Both the uniform strain rate and the manually stress regulated tests are similarly performed, the main differences being the method of data collection and as the

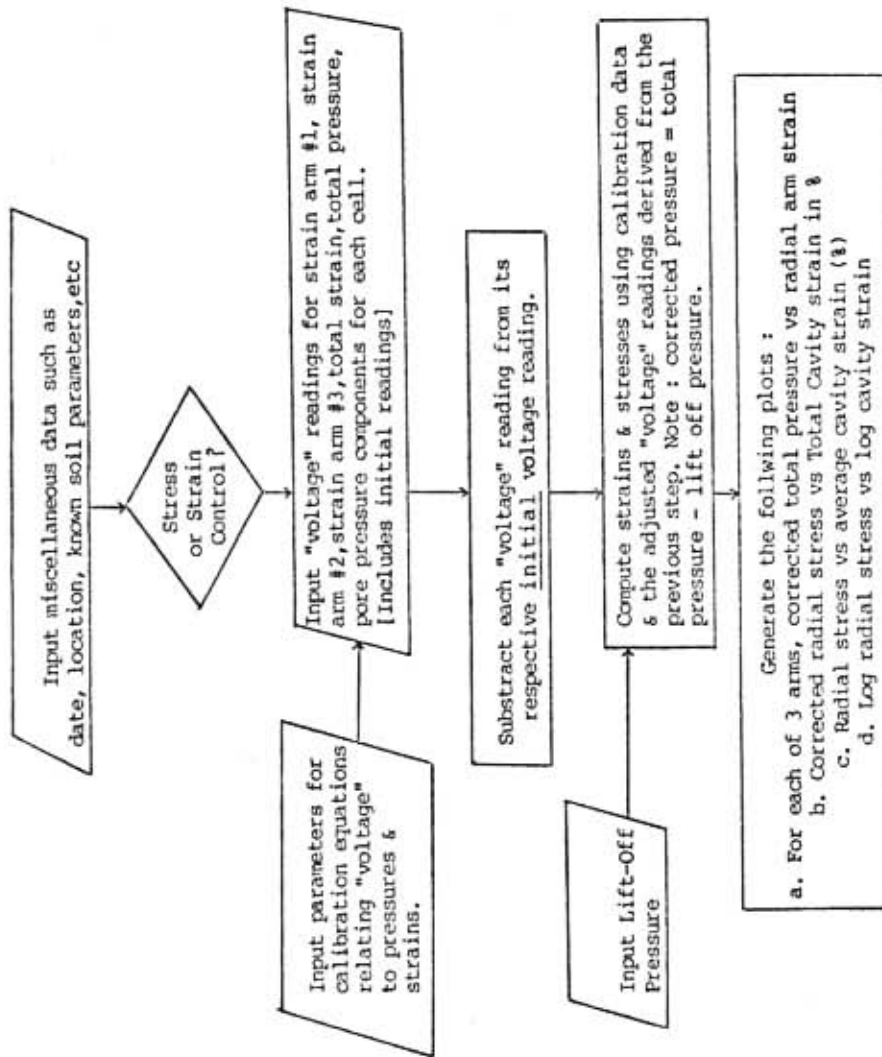


Figure 4.5 Self-Boring Pressuremeter Test Data Processing Flowchart

terminology suggests, the internal pressure is manually varied for stress-controlled testing while the control unit is used for spontaneous controlled strain testing. Presently, equipment at the University of Florida does not permit the automatic retrieval of test data during the stress regulated test, but the strain control unit has a modern data capture unit which outputs the data at prescribed time intervals to an electrostatic printer.

In order to plot the modulus loop used in the determination of the shear modulus, G , the expansion phase of the test is reversed at a predetermined stress or strain level, and cavity pressure vs radial displacement readings are continually observed during this restrained contraction and re-expansion of the cavity. The magnitude of the shear modulus (i.e. unload-reload) loop is important because different failure modes may be induced by the dominance of the circumferential stress over the radial stress (Wood & Wroth, 1977); to circumvent this problem, it is suggested that the unloading loop do not exceed twice the undrained shear strength (c) of the insitu clay. A similar elastic analysis may be performed for sands to ensure that the circumferential stress never becomes the major principal stress. The membrane is then reloaded to a maximum expansion of 10% strain, and at this stage, the pressuremeter probe may be deflated and, if necessary, lowered to the next test depth. Wroth (1982), however, points out the significance of the unloading phase after

maximum cavity expansion has been achieved: a flat plateau will be noted on the descending portion of the total stress vs strain plot for a saturated sand which gives a direct reading of the pore water pressure. This phenomena can be attributed to the drainage of pore water into the region of collapsed soil surrounding the deflated membrane. As would be expected, a similar trend is not observed in clayey soil owing to the low permeability characteristics which do not permit rapid drainage of pore water into the collapsed zone.

4.2.3 Advantages and disadvantages of the SBPM

The commercial manufacturer of the present-day self boring pressuremeter device lists the following advantages and handicaps of SBPM field testing;

ADVANTAGES

The tests are performed on virtually undisturbed soil, although some slight disturbance is inevitable, it will be very greatly less than the disturbance associated with so-called "undisturbed" sampling or with pressuremeter tests in pre-drilled boreholes.

A number of soil parameters may be obtained from a single test:

Clays - undrained shear strength, shear modulus or undrained Young's modulus, and insitu horizontal total stress.

Sands - angle of internal friction & angle of dilation.

Parameters can be derived from the test results using well developed theories of cavity expansion without resorting to empirical correlation factors. The data is less scattered than other types of testing; variables associated with other types of testing include disturbance due to sampling or trimming, time between borehole preparation and testing, and the effects of piping in a borehole in sand below the water table.

Quick turnaround time for data processing.

DISADVANTAGES

Will not penetrate gravel, boulder clay, claystones, etc.

The orientation of the failure plane and mode of deformation will usually be inappropriate to the field situation.

No control of total or effective stress path - only two stress paths, drained or undrained. [Unlike a triaxial test where the magnitudes of the principal stresses are known, the complete stress and strain history during a pressuremeter test is unknown and depends on the choice of constitutive law].

To reduce the effects of drainage, undrained tests have to be performed at undesirably high rates of strain.

Instrument is complex by modern standards.

4.3 Laboratory Study of the Pressuremeter Test in Sand

A series of self boring pressuremeter tests were performed in the University of Florida geotechnical testing chamber as the first phase of a study (Davidson et al., 1983) to investigate the behavior of both loose and dense sand during SPBM testing. In this research report, the Hughes et al. (1977) method of interpretation of SPBM test results was evaluated and compared to soil parameters obtained from both conventional triaxial compression (CTC) tests and dilatometer tests. It is this report (Davidson et al., 1983) which provides the major portion of the triaxial test data used in calibrating the Bounding Surface plasticity model (by procedures previously outlined in chapter 3), and the "controlled-environment" SPBM test results which were used for comparison to predictions

obtained by the finite element method (as will be discussed in the following chapter).

4.3.1 Soil description

The Reid Bedford sand used in this test program was selected because its behavior has been well documented through research efforts at the University of Florida and at the Corp of Engineers Waterways Experiment Station at Vicksburg, Mississippi. The soil description that follows is only a summary of the more detailed presentations of the material properties that can be found in Lheur (1976) or Davidson et al. (1983).

Color & type: light brown, clean, fine sand.

Grain shape: varying from subrounded to subangular.

Mineralogy: 89% quartz, 9% feldspar, 2% ferromagnesian and "heavies".

Maximum dry unit weight: 107.1 pcf

Minimum dry unit weight: 88.7 pcf

D_{60} : 0.217 mm (see figure 4.6)

D_{10} : 0.160 mm

Coefficient of uniformity, C_u : 1.36

Specific gravity, G_s : 2.66

Unified Soil Classification: SP

Maximum void ratio, e_{max} : 0.871

Minimum void ratio, e_{min} : .550

4.3.2 The test chamber

This triaxial test chamber (as described by Laier, Schmertmann & Schaub, 1975) was specially designed to

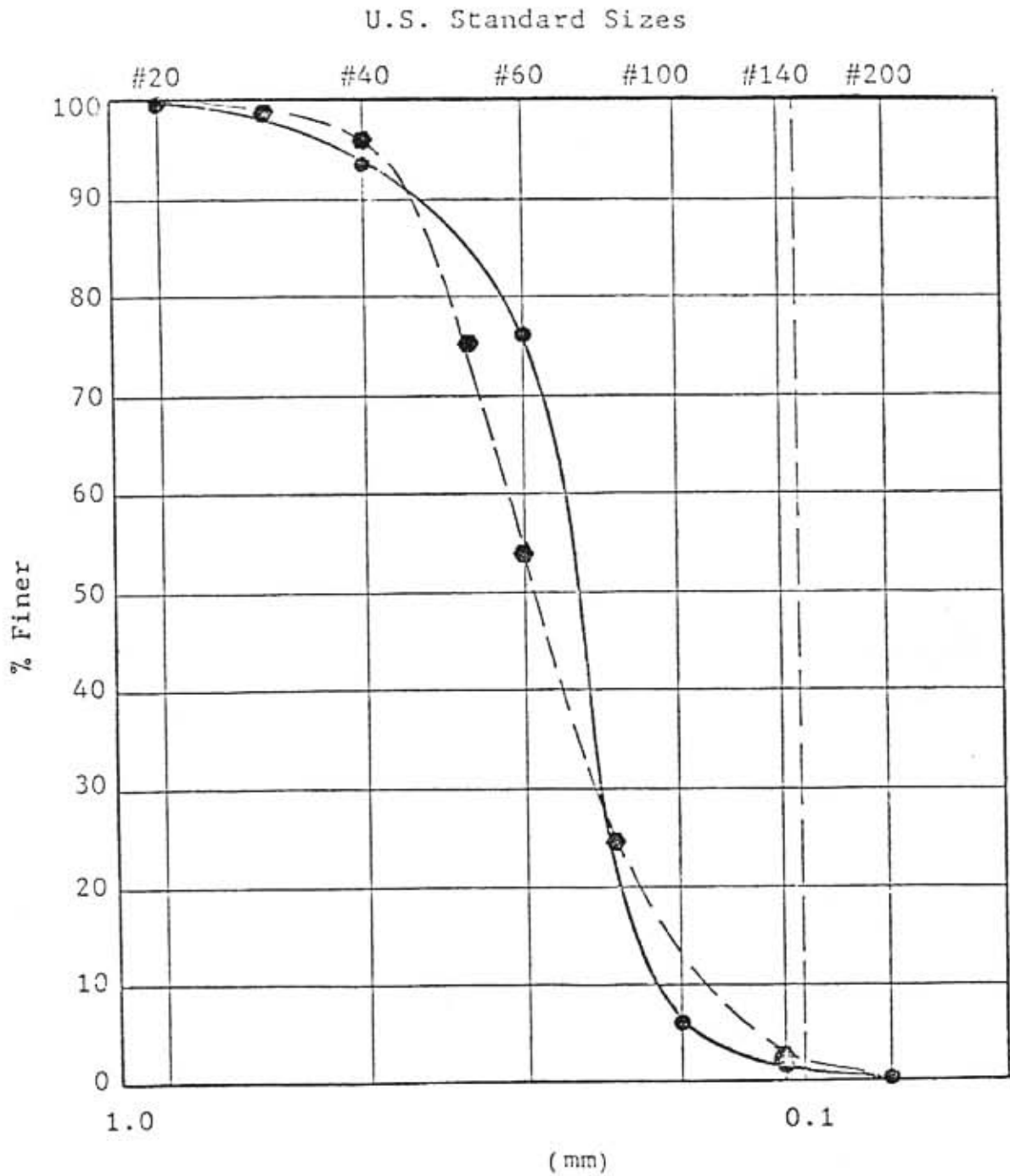


Figure 4.6 Grain Size Distribution Curve for Reid Bedford Sand. Solid Line 1983, Dashed Line 1976 (from Lheur) (After Davidson et al., 1983)

calibrate and to study under controlled conditions the performance of insitu testing equipment. The main feature of the chamber is that the vertical and horizontal boundary stresses can be independently applied to the sides and base of the sample; it is also possible to restrain displacement at either of these boundaries (i.e., no horizontal or vertical strain). Figure 4.7 illustrates the stresses acting on the boundary of the chamber in which the pressuremeter probe has been cast in place into a sand specimen (in this figure, $a = 1.606''$ & $b = 23.907''$), and figure 4.8 is included as an example of a pressuremeter test result in this chamber. Considering the possible combinations of prescribed horizontal and vertical stresses or strains, it can be shown that there exists four potential boundary conditions (BC):

- a. BC #1 - no change in vertical or horizontal stresses
- b. BC #2 - no change in horizontal stress or vertical strain
- c. BC #3 - no change in vertical stress or horizontal strain
- d. BC #4 - no change in vertical or horizontal strain

All of the pressuremeter tests were performed under BC #1 or BC #3, and as will be noted in the following chapter, this proved somewhat inconvenient in the finite element idealization since the constant stress boundary condition could not be modelled with the present computer code. At this stage, it should also be mentioned that no attempt was

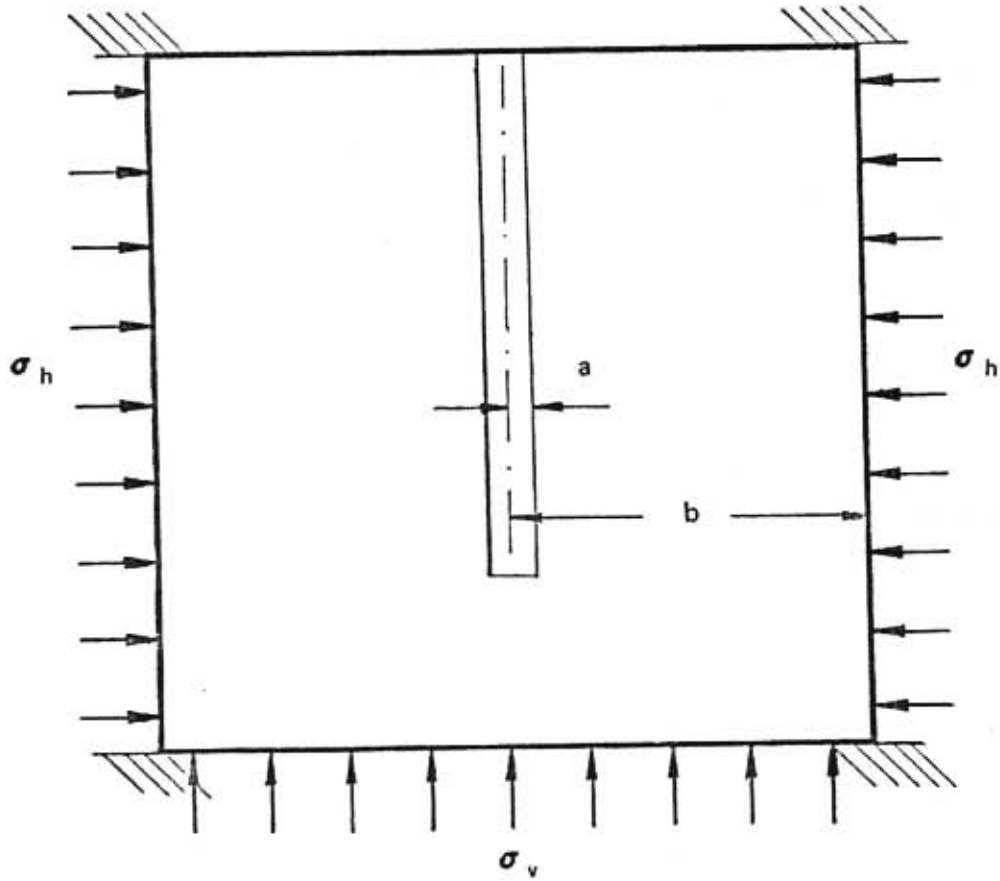


Figure 4.7 Calibration Chamber Situation During Pressuremeter Test (After Davidson et al., 1983)

made to numerically simulate the pressuremeter test in loose sand since the bounding surface elasto-plastic constitutive law was originally intended for stiff clays or dense sands, and has not yet been validated or modified for predicting the stress-strain response of loose material.

Further details of the testing procedure and the sample preparation by the sand rain method can be found in the Davidson et al. (1983) reference or in other reports relating to a similar series of tests performed at the University of Cambridge (ex. Jewell, Fahey & Wroth, 1980).

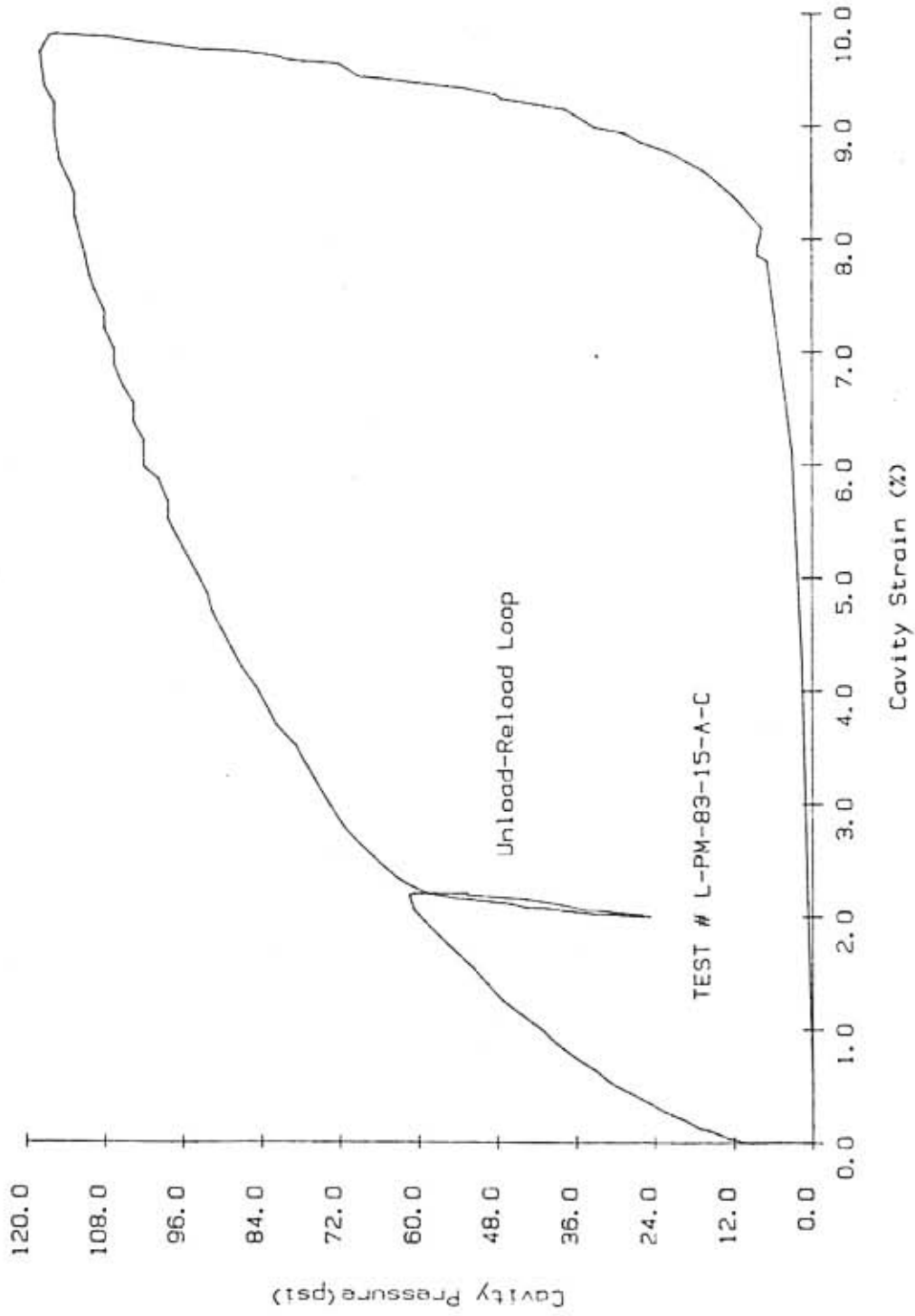


Figure 4.8 Sample Results of SBPM Tests in Chamber

CHAPTER 5
PRESSUREMETER ANALYSIS BY THE FINITE ELEMENT METHOD

5.1 Introduction

The typical stress-strain response obtained during a pressuremeter test can be mechanically modeled by a thick-walled cylinder subjected to an internal pressure. The currently available theoretical solutions to this loading condition consider materials whose behavior may be characterized as either elastic or elastic-plastic (Tresca or Von Mises yield criteria). The elastic solution can be found in many texts including Timoshenko and Goodier (1970), Hill (1950), and Little (1973). Hodge and White (1950) derived the solution for cavity expansion in an elastic-perfectly plastic medium based on a Mises yield criteria; however, their approach requires the numerical solution of a complicated system of non-linear partial differential equations. Koiter (1953) presented the elastic-plastic closed-form derivation for a Tresca material which was later extended to include work hardening Tresca materials (Mendelson, 1978). These hypothetical solutions to the stress and strain distributions within the media are governed by simplifying assumptions regarding the imposed boundary conditions on the "thick-walled cylinder" and the intrinsic nature of the material. The importance of

boundary specification is well illustrated by Aboim (1981) who, in his finite element analysis of pressuremeter expansion, concludes that different outer boundary constraints cause differences in material behavior that are more important than the ones produced by conditions of plane stress or plane strain during loading.

Owing to the fact that the bounding surface (henceforth abbreviated to B.S.) plasticity constitutive relationship is strain history dependent, it is doubtful that there is a realizable academic solution to the cylindrical cavity expansion in a medium characterized by a B.S. rheological formulation. It was therefore necessary to rely upon numerical techniques to investigate this boundary-value problem. The finite element process was chosen as the "standard discrete system" research tool to approximate this continuum problem; the foremost reason influencing this selection was the availability of a computer program which conceptually did not require too much modification effort to accommodate the B.S. elasto-plastic constitutive law.

5.2 Theory

The general concepts of the finite element method approximation technique can be outlined by these steps (Zienkiewicz, 1982):

- a). The continuum is separated by imaginary lines or surfaces into a number of finite elements.
- b). The elements are assumed to be interconnected at a discrete number of nodal points situated on their

boundaries. The displacements of these nodal points will be the basic unknown parameters of the problem.

- c). A set of functions is chosen to define uniquely the state of displacement within each finite element in terms of its nodal displacements.
- d) The displacement functions now define uniquely the state of strain within an element in terms of the nodal displacements. These strains, together with any initial strains and the constitutive properties of the material will define the state of stress throughout the element and, hence, also on its boundaries.
- e). A system of forces concentrated at the nodes and equilibrating the boundary stresses and any distributed loads is determined resulting in a stiffness matrix relating nodal forces to nodal displacements.
- f). Assembly and analysis of the system of elements is accomplished by invoking the conditions of displacement compatibility and equilibrium for the whole "structure". After insertion of the prescribed boundary conditions, numerical methods are employed to solve the equation system.

The application of the finite element method to the structural analysis of axisymmetric solids was first

presented by Wilson (1965). This procedure was incorporated into a computer program for elastic analysis which was later altered by Duncan (Duncan and Chang, 1970) to perform non-linear incremental analysis for soils. It is this computer program by Duncan which has been further modified in this thesis to execute the B.S. elasto-plastic incremental analysis. It is therefore most appropriate in this context to discuss the finite element idealization as it pertains to bodies of revolution subject to axisymmetric loads such as the pressuremeter expansion.

5.2.1 Element characteristics

5.2.1.1 Displacement function

Consider the cross-section of a typical triangular ring element as shown in figure 5.1 and 5.2, with nodes i,j,k numbered counter clockwise.

The displacements of a nodal circle, such as i, have two components

$$\underline{u}^i = [u^i] = \begin{bmatrix} u_r^i \\ u_z^i \end{bmatrix}^T \quad (5.1)$$

and the six components of element displacements are listed on a vector

$$\underline{u}^e = \begin{bmatrix} u^i \\ u^j \\ u^k \end{bmatrix} = \begin{bmatrix} u_r^i & u_z^i \\ u_r^j & u_z^j \\ u_r^k & u_z^k \end{bmatrix} \quad (5.2)$$

The displacements in terms of these six components (eq. 5.2) in the r - z plane within an element are defined by two linear polynomials

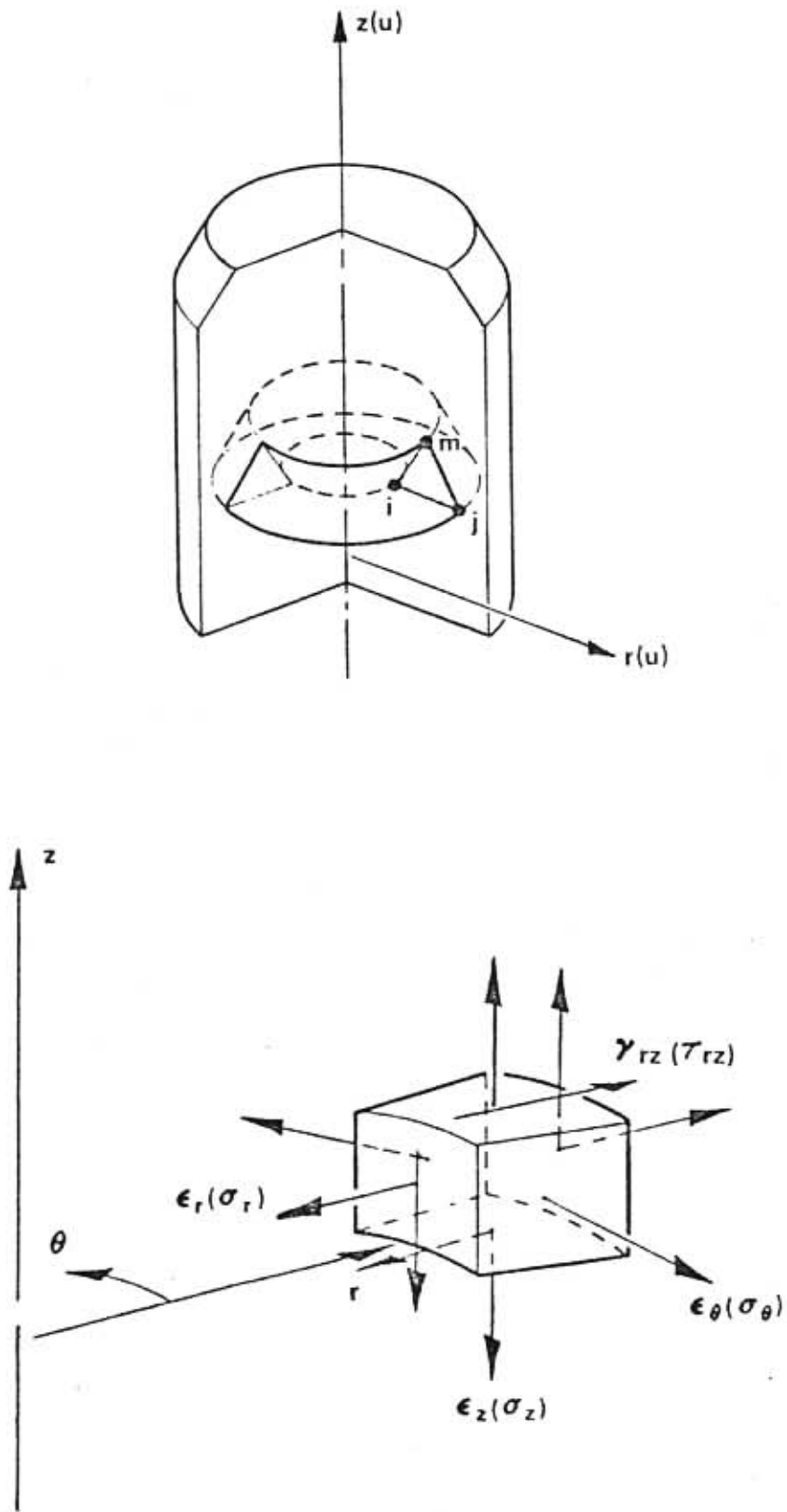


Figure 5.1 Strains and Stresses Involved in the Analysis of Axi-Symmetric Solids

$$u_r(r,z) = b_1 + b_2r + b_3z \quad (5.3a)$$

$$u_z(r,z) = b_4 + b_5r + b_6z \quad (5.3b)$$

This linear displacement field assures continuity between elements because the displacements vary linearly along any side of the triangle, and with identical displacement imposed at the nodes, the same displacement will clearly exist along an interface. The six constants b_i can be evaluated easily by solving two sets of three simultaneous equations which will arise if the nodal co-ordinates are inserted and the displacements equated to the appropriate nodal displacements; for instance

$$u_r^i = b_1 + b_2r_i + b_3z_i \quad (5.4a)$$

or in general, the following matrix equation is obtained

$$\begin{bmatrix} u_r^i & u_z^i \\ u_r^j & u_z^j \\ u_r^k & u_z^k \end{bmatrix} = \begin{bmatrix} 1 & r_i & z_i \\ 1 & r_j & z_j \\ 1 & r_k & z_k \end{bmatrix} \begin{bmatrix} b_1 & b_4 \\ b_2 & b_5 \\ b_3 & b_6 \end{bmatrix} \quad (5.4b)$$

From eqn. 5.4b, it is now easy to solve for the constants b_i in terms of the displacement at the vertices.

$$\begin{bmatrix} b_1 & b_4 \\ b_2 & b_5 \\ b_3 & b_6 \end{bmatrix} = [D] \begin{bmatrix} u_r^i & u_z^i \\ u_r^j & u_z^j \\ u_r^k & u_z^k \end{bmatrix} \quad (5.5a)$$

where

$$[D] = \frac{1}{\lambda} \begin{bmatrix} r_j z_k - r_k z_j & r_k z_i - r_i z_k & r_i z_j - r_j z_i \\ z_j - z_k & z_k - z_i & z_i - z_j \\ r_k - r_j & r_i - r_k & r_j - r_i \end{bmatrix}$$

in which $\lambda = \text{area of triangle } i, j, k = r_j(z_k - z_i) + r_i(z_j - z_k) + r_k(z_i - z_j)$

eqn. 5.5a may be restated symbolically as

$$[b] = [h][u] \quad (5.5b)$$

By reckoning the values of the constants b_i , we have approximated an expression for the displacements $[u^e]$ within a typical element e in terms of the nodal circle displacements $[u]$

$$[u^e] = [N_i, N_j, N_k] \begin{bmatrix} u^i \\ u^j \\ u^k \end{bmatrix} \quad (5.6)$$

where $N_i = N_i[I]$ in which $[I] = 2 \times 2$ identity matrix

The functions N_i, N_j, N_k were chosen so as to give the appropriate nodal displacements when the co-ordinates of the appropriate nodes are inserted in equation 5.4a. In general,

$$N_i[r_i, z_i] = [I]$$

$$\text{when } N_i(r_j, z_j) = N_i(r_k, z_k) = 0 \quad (5.7)$$

These components of N are prescribed functions of position and it was shown that the linear function of r and z in eqn. 5.4a satisfies the criteria stated in equation 5.7. The functions N are called shape functions and they perform an important role in the general formulation of finite element analysis.

5.2.1.2 Strains

The strains and associated stresses involved in the analysis of axi-symmetric solids depicted in figure 5.1b are obtained by differentiating equations 5.3(a) and 5.3(b),

$$\text{Radial strain, } \epsilon_r = \frac{\partial u_r}{\partial r} = b_2$$

$$\text{Axial strain, } \epsilon_z = \frac{\partial u_z}{\partial z} = b_6$$

$$\text{Circumferential strain, } \epsilon_\theta = \frac{u_r}{r} = \left(\frac{1}{r}\right)b_1 + b_2 + \left(\frac{z}{r}\right)b_3$$

$$\text{Shear strain, } \gamma_{rz} = \frac{\partial u_r}{\partial z} + \frac{\partial u_z}{\partial r} = b_3 + b_5$$

which may be written in matrix form as

$$\epsilon = \begin{bmatrix} \epsilon_r \\ \epsilon_z \\ \epsilon_\theta \\ \gamma_{rz} \end{bmatrix} = \begin{bmatrix} 0 & 1 & 0 & 0 & 0 & 0 \\ 0 & 0 & 0 & 0 & 0 & 1 \\ 1/r & 1 & z/r & 0 & 0 & 0 \\ 0 & 0 & 1 & 0 & 1 & 0 \end{bmatrix} \begin{bmatrix} b_1 \\ b_2 \\ b_3 \\ b_4 \\ b_5 \\ b_6 \end{bmatrix} \quad (5.8a)$$

or symbolically

$$[\epsilon] = [g][b] \quad (5.8b)$$

but $[b] = [h][u]$ from eqn. 8.5(b)

$$\text{therefore } [\epsilon] = [g][h][u] \quad (5.9)$$

which is an expression showing that once the displacements of all nodal points of an element e are known, it is possible to compute the strain vector $\underline{\epsilon}^e$ at any point in the element. The strain-displacement transformation (a^e), for an element can be extracted from equation 5.9 as

$$[a^e] = [g][h] \quad (5.10)$$

$$\text{Therefore } [\epsilon] = [a^e][u]$$

5.2.1.3 Element stiffness matrix

Listing the forces acting on the element shown in figure 5.2 as a matrix, we have

$$\underline{q}_i^e = \begin{bmatrix} q_i^e \\ q_j^e \\ q_k^e \end{bmatrix} ; \quad \underline{q}_{i1}^e = \begin{bmatrix} q_r \\ q_z \end{bmatrix}, \text{ etc.} \quad (5.11)$$

which corresponds to the nodal displacements \underline{u}^e of equation 5.2. Note that \underline{q}_i^e and \underline{u}_i^e always possess the same number of components or degrees of freedom. The characteristic relationship linking \underline{q}^e to \underline{u}^e is of the form

$$\underline{q}^e = \underline{k}^e \underline{u}^e + \underline{f}_p^e + \underline{f}^e \epsilon_0 \quad (5.12)$$

where \underline{k}^e = element stiffness matrix for element e

\underline{f}_p^e = nodal forces req'd to balance any distributed loads on the element

$f_{\epsilon_0}^e$ = nodal forces req'd to balance any initial strains as may be caused by temperature change.

The stiffness matrix of the element, $[k^e]$, will always be square and of the form

$$\tilde{k}^e = [k^e] = \begin{bmatrix} k_{ii}^e & k_{ij}^e \dots k_{ik}^e \\ k_{ki}^e \dots \dots \dots k_{kk}^e \end{bmatrix} \quad (5.13)$$

in which k_{ii}^e , etc are submatrices which are also square and of the size $l \times l$, where l is the number of force components to be considered at the nodes.

The displacement approach is now employed to originate the definition of the element stiffness matrix. We must first let \tilde{q}^e (as expressed in equation 5.11) define the nodal forces which are equivalent statically to the boundary stresses and distributed loads on the element. The distributed loads, (or body forces), \tilde{b}^e , are defined as those acting on a unit volume of material within the element with directions corresponding to those of the displacements \tilde{u}^e at that point.

A simple procedure is adopted to make the nodal forces statically equivalent to the actual boundary stresses and distributed loads: impose an arbitrary (virtual) nodal displacement and equate the external and internal work done

by the various forces and stresses during that displacement. Let such a displacement be \underline{u}^e at the nodes; therefore, by equations 5.6 and 5.10, the displacements and strains within the element are equal to

$$\underline{\delta u}^e = \underline{N} \begin{bmatrix} \delta u_i \\ \delta u_j \\ \delta u_k \end{bmatrix} \quad \text{and} \quad \underline{\delta \epsilon} = [\underline{a}^e] \begin{bmatrix} \delta u_i \\ \delta u_j \\ \delta u_k \end{bmatrix} \quad (5.14a)$$

and by renaming

$$\begin{bmatrix} \delta u_i \\ \delta u_j \\ \delta u_k \end{bmatrix} \quad \text{to} \quad \underline{\delta d}^e, \quad \text{equation 5.14a may be}$$

expressed more compactly as

$$\underline{\delta u}^e = \underline{N} \underline{\delta d}^e \quad \text{and} \quad \underline{\delta \epsilon} = \underline{a}^e \underline{\delta d}^e \quad (5.14b)$$

The work done by the nodal forces is equal to the sum of the products of the individual force components and corresponding displacements, i.e.

$$\underline{\delta d}^{eT} \underline{q}^e \quad (5.15)$$

while the internal work per unit volume done by the stresses and distributed forces is

$$\underline{\delta \epsilon}^T \underline{\sigma} - \underline{\delta u}^{eT} \underline{b}^e \quad (5.16)$$

and substituting equation 5.14b in equation 5.16 leads to

$$\underline{\delta d}^T (\underline{a}^{eT} \underline{\sigma} - \underline{N}^T \underline{b}^e) \quad (5.17)$$

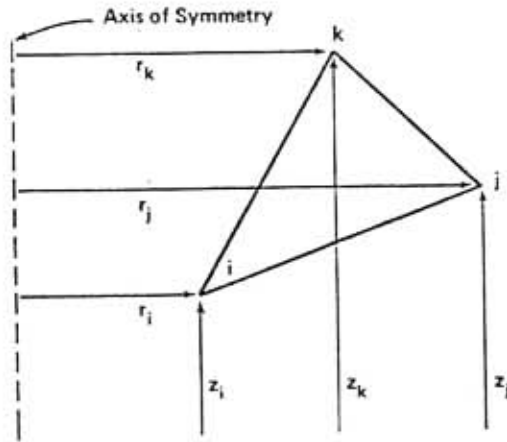


Figure 5.2 Triangular Element

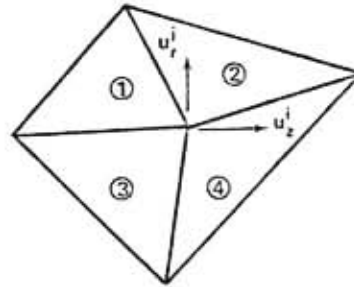


Figure 5.3 Assembly Process

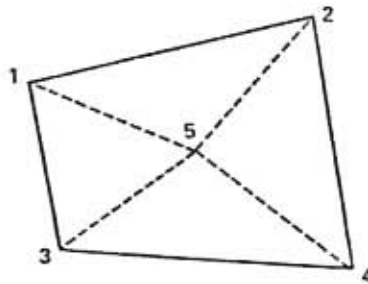


Figure 5.4 Quadrilateral Element

Equating the external work with the total internal work obtained by integrating over the volume of the element, v^e , results in

$$\delta \underline{d}^e T \underline{q}^e = \delta \underline{d}^e T \left(\int_{v^e} \underline{a}^e T \underline{\sigma} d(\text{vol}) \right) - \int_{v^e} \underline{N}^T \underline{b}^e d(\text{vol})$$

thus

$$\underline{q}^e = \int_{v^e} \underline{a}^e T \underline{\sigma} d(\text{vol}) - \int_{v^e} \underline{N}^T \underline{b}^e d(\text{vol}) \quad (5.18)$$

The assumed relationship between stress and strain is of the following form

$$\underline{\sigma} = [CL] (\underline{\epsilon} - \underline{\epsilon}_0) + \underline{\sigma}_0 \quad (5.19)$$

where $CL = [CL]$ = constitutive relationship as derived the chapter on the B.S. plasticity model

$\underline{\epsilon}_0$ = initial strains as may be due to shrinkage, etc

$\underline{\sigma}_0$ = initial residual stresses

Substituting for $\underline{\sigma}$ (equation 5.19) in equation 5.18 leads to

$$\underline{q}^e = \int_{v^e} \underline{a}^e T [CL] \underline{\epsilon} d(\text{vol}) - \int_{v^e} \underline{a}^e T [CL] \underline{\epsilon}_0 d(\text{vol}) + \int_{v^e} \underline{a}^e T \underline{\sigma}_0 d(\text{vol}) - \int_{v^e} \underline{N}^T \underline{b}^e d(\text{vol}) \quad (5.20)$$

Comparing equation 5.20 with equation 5.12 leads to the following separation of components.

$$\underline{k}^e \underline{u}^e = \int_{v^e} \underline{a}^e T [CL] \underline{\epsilon} d(\text{vol}) \quad (5.21)$$

and

$$\underline{f}_p^e + \underline{f}_o^{\epsilon} = - \int_{vol} \underline{N}^T b d(vol) - \int_{vol} \underline{a}^T CL \underline{\epsilon}_o d(vol) + \int_{vol} \underline{a}^T \underline{e} g d(vol) \quad (5.22)$$

Substituting $[\epsilon] = [a^e][u]$ from equation 5.10 into equation 5.21 yields the definition of the element stiffness matrix as,

$$\underline{k}^e \underline{u}^e = \int_{vol} \underline{a}^T CL \underline{a}^e \underline{u}^e d(vol)$$

Therefore

$$\underline{k}^e = \int_{vol} \underline{a}^T CL \underline{a}^e d(vol) \quad (5.23)$$

Substituting $[a^e] = [g][h]$ from eqn 5.10 into 5.23, give the element stiffness matrix for a triangular ring element with the B.S. elasto plastic constitutive characterization,

$$\underline{k}^e = [h]^T \int_{vol} [g]^T [CL] [g] dV [h] \quad (5.24)$$

The terms under the integral in equation 5.24 may be explicitly expressed as shown in figure 5.5.

5.2.2 Generalization to the Whole Region

Having established the conditions of overall equilibrium within a single typical element, it is now necessary to assemble and analyze the hypothetical structure in which all the elements participate. In order to obtain this solution, two conditions must be satisfied: a) displacement compatibility, and b) juncture equilibrium; these operations will produce a set of force vs.

$$[g]^T [CL] [g] = \begin{bmatrix} \frac{1}{r} CL_{33} & \left(\frac{1}{r}\right) (CL_{13} + CL_{33}) & \frac{1}{r} (z CL_{33} + CL_{34}) & 0 & \left(\frac{1}{r}\right) CL_{34} & \left(\frac{1}{r}\right) CL_{23} \\ \frac{1}{r} (CL_{13} + CL_{33}) & CL_{11} + 2CL_{13} + CL_{33} & \frac{z}{r} (CL_{13} + CL_{33}) + CL_{14} + CL_{34} & 0 & CL_{14} + CL_{34} & CL_{12} + CL_{23} \\ \frac{1}{r} (z CL_{33} + CL_{43}) & \frac{z}{r} (CL_{31} + CL_{33}) + CL_{41} + CL_{43} & \frac{z}{r} (z CL_{33} + CL_{43} + C_{34}) + CL_{44} & 0 & CL_{44} + \left(\frac{z}{r}\right) CL_{34} & \left(\frac{z}{r}\right) CL_{23} + CL_{42} \\ 0 & 0 & 0 & 0 & 0 & 0 \\ CL_{43}/r & CL_{41} + CL_{43} & CL_{44} + \left(\frac{z}{r}\right) CL_{43} & 0 & CL_{44} & CL_{42} \\ (1/r) CL_{23} & CL_{12} + CL_{23} & (z/r) CL_{23} + CL_{24} & 0 & CL_{24} & CL_{22} \end{bmatrix}$$

Figure 5.5 Elements of the Matrix $[g]^T [CL] [g]$

displacement equations for the nodes which will inter-relate the elements.

$$[Q] = [K][u] \quad (5.25)$$

where $[Q]$ = load matrix which encompasses external forces applied at the nodes in addition to the distributed loads applied to the individual elements.

$[K]$ = global stiffness matrix

$[u]$ = global displacement matrix for all nodes in the system

To illustrate this procedure, consider the equilibrium conditions of a typical node "i" in the assembled analytical model shown in figure 5.3.

Each component of Q_i has to be equated to the sum of the component forces contributed by the elements meeting at the node; thus

$$Q_i = \sum_{e=1}^m q_i^e = q_i^1 + q_i^2 + \dots \quad (5.26)$$

in which q_i^1 is the force contributed to node i by element 1, q_i^2 by element 2, etc., and m is the total number of elements in the structure. Evidently, only the four elements which include point i will contribute non-zero forces, but all the elements are included in the summation since it is relevant to the assembly process. Substituting

the relationship of equation 5.12 into equation 5.26 yields the following

$$\underline{Q}_i = \left(\sum_{e=1}^m k_{i1}^e \right) \underline{u}_1 + \left(\sum_{e=1}^m k_{i2}^e \right) \underline{u}_2 + \dots + \underline{f}_i^e \quad (5.27)$$

$$\text{where } \underline{f}_i^e = \underline{f}_p^e + \underline{f}_{i0}^e$$

Here again, the summation only includes the elements which contribute to the node i , and when all such equations are assembled (for convenience we omit the \underline{f}_i^e term), the result is the relationship (eqn. 5.25) which we intended to define at the outset,

$$\underline{Q} = \underline{K} \underline{u} \quad (5.28)$$

$$\text{where } \underline{K} = [\underline{K}] = \sum_{e=1}^m [k^e]$$

5.2.3 Boundary Conditions

In any boundary value finite element problem, it is imperative that every boundary node have either a prescribed traction or displacement field. Without this boundary information, the solution to the system of equations in equation 5.28 are no longer unique; in a situation like this, the \underline{K} matrix becomes singular. Mixed boundary conditions - i.e. specified nodal point forces and specified nodal displacements - are considered by rewriting equation 5.28 as a partitioned matrix:

$$\begin{bmatrix} Q_a \\ Q_b \end{bmatrix} = \begin{bmatrix} K_{aa} & K_{ab} \\ K_{ba} & K_{bb} \end{bmatrix} \begin{bmatrix} u_a \\ u_b \end{bmatrix} \quad (5.29)$$

where

$[Q_a]$ = specified nodal forces

$[Q_b]$ = unknown " "

$[u_a]$ = unknown nodal displacement

$[u_b]$ = specified nodal displacement

The upper portion of equation 5.29 may be written separately as:

$$[Q_a] = [K_{aa}][u_a] + [K_{ab}][u_b] \quad (5.30)$$

Since $[u_b]$ and $[K_{ab}]$ are known, equation 5.30 may be reduced as

$$[Q_a] - [K_{ab}][u_b] = [K_{aa}][u_a]$$

and letting the left hand side of the equation be redefined as the modified load vector, $[Q^*]$, we now have

$$[Q^*] = [K_{aa}][u_a] \quad (5.31)$$

The solution procedure requires the determination of the nodal displacements from equation 5.31 followed by the substitution of these displacements into equation 5.10 to compute the strains within any element. Knowing the strains, the stresses within the elements can in turn be reckoned from the stress-strain relation in equation 5.19.

5.2.4 Quadrilateral Element

A quadrilateral element, comprising four triangular elements as shown in figure 5.4 is considered advantageous over the use of individual triangular elements for two reasons: a) a quadrilateral geometry is more convenient for automatic mesh generation, and b) the condensation procedure

which factors out the internal node (i.e. node 5) produces a set of equilibrium equations which has fewer unknowns.

The equilibrium equations for the quadrilateral as developed by the standard direct stiffness techniques involve ten equations, which are written in the following matrix form (this differs slightly from that presented by Wilson (1965) in that the thermal load matrix, which is not important in soil mechanics problems, has been excluded):

$$\begin{bmatrix} S_a \\ S_b \end{bmatrix} = \begin{bmatrix} k_{aa} & k_{ab} \\ k_{ba} & k_{bb} \end{bmatrix} \begin{bmatrix} u_a \\ u_b \end{bmatrix} \quad (5.32)$$

where $[S]$ = matrix of concentrated nodal loads and $[S_a]$ and $[u_a]$ are associated with the nodal points 1,2,3, & 4 while $[S_b]$ and $[u_b]$ are associated with node #5 in figure 5.4.

This partitioned matrix representation may be separated into its two constituent equations:

$$[S_a] = [k_{aa}][u_a] + [k_{ab}][u_b] \quad (5.33a)$$

$$[S_b] = [k_{bb}][u_b] + [k_{ba}][u_a] \quad (5.33b)$$

Equation 5.34b may be arranged to solve for the displacement of node #5,

$$[u_b] = - [k_{bb}]^{-1} [k_{ba}][u_a] + [k_{bb}]^{-1}[S_b] \quad (5.34)$$

Substituting equation 5.34 into equation 5.33a renders the expression relating the forces at points 1 to 4 to the unknown displacements at these locations,

$$[S_a] = [k_{aa}][u_a] \quad ((5.35)$$

where

$$[k_{aa}] = [k_{aa}] - [k_{ba}][k_{bb}]^{-1}[k_{ba}]$$

and an additional term

$[k_{ab}][k_{bb}]^{-1}[S_b]$ which must be added to $f_{\epsilon_0}^e$ in equation 5.12.

5.3 Computer Procedure

5.3.1 Introduction

The most time-consuming phase of this research effort was the enhancement of the capability of an existing finite element method (FEM) program (AXSYM) to include the bounding surface elasto-plastic constitutive law. Several alterations to the original program were effected in order to accommodate the more complex B.S. stress-strain relationship, but the dominant feature throughout the modification process was the identification of and replacement of the elastic rheological equations by the [CL] matrix as presented in chapter 3. It is not possible to discuss every aspect of the program, and hence, for economy of presentation, the format for this section of the chapter will consist of abridged descriptions depicted in simple flowcharts.

5.3.2 Preliminary Information

With regards to its physical characteristics, the source listing of the computer program (see appendix B) is composed of approximately 2000 lines (or 250 blocks) written in the FORTRAN "language" which is currently available on the University of Florida's DEC (Digital Equipment Corporation) VAX computer system. In its present form, the program's execution time is about .18 seconds of

CPU (central processing unit) time per element per load step; this processing time can be less abstractly envisaged by saying that a typical pressuremeter mesh (20 elements) will allow a maximum of 500 load steps for a 30-minute execution period (which is presently the maximum CPU access time on U. of Florida's VAX computer). The output consists of an echo-print of the input information and the results of the analysis: a) displacements in the radial (R) and vertical (Z) direction for each node, and b) the stresses at the center of each element (radial, tangential, vertical, shear, and the principal values of the stress tensor). For larger finite element meshes, the generated output can require significant disk capacity for storage; again, in more pertinent terms, the disk quota needed to store the output of a 500 load step pressuremeter mesh analysis with a 25-step print interval is about 1000 blocks. In conclusion, the above-mentioned statistics reveals that the computing capacity demanded in the execution of this program is quite significant, and may prove to be costly to the geotechnical engineer whose computing time is only available on a pro-rata basis.

5.3.3 General procedure

The finite element program can be separated into two basic parts: a) data input module and preprocessor, and b) solution and output modules to carry out the actual analysis. Typical input data for the problems analyzed in this thesis include the following:

1. Title, number of nodal points, number of elements, number of different materials, and number of nodes where the boundary conditions are specified.
2. Radius of loaded area & atmospheric pressure in consistent units.
3. Material properties for each material type: density, coefficient of lateral earth pressure, & B.S. plasticity model constants - $G, K, R, S, W, D, N, Q, H_u, H_r$
4. Position of boundaries between elements.
5. Boundary restraint conditions.
6. Print Interval
7. Pressure boundary conditions are read before the solution procedure for each load step; an example of these boundary conditions may be the incremental cavity pressure for stress-controlled analysis of the cylindrical cavity expansion.

The flow chart in figure 5.6 provides a synopsis of the computational procedure while figures 5.7 and 5.8 furnish outlines of subroutines SAND and STRESS, both of which play an instrumental role in the solution technique of this contemporary finite element formulation.

5.3.4 Limitations

Even though it is possible to simulate a variety of loading and boundary conditions with the program in its present form, there are two major restrictions, only one of

which is of consequence in this report, that should be noted: 1) the inability to model a plane stress (i.e. constant σ_z) boundary stipulation, and 2) the incapability to accurately solve the resulting system of equations from the non-symmetric global stiffness matrix whose non-symmetry is attributable to the use of a non-associative flow rule (Prevost and Hjorth, 1980).

Neither of these problems is insurmountable, but any attempt to make accommodations for either of these restraints were relinquished because of the excessive time that would be required to implement these changes. The problem of the plane stress boundary condition can be overcome by assimilating into the program a routine similar to those used in other finite element codes (ex. Mana, 1978) to model boundary conditions of this type. This boundary condition restriction hindered research effectiveness since it only permitted finite element meshes with specified nodal displacements.

Inasmuch as the original version of the FEM program was intended for elastic materials, the Hookean constitutive relationship dictates that the element stiffness matrices and hence the global stiffness matrix are symmetric. This symmetry feature facilitates a convenient solution of the system of equations; if, however, this program is to be used as a research tool to study non-associative flow, it will be necessary to replace the numerical procedure for solving the system of equations by one which can evaluate non-symmetric

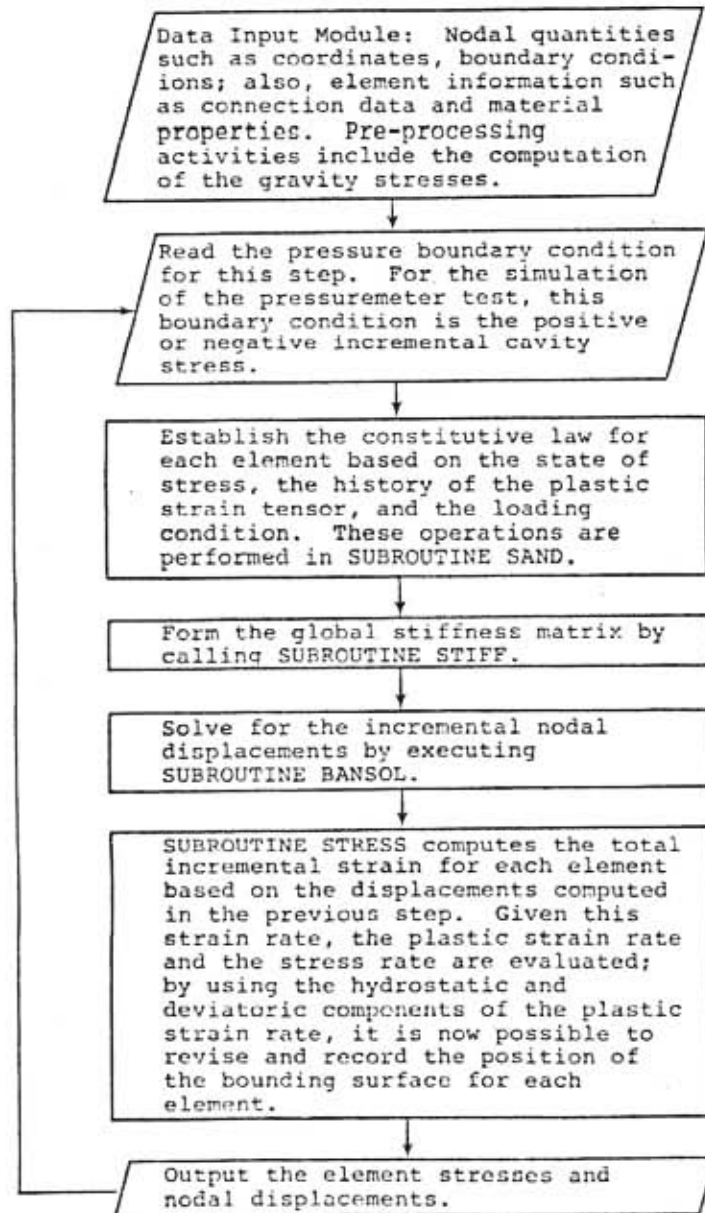


Figure 5.6 General Computational Procedure

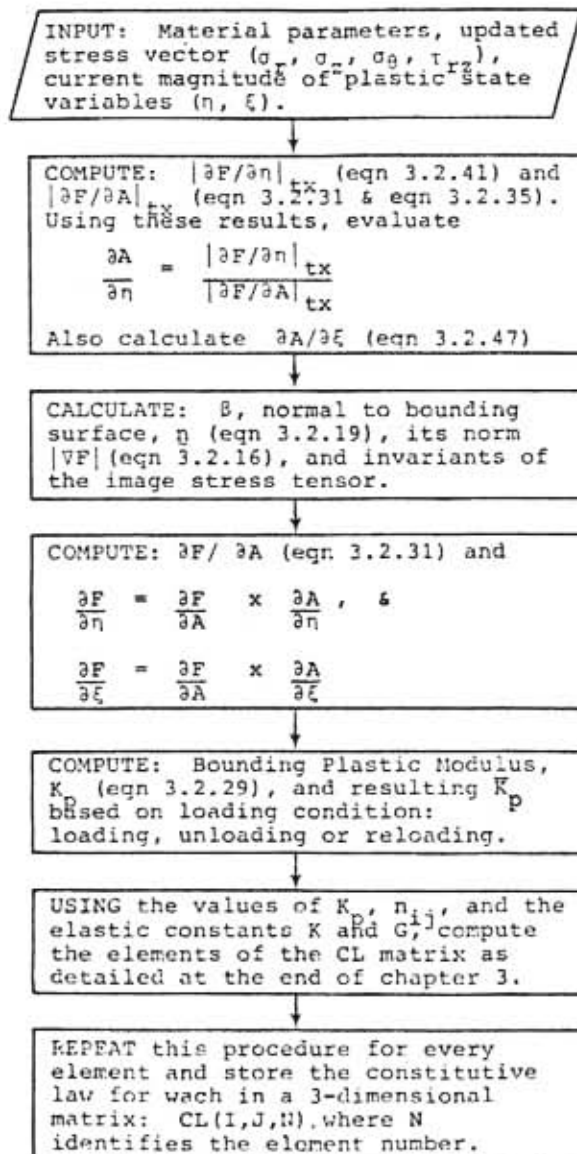


Figure 5.7 Subroutine Sand

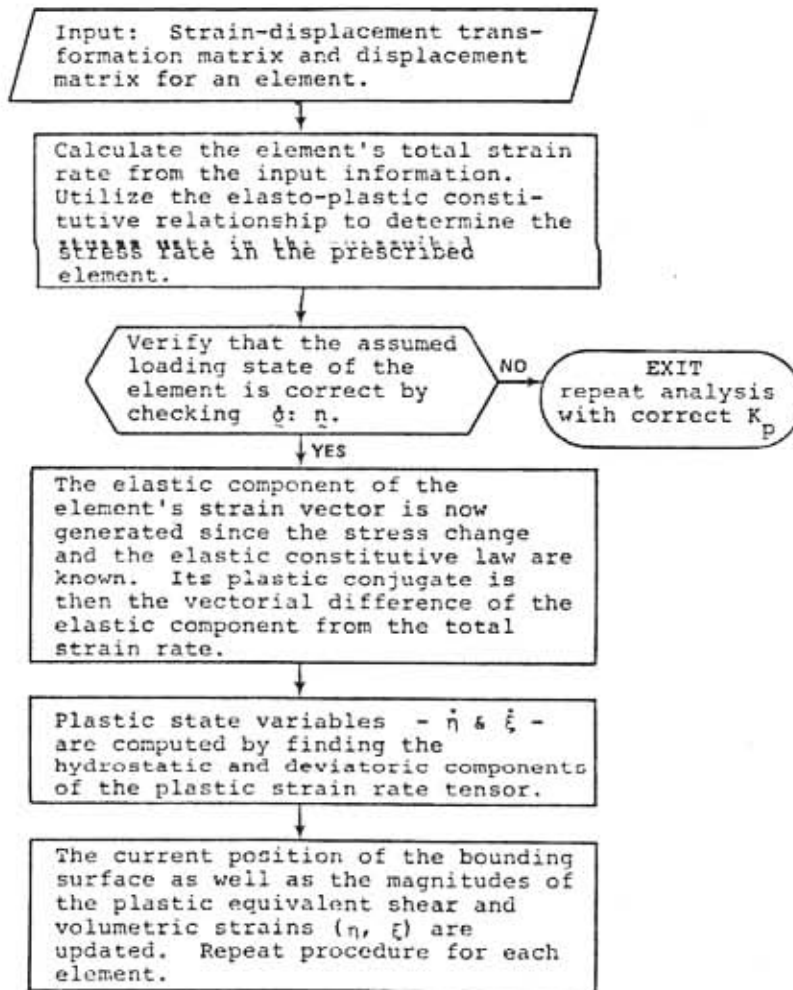


Figure 5.8 Subroutine Stress

stiffness matrices. During the course of this study, none of the stress paths under investigation necessitated the use of the non-associative flow law and therefore this restriction did not pose a problem in analysis.

One of the less important constraints that deserves mention is that the computer program is strictly used for stress-controlled loads while, on the other hand, the pressuremeter tests in the calibration chamber (previously discussed in chapter 4) were strain-control.

5.4 Conclusion

In this chapter, the finite element method of analysis was proposed as the technique by which to study the expansion of a cylindrical cavity in an elasto-plastic medium. The theoretical as well as the computational aspects of the procedure were emphasized with regards to the bounding surface plasticity model although the framework of the program will allow the introduction of most plasticity models. The following chapter will present, discuss, and compare the results of the finite element analyses of the pressuremeter test to the actual test data from the calibration chamber.

CHAPTER 6
DISCUSSION AND PRESENTATION OF RESULTS

6.1 Introduction

This chapter compares the theoretical results of the finite element simulation of the controlled-environment pressuremeter test (PMT) to its related experimental data so that conclusions may be made with regards both to the generality of the bounding surface plasticity model and to the influence of the restrictions inherent in the finite element computer code. The tasks involved in this comparison include: a) the determination of model parameters from triaxial tests, b) the selection of a representative set of these model parameters to be used in the simulation of the pressuremeter test, c) the determination of the magnitude of the coefficient of lateral earth pressure which, although not immediately apparent, has a significant influence on the stress-strain behavior during cylindrical cavity expansion in soil, and d) the selection of the appropriate finite element mesh to model the boundary conditions in the calibration chamber to which the cast-in-place pressuremeter was subjected. In addition to the prediction of the stress-strain response, this standard discrete numerical method of analysis manifests additional important information such as the stress paths and the

distribution and magnitudes of the principal stresses for elements of soil within the zone of influence of the expanding pressuremeter cavity. This data can be extremely useful especially in the selection of approximate stress functions to be used in closed-form solutions to determine soil strength parameters and constitutive properties based on pressuremeter stress-strain results.

Before undertaking the numerical analyses described in the previous paragraph, it is necessary as a first step in the implementation of any new computer program to substantiate the preciseness of the digital solution technique by checking the computer results against a manual calculation. Closed-form solutions for two known stress paths - i.e., the isotropic consolidation path and the triaxial stress path - were used to judge the degree of accuracy of the computer program; excellent agreement was established for both loading conditions. Figure 6.1 shows the element mesh used in both these simulations while figure 6.2 contrasts the numerical solution to the academic result of the hydrostatic compression loading.

Since this computer coded finite element method provided the capability to subject specimens to arbitrary boundary displacement conditions, it was possible to hypothetically examine the performance of the constitutive law under another pertinent loading state: K_0 consolidation. Well documented experimental values of the coefficient of lateral earth pressure of this Reid-Bedford

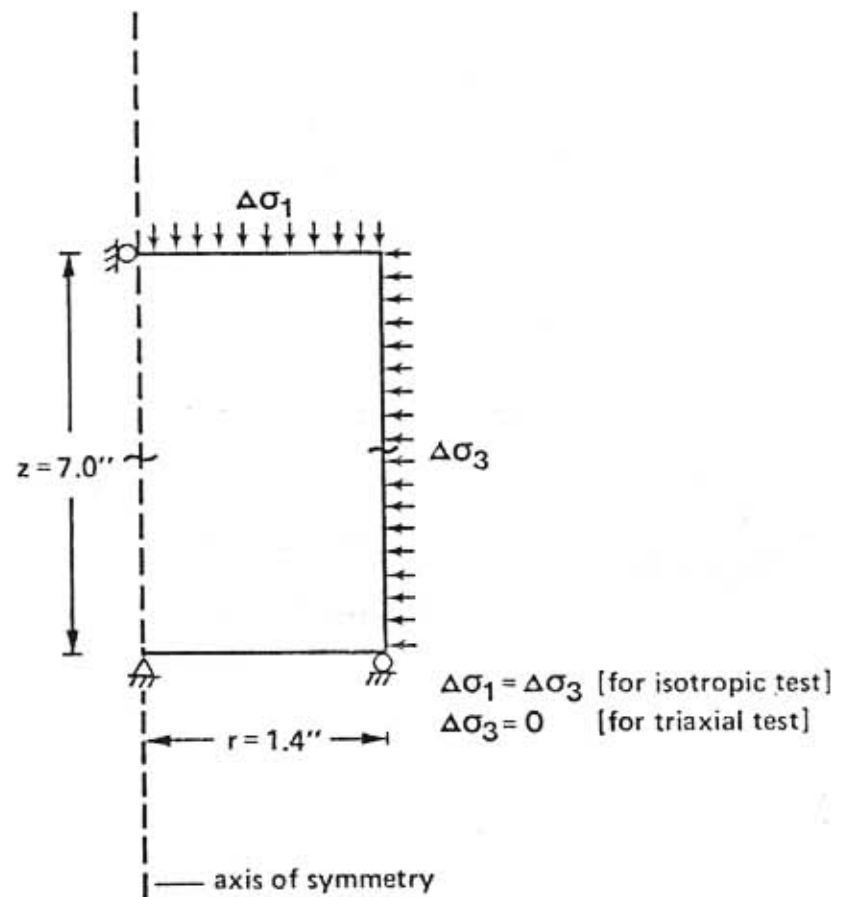


Figure 6.1 Finite Element Used for Simulation of Triaxial Test and Isotropic Compression Test

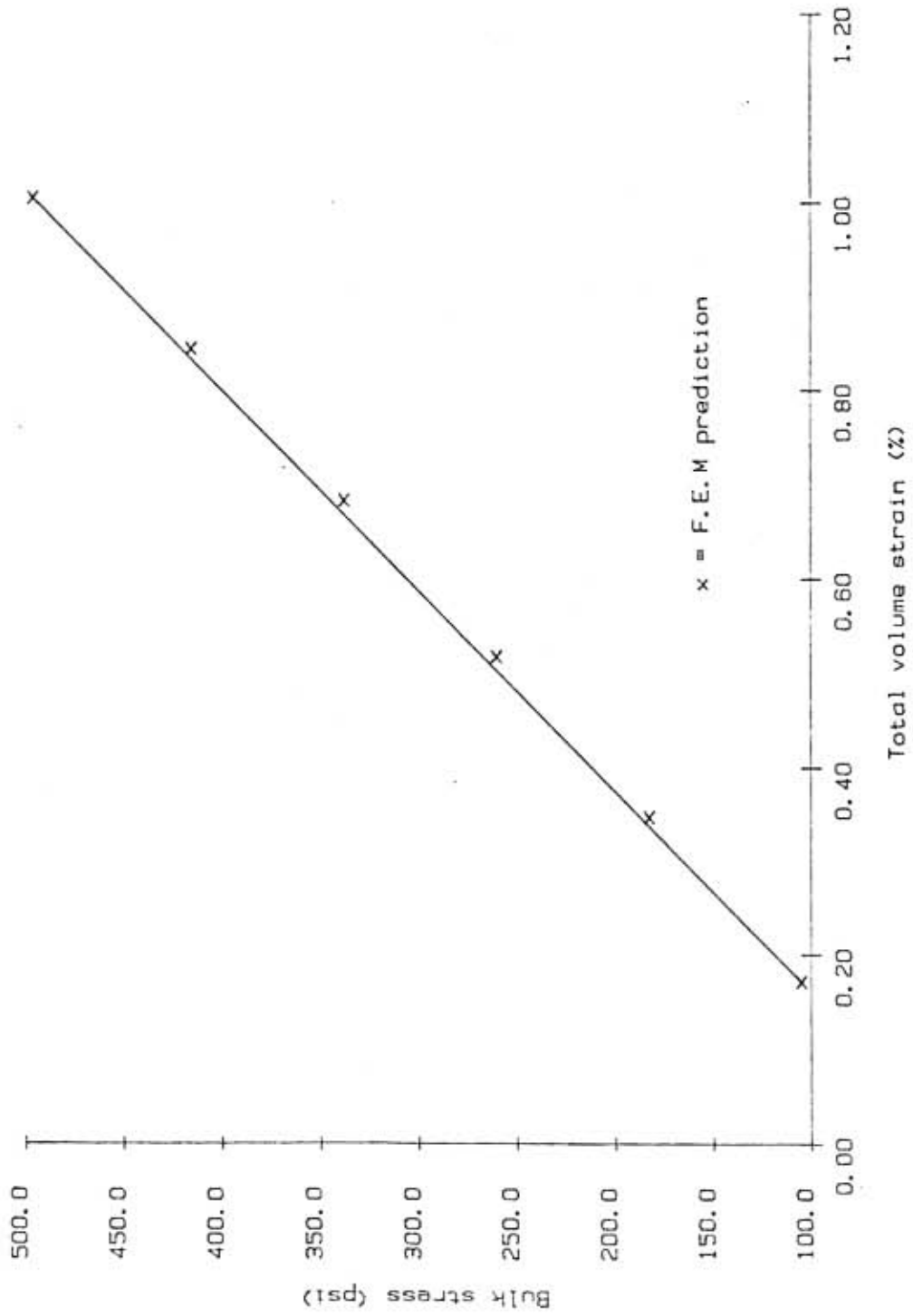


Figure 6.2 F.E.M. Versus Closed-Form Solution for Isotropic Compression Test

sand were available for comparative purposes, and this analysis, together with the cylindrical cavity expansion model, permitted further insight into the general applicability of the B.S. plasticity model.

6.2 Determination of Model Parameters from Triaxial Tests

Although data from a single test would have sufficed, the results of four conventional triaxial compression tests on dense Reid-Bradford sand were utilized in the determination of the bounding surface model parameters R , S , and N . As previously defined in Chapter 4, but repeated here for convenience, R and S are the intercept and slope respectively of the transformed hyperbolic stress (i.e. 2nd invariant of the stress deviator) versus strain (i.e. plastic equivalent shear strain) curve, and N is the slope of the critical state line which can be physically interpreted as the critical combination of deviatoric and hydrostatic stress which signals the initiation of dilation in a dense soil. Three of the experiments - at confining pressures 25, 35 and 45 psi - were carried out by another research student, Karsten Heidebrecht, and can be found in the Davidson et al. (1983) reference, while the fourth test, at a 50 psi confining pressure, was performed by the author under the supervision of Dr. Frank Townsend. Photographs of the laboratory equipment used in this investigation are exhibited in Figure 6.3.

Following data reduction procedures outlined in Chapter four, the model parameters were computed and the results are

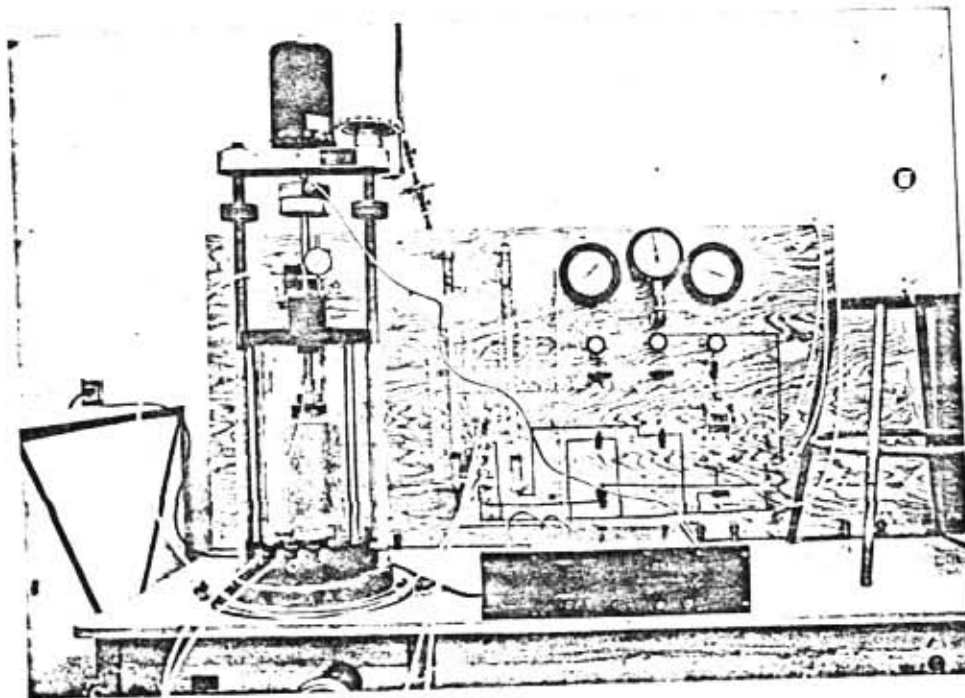
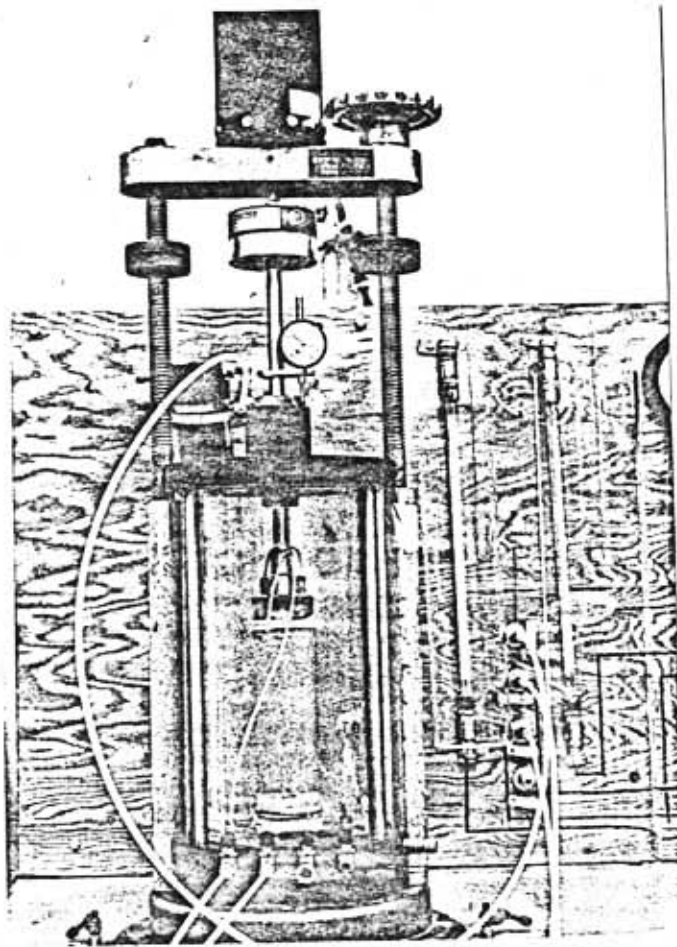


Figure 6.3 Photographs of Triaxial Test Apparatus

tabulated below (detailed data sheets can be found in Appendix A).

TABLE 6.1
MODEL PARAMETERS FROM CTC TESTS

Unit Weight (pcf)	Confining Pressure (psi)	R	S	N	Correlation Coefficient (R^2)
102.9	25	.13	.34	.26	.99
103.6	35	.12	.40	.26	.99
104.0	45	.16	.41	.24	.99
103.6	50	.09	.46	.25	.99

According to the postulated relationship between shear stress and plastic shear strain (Aboim & Roth, 1982, and modified by Taesiri et al., 1983), the values of the parameters R and S should be independent of the confining pressure so long as the samples were identically prepared at the same relative density. As can be noted from table 6.1, the unit weights (and hence the relative densities) do indeed vary slightly among the samples but it is not considered important enough to have such a marked influence on the variation in the computed values of R and S. If one were to neglect the test at 45 psi confining pressure, a distinct relation emerges between the parameter S and the confining pressure. In a more classical sense, this can be interpreted as fitting a curved Mohr-Coulomb failure envelope since S, in a most crude manner, can be interpreted as being inversely proportional to the friction angle in sands (or slope of the Mohr-Coulomb envelope). It is

obvious from the variation in the values of the model parameters R and S that still further research is necessary to examine the postulation that the triaxial stress-strain results can be normalized by the confining pressure. The possibility exists that there may be a more appropriate equation, such as one in which the confining pressure raised to a certain power, can be used to more effectively normalize the stress-strain data and so enable a consistent set of model parameters to be obtained from a single triaxial test.

Quite contrary to the queries concerning the generality of the parameters R and S, there is no uncertainty in stating that the hyperbolic function was most suited to model this relationship (\sqrt{J} vs. η); in all cases, correlation coefficients close to unity attested to a near perfect fit of the data. This close agreement is reflected in figure 6.4 where the actual triaxial stress-strain results are plotted together with the predicted stress-strain response based on the derived model parameters R and S shown in Table 6.1; for purposes of clarity, only three of the four tests were graphed in this figure. Besides knowing the values of R, S, and N, it was necessary to estimate some other model parameters (i.e. K, G, & Q) before the predictions (of fig. 6.4) along the triaxial stress path could be accomplished. Since an unload-reload cycle was not performed in any of the triaxial tests, the elastic bulk modulus, K, and shear modulus, G,

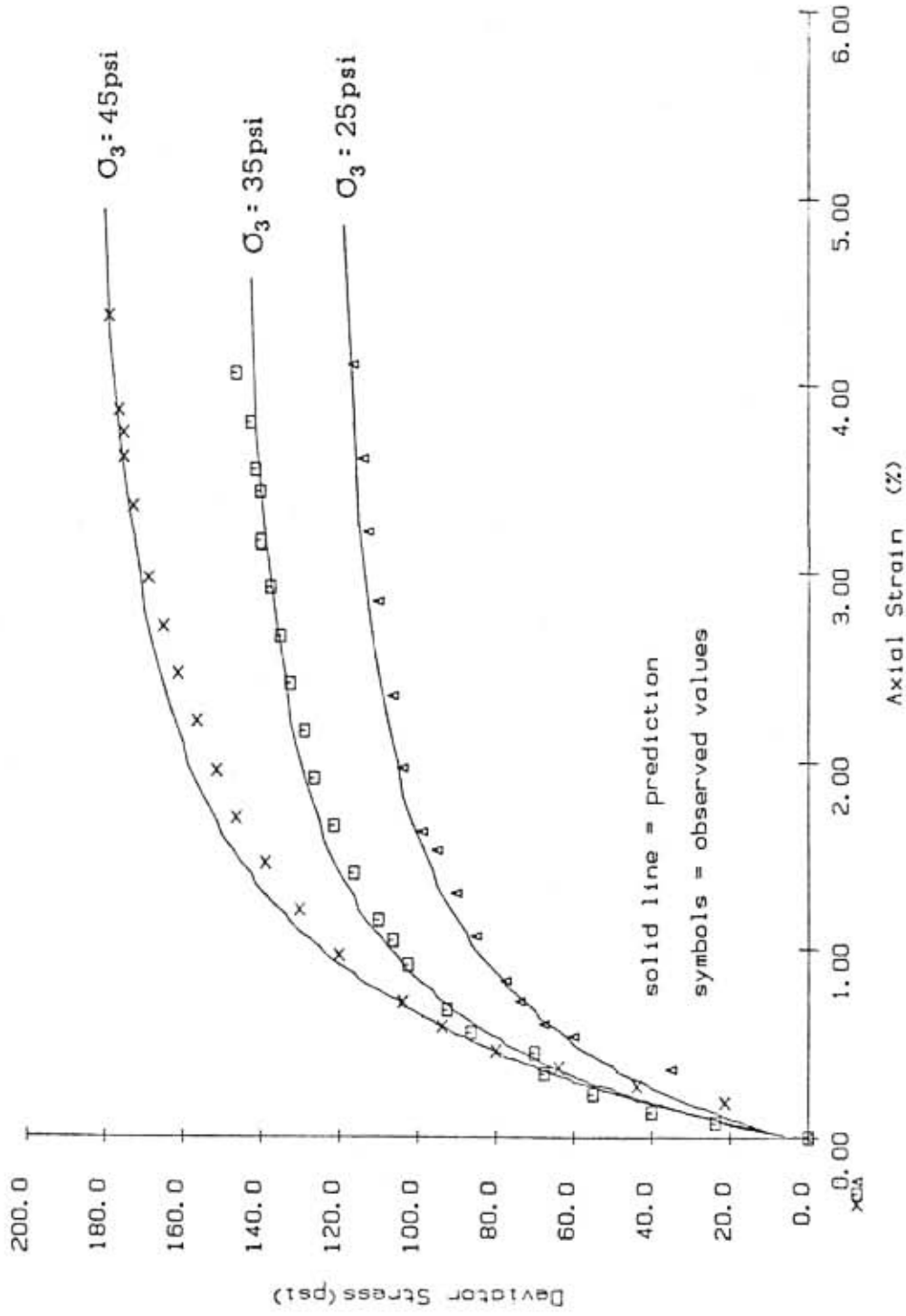


Figure 6.4 Actual Versus Predicted Triaxial Test Results

had to be reckoned from assumed values of the Young's modulus, E , and Poisson's ratio; based on values akin to those obtained by Taesiri et al. (1983) in his study of another dense sand, K was chosen as 36000 psi while G was assumed to be 21600 psi (or in terms of more familiar elastic parameters, $E = 54000$ psi and $\nu = .25$). Several trial values of these elastic constants were examined and the solutions to several problems were found not to be sensitive to these input parameters; as a result, it was not considered imperative to perform a triaxial test solely for the purpose of determining these elastic moduli.

The ratio of the major to minor axes of the elliptic portion of the bounding surface is equal to $(Q-1)/N$ where Q is a "trial and error" parameter and N has been previously mentioned above as the slope of the critical state line. Describing Q as a "trial and error" parameter in no manner insinuates that this parameter has no physical significance or there are no established guidelines for its determination. On the contrary, the constant Q singly controls the ratio of the deviatoric to volumetric component of the strain since its magnitude directly influences the shape of the elliptic portion of the bounding surface from which the plastic strain rate direction is computed; in quantitative terms, higher values of Q induce larger shear/volumetric strain ratios. The magnitude of Q however exerts no influence on the logarithmic portion of the surface and hence there is little control of the

shear/volumetric strain ratio when dilation begins (i.e., when the image stress tensor is on the log surface). A value of Q equal to 4.0 was found satisfactory for modeling each triaxial test during its compressive phase.

The references to strain in the previous discussion all dealt with the axial strain while no mention was made of the dilatation or volume strain predicted by the B.S. hypothesis. Figure 6.5 a, b, and c show predicted versus actual volumetric behavior during the triaxial tests. In both a quantitative and qualitative sense, the predicted volume strain concur reasonably well with the observed data until the point at which the sample begins to expand under the shear stress. Beyond this point, the qualitative agreement still endures but the constitutive model starts overestimating the volume expansion of the specimen, and a possible reason for this has been previously suggested in the discussion of the model parameter Q . This divergency is *not as critical as it may initially seem in the simulation of the pressuremeter test since, as will be discussed later, the elements of soil surrounding the pressuremeter probe reside only briefly, if ever, on stress states which induce dilative behavior.* It should also be remarked that this inconsistency occurs only when the image stress state is located on the logarithmic portion of the bounding surface; present discussion at the University of Florida indicates that this log surface will be replaced by a more functional surface in future versions of the model, and hopefully, will

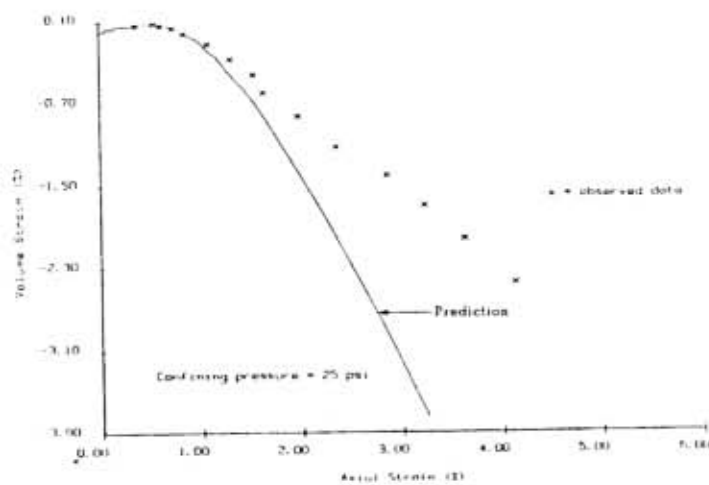
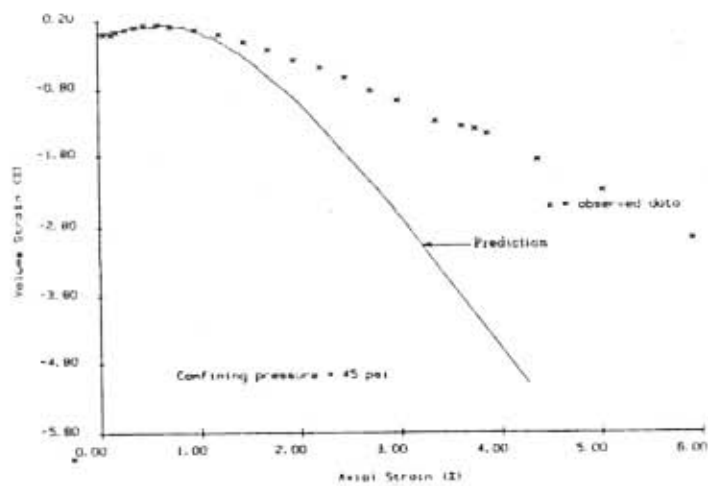
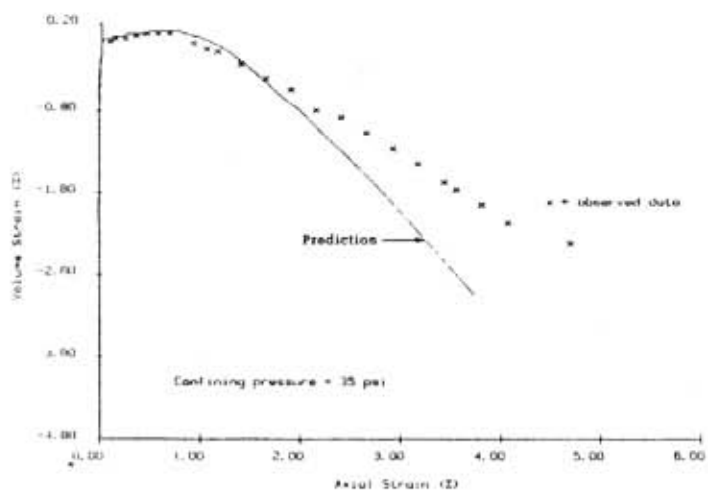


Figure 6.5 Actual Versus Predicted Volume Strain for Triaxial Tests

thus lead to an improvement in volumetric strain predictive capability for stress states above the critical state line.

Hardening along the hydrostatic axis is patterned by the parameters D and W ; for this sand, D and W were evaluated to be .0005 and .028 respectively. These constants are assessed by fitting a curve through the bulk stress vs. plastic volumetric strain results of an isotropic consolidation test. The data sheet containing this test result is included together with the CTC data in appendix A, and the predicted versus observed stress-strain plot is presented in figure 6.6. An important observation is that the level of bulk stress attained in the pressuremeter tests was considerably higher than that achieved in the isotropic consolidation test which made it necessary to extrapolate the calibration data in order to fit a curve which would produce realistic estimates of the parameters D & W .

The last two model parameters that remain to be determined are the unload and reload constants, H_u and H_r . Trial and Error techniques are usually employed to obtain estimates of the magnitudes of these parameters which exclusively serve to manage the amount of hysteresis in the unload-reload loops of the stress-strain curves. Since all of the triaxial tests on the Reid-Bedford sand were subjected only to monotonic loads, it was not possible to evaluate these parameters from the pool of available triaxial test data; alternatively, it was decided to reckon these values based on estimates made by Taesiri (1983) for

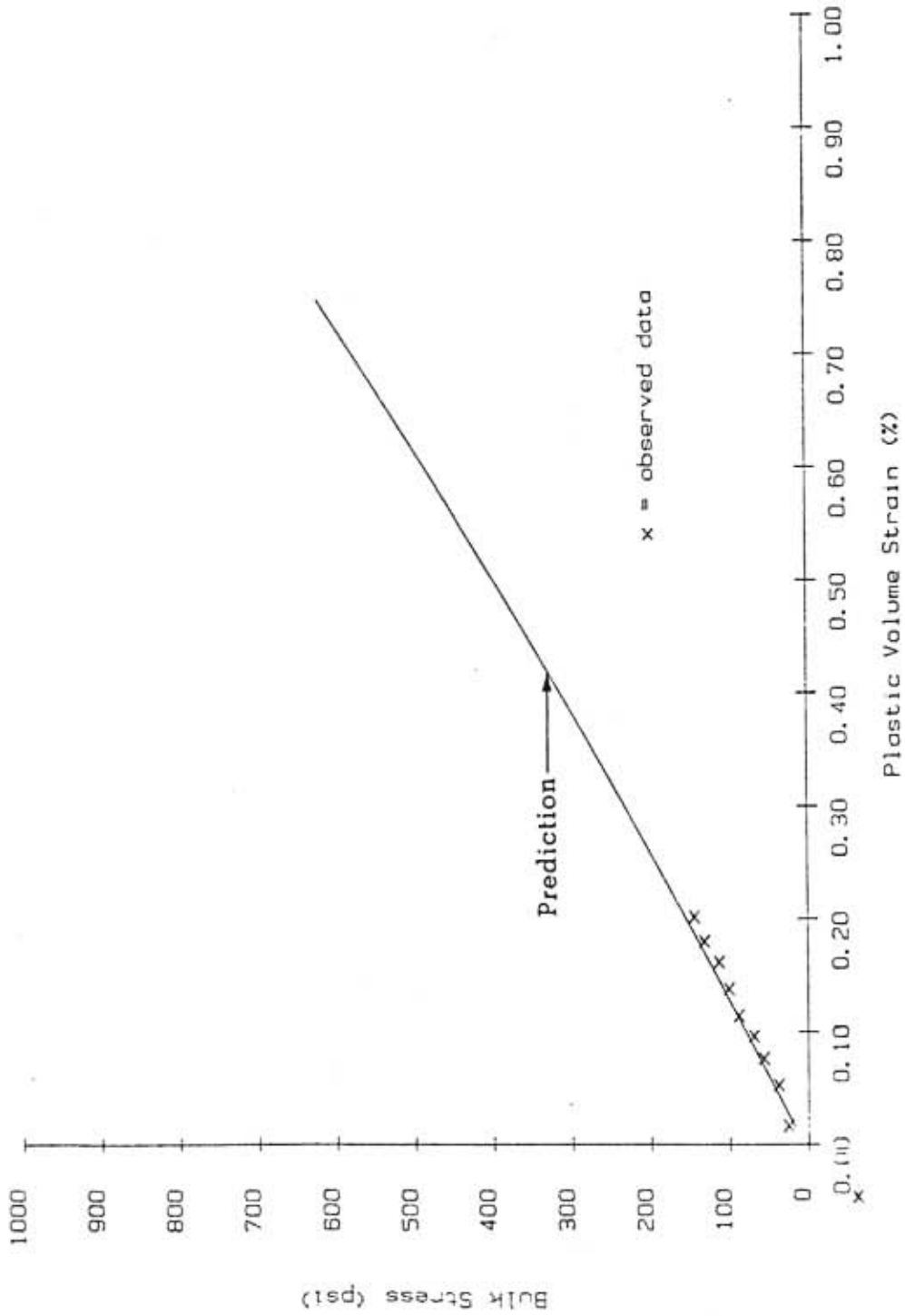


Figure 6.6 Actual Versus Predicted Isotropic Compression Results

the sand he investigated. H_u and H_r were assumed to be equal to 50,000 and 150,000 respectively for dense Reid-Bedford sand.

6.3 Coefficient of Lateral Earth Pressure, K_o

Ideally, the magnitude of the coefficient of lateral earth pressure, which is a prerequisite input parameter in the cylindrical cavity expansion model, should have been derived from a finite element simulation of this loading path. Results of this study (see figure 6.7) indicate that the present bounding surface plasticity constitutive model yields values of K_o which diverge considerably from experimental estimates of this soil parameter. Figure 6.8 summarizes the results of a detailed laboratory investigation of K_o consolidation by Al-Hussaini and Townsend (1975). Two important conclusions can be inferred from a comparison of these predicted and observed values of K_o ; first, it is clear that the magnitudes of K_o predicted by the B.S. constitutive model are considerably higher than the experimentally determined ratio of lateral stress (σ_h) to the vertical stress (σ_v) for the zero lateral strain boundary condition. The second comment on the experimental versus theoretical comparison of K_o centers on the variation in the magnitude of K_o with stress level; the laboratory study indicates that K_o of 0.4 was representative of the dense sand investigated in this thesis, whereas the elasto-plastic analysis shows values of K_o decreasing from

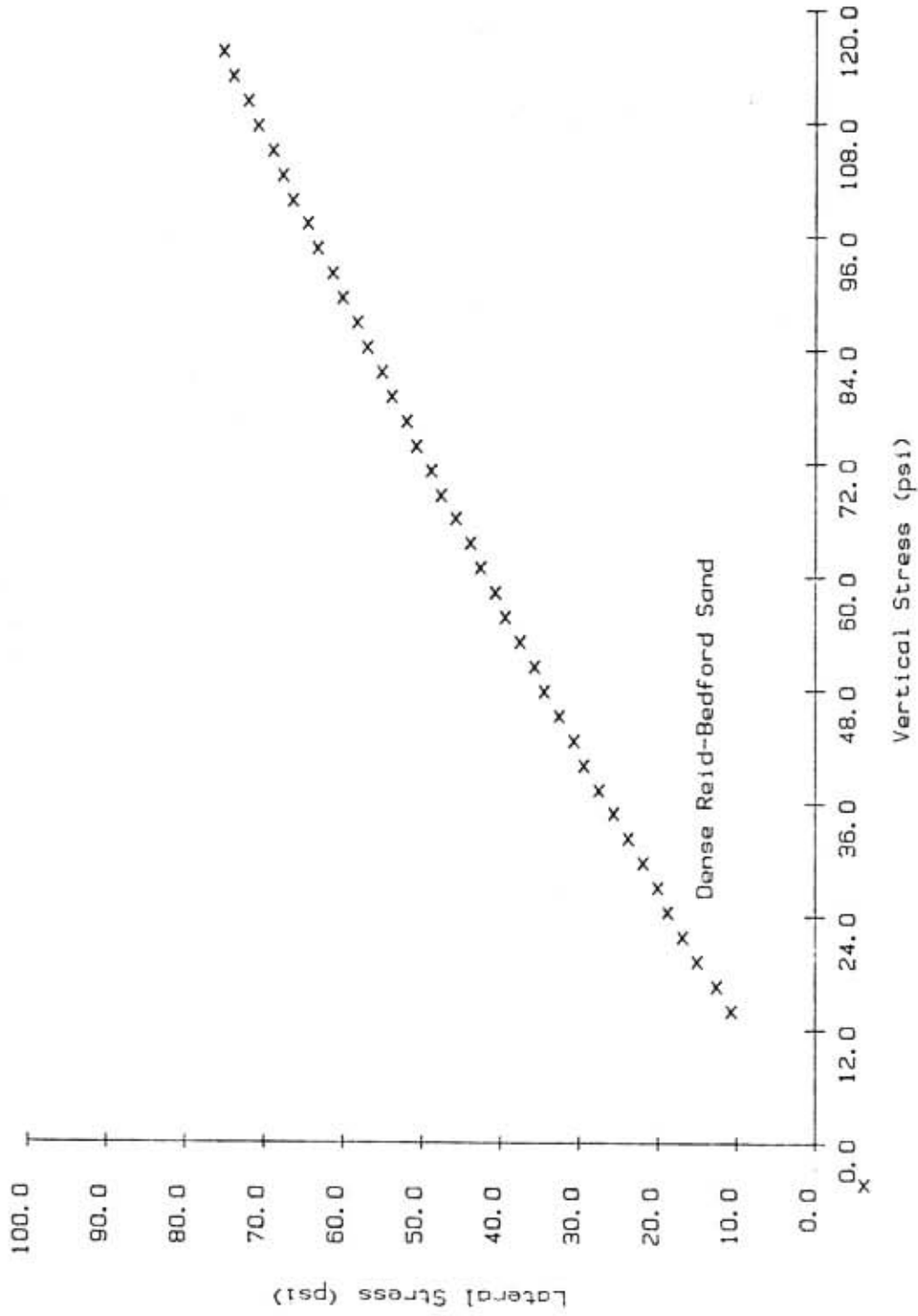


Figure 6.7 K_0 Consolidation Simulation Using B.S. Constitutive Law

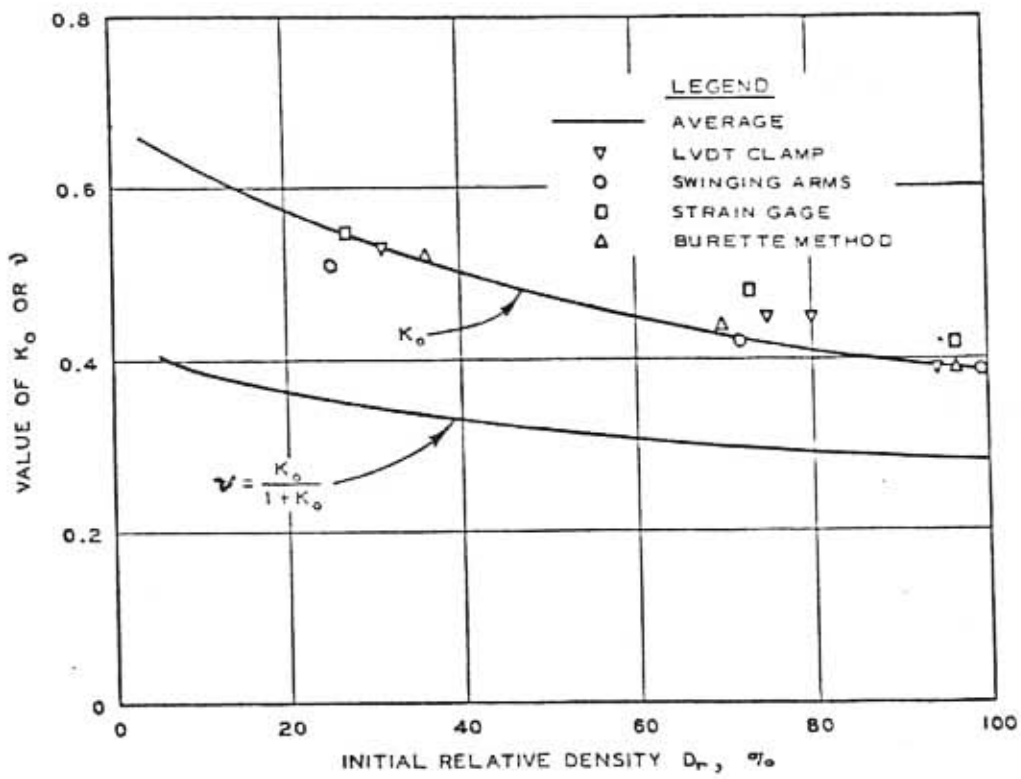


Figure 6.8 Relationship Between K_o , v , and D_r for Reid Bedford Sand
(After Al-Hussaini & Townsend, 1975)

.81 at $\sigma_v = 11.3$ psi to .65 at $\sigma_v = 115.3$ psi. This postulated variability of K_o agrees with the following theoretical considerations: at higher levels of stress, the hardening rule along the hydrostatic axis (modeled as a negative exponential function) generates smaller increments of plastic volumetric strain for a given stress increment. This means that the plastic modulus, K_p , increases as the first invariant of stress, I , increases along this particular stress path. As the value of K_p becomes large in comparison to the elastic constants K and G , a review of the CL matrix (i.e., the constitutive law) in Chapter 3 reveals that this matrix takes the form of a constitutive relationship dominated by the bulk modulus, K , and the shear modulus, G . It is therefore logical to assume that the limiting value of K_o at very high stresses, where K_p is numerically much greater than K or G , is equal to the theoretical value based on an elastic analysis, i.e. $K_o = \nu / (1 - \nu)$ where ν is the Poisson's ratio. Since ν has been previously assumed equal to .25 (see section 6.1), the ultimate value of K_o will be .33 which turns out to be a closer approximation to the experimentally observed magnitude of this parameter.

The validity of the K_o consolidation data presented by Al-Hussaini and Townsend (1975) is reinforced by the boundary pressure data recorded in the triaxial calibration chamber during the preparation of the pressuremeter test samples referred to in Chapter 4. After considering the

cogent assembly of experimental data which contradicted the B.S. K_0 simulation, it was finally resolved to abort the original intention of using the constitutive model to provide preliminary estimates of K_0 , and to use instead the K_0 parameters documented during the sample preparation in the U.F. calibration chamber. Note however that in a few instances of sample preparation, including a test investigated in this thesis, the value of σ_h was increased after the K_0 consolidation phase, and hence, the lateral/vertical stress ratio was in fact greater than K_0 .

It is evident from the discussion so far presented in this section that further research is required to evaluate the utility of the B.S. elasto-plastic model in the simulation of K_0 consolidation. Other elasto-plastic models, such as the Lade model presented in Chapter 2, demonstrate the capability to simulate K_0 consolidation, and any further research on this bounding surface plasticity model will warrant an investigation into the dissimilarities between the bounding surface formulation and its counterparts (ex. Lade's model) which lead to this inconsistent prediction along the K_0 stress path.

Having described the problems of simulating K_0 , it is now instructive to illustrate the significance of its magnitude in the mathematical modeling of the pressuremeter test. K_0 determines the initial values of the radial and hoop stresses which exist in the soil mass prior to the expansion of the cavity, i.e. $\sigma_r = \sigma_\theta = K_0 \sigma_z$. By using the

definitions of the invariants of the stress tensor and some mathematical manipulation, we find for the insitu stress state,

$$\frac{\sqrt{J}}{I} = \frac{(2K_o^2 + 2 - 4K_o)^{1/2}}{6(1 + 2K_o)}$$

But it is known that N is defined as the ratio \sqrt{J}/I which determines the critical stress state for dilation to occur, and this, coupled with the phenomena that dense sands under shear stresses always undergo an initial compression before dilation, leads one to expect that the initial \sqrt{J}/I ratio based on the magnitude of K_o would be less than the parameter N. This criteria aided in the selection of the representative numerical value of N from the data in table 6.1; for example, consider a case where K_o was equal to .30 - this automatically yields an insitu \sqrt{J}/I ratio of .25 based on the equation presented above. Consequently, to enforce the condition that some initial compression must take place before the dilation phase, it will be necessary to select a value of N greater than .25 and if presented with the data of table 6.1, the values of N = .24 or .25 will be discarded in favor of N = .26. In less technical terms, this criteria can be construed as follows: a lower value of K_o leads to a greater deviatoric (or shear) component of the stress tensor for the insitu state, and since some initial compression must be observed upon load application, the position of the critical state line must reside above the coordinates of the insitu stress tensor in

principal stress space. Emphasis has been fixed on this hypothetical case because it represents a situation that actually occurs in simulating one of the pressuremeter test analyzed in this report.

6.4 Simulation of Pressuremeter Test

Typical output of the finite element analysis, including nodal displacements and principal stresses at the center of each finite element, allowed an examination of the following characteristics of the cylindrical cavity expansion model:

a) comparison of the actual versus predicted cavity stress-strain plots (including the unload-reload modulus loops) which serve primarily to corroborate or invalidate the suitability of the bounding surface constitutive law in simulating generalized cyclic loading paths.

b) superior comprehension of the stress paths to which the soil elements are subjected during the pressuremeter test; this information will be crucial for controlled laboratory similitude studies which attempt to model the progression of the stress state of soil elements subject to cylindrical cavity pressure.

c) establishing the radius of influence within the soil mass due to the cavity pressure; this is investigated by inspecting the distribution of radial, circumferential, and vertical principal stresses as a function of distance from the axis of the pressuremeter.

d) variation in the three principal stresses - σ_r , σ_z , σ_θ - with the pressure level in the cavity; again as in b), this information is important in laboratory simulation.

It is convenient at this point, before discussing numerical results of the pressuremeter analysis, to summarize in Table 6.2 the bounding surface model parameters (suggested in Section 6.2) which were used in the simulation of these tests.

TABLE 6.2

SUMMARY OF MODEL PARAMETERS FOR DENSE REID BEDFORD SAND

NO.	PARAMETER	MAGNITUDE
1	R	.12 %
2	S	.460
3	W	2.80 %
4	D	.0005
5	N	.26
6	K	36000 psi
7	G	21600 psi
8	Q	4.0
9	H^u	50000
10	H^u_r	150000

6.4.1 Boundary conditions.

As described in chapter 4, the cast-in-place self-boring pressuremeter tests were performed under two boundary conditions; boundary condition #1 (B.C. #1) allowed no change in stress at the radial boundary and also restrained vertical displacements at the specimen's periphery while, conversely, B.C. #3 permitted no lateral displacement along the perimeter of the sample and no change in stress at the top and bottom of the specimen. These

boundary conditions obviously controlled the selection of the nodal displacement restrictions for the finite element meshes used to represent each situation, and taking into consideration the relatively small magnitude of the ratio of the chamber radius (24") to the pressuremeter radius (1.6"), it was found, as anticipated, that the boundary stipulations did indeed have a significant influence on the predicted stress-strain behavior. It can be unequivocally stated at the outset that the finite element mesh boundary conditions, together with the model parameters R, S, D and W, were the predominant factors governing the simulated pressuremeter stress-strain behavior.

One of the inherent limitations of the computer code, aforementioned in chapter 5, is its inability to treat a constant stress boundary stipulation. Unfortunately, such a requirement exists for both B.C. #1 and B.C. #3 at the lateral and vertical confines respectively. Figures 6.9 and 6.10 show the F.E.M. (finite element method) meshes used in an endeavor to overcome the problem of the constant stress restrictions for both conditions. For B.C. #1, the fixed stress at the outer radial boundary is approximated by using a longer element at the border such that the finite element mesh is about twice the actual length of the sample in the chamber (24" vs 55"); note that this artificial element at the end will produce stress-strain results which more closely model an assumed plane strain field situation. Judging from the results to be presented, it appears that

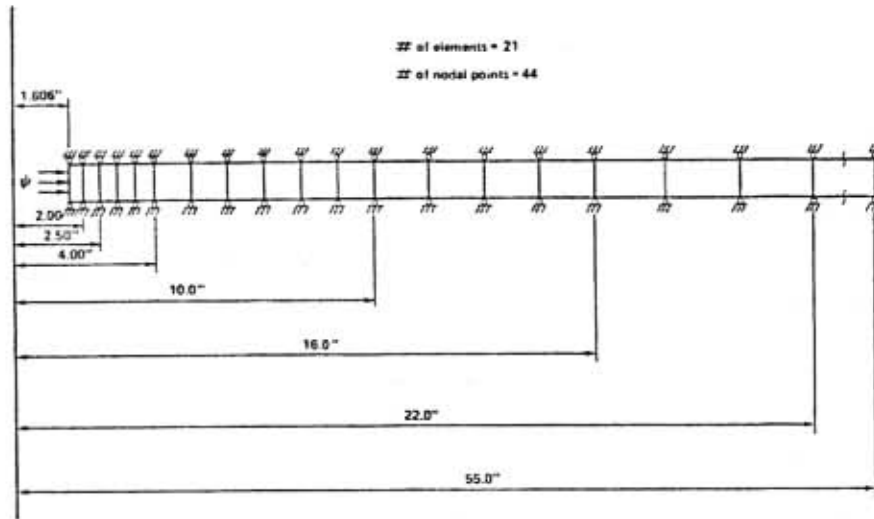


Figure 6.9 F.E.M. Mesh for Simulation of B.C. #1

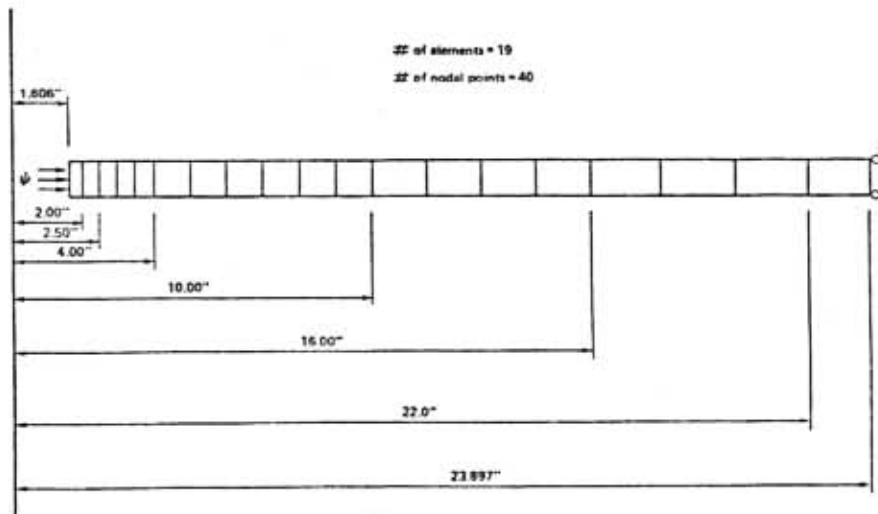


Figure 6.10 F.E.M. Mesh for Simulation of B.C. #3

the attempt to model B.C. #3 was much less successful; the "rollers", which were used to prevent vertical displacement of the nodes in B.C. #1, were eliminated while two additional "rollers" were prescribed at the outer boundary to prevent radial movement at the sample's perimeter. The removal of the "rollers" used to prevent vertical movement is somewhat ambiguous since it is known from radiographic evidence that expansion of the pressuremeter membrane produces no axial movements (Wood & Wroth, 1977).

It can be concluded therefore that neither of the actual chamber boundary conditions could be reproduced exactly for input into the computer program, and it was therefore considered necessary to make some rational allowances in the finite element meshes to compensate for the expected deviations from the exact solution.

6.4.2 Actual versus predicted SBPM results.

The comparison of predicted vs. observed stress-strain results of the pressuremeter tests are exhibited in figures 6.11 and 6.12; review of these graphs evinces either of three possibilities: 1) a misrepresentation in the boundary provisions of B.C. #3, 2) an intrinsic limitation of the B.S. model, or 3) a discrepancy in the selected model parameters. The latter is unlikely since the sand raining technique used in sample preparation of dense sands assures a fairly high degree of uniformity (Jewell, Fahey & Wroth, 1980), and it is presumed that the measured relative density is representative of the soil elements at the mid-plane of

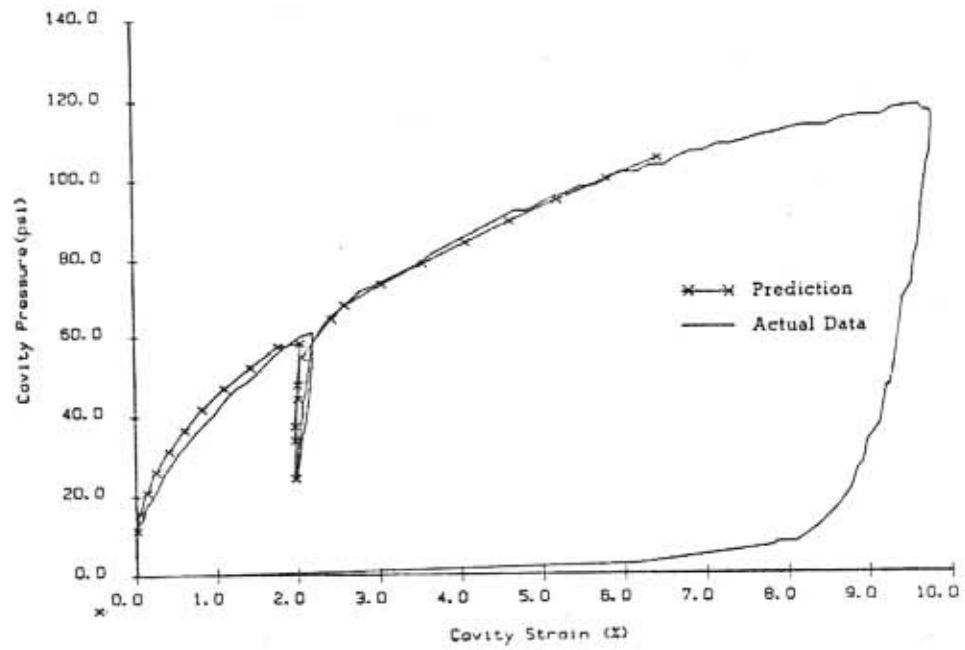


Figure 6.11 Actual vs. Predicted SBPM Results for B.C. #1

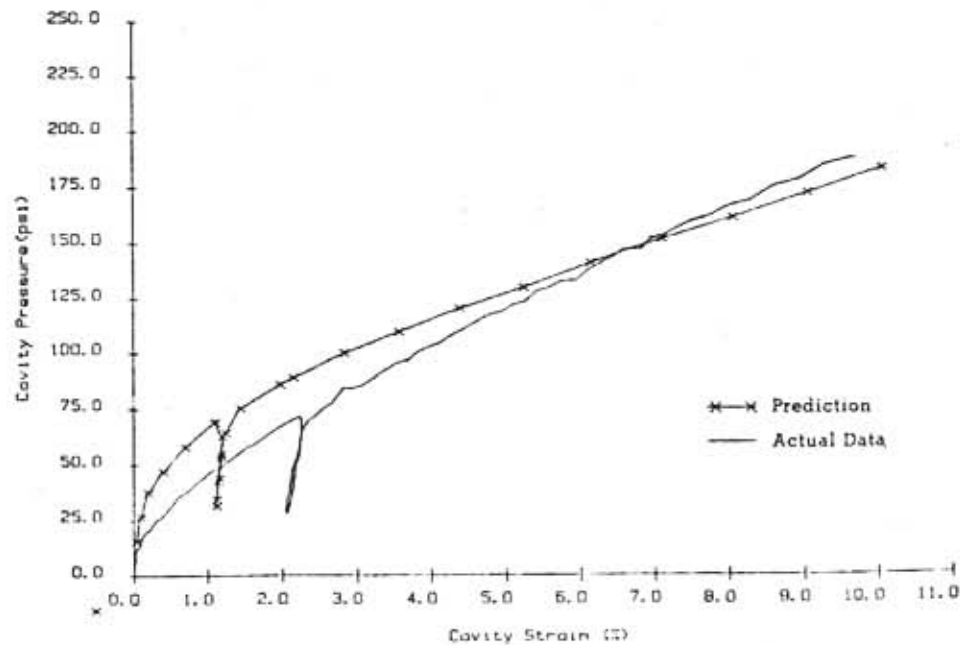


Figure 6.12 Actual vs. Predicted SBPM Results for B.C. #3

the pressuremeter. The second possibility, although not totally out of the question, is contradicted by the good results of the B.C. #1 simulation. As a matter of information, a variety of boundary conditions were tested for B.C. #3, and although quite divergent from the actual stress-strain data, the F.E.M. mesh chosen in this thesis (fig. 6.10) yielded the most realistic results. Another probable source of error which was investigated and systematically ruled out was the magnitude of the stress increment used in the numerical analysis (B.C. #3 = 0.4 psi); smaller increments (0.1 and 0.2 psi) resulted in virtually the identical stress-strain prediction shown in figure 6.12. The same, however, does not apply to B.C. #1 in which a stress increment of 0.2 psi had to be used instead of 0.4 psi in order to avoid numerical instability emanating from the incremental plasticity theory. As a consequence of this lower required stress increment for B.C. #1, it was not possible to access enough computer time to completely model the test to its ultimate cavity strain of 10%; nevertheless, the maximum cavity strain achieved, about 7% was sufficient to make a rational analogy to the observed data.

Jewell et al. (1980), in a series of controlled environment SBPM tests on dense sands at Cambridge University, notes that it is likely that the suspended pressuremeter has an influence locally on the sand rain, thus producing around the pressuremeter a thin annulus of

sand with random density variations, though these variations need not significantly affect the overall average density measured. Based on this observation, the author postulates that the sand immediately next to the cavity wall is in fact slightly less dense than the surrounding soil; this hypothesis is founded on examining several numerical simulations (including B.C. #1 and B.C. #3 in this thesis) where the initial predicted response (say less than 1.75% strain) is always stiffer than the observed data until some level of cavity stress above which the effect of this local variation seems to be obliterated.

Gathering from the results presented in this section, it can be asserted that the excellent correspondence between the predicted and observed data for B.C. #1 substantiates the claim of stress path independence for the bounding surface philosophy. It is worth reminding the reader that this statement is based solely on the results of section 6.4, and if one were to support his conclusions with only the K_0 simulation data (in section 6.3), it is feasible that the conclusions might be reversed.

6.4.3 Stress paths.

In the current approaches adopted to determine soil strength and elastic parameters from the pressure meter curve, such as Hughes et al. (1977) method, various assumptions about the principal stresses are implicit in the theoretical development of these interpretation procedures. The results of this numerical study of the pressuremeter

expansion thus furnishes useful information on the stress paths and stress distributions which can be employed in future academic attempts to infer the magnitude of soil constitutive and limiting equilibrium design parameters from pressuremeter test results. It is not attempted herein to present a new interpretation scheme, but rather to present data on the typical stress paths followed by dense sand elements of which the stress-strain constitution can be characterized by the bounding surface model. Furthermore, since the boundary condition #1 simulation realized more precise predictions than B.C. #3, it was decided to present the data of this supplementary stress distribution analysis only for B.C. #1 because of the possibility of anomalous results inherent in the B.C. #3 idealization.

In terms of elastic analysis, the plane strain expansion of a hollow cylinder subjected to internal pressure produces successive stress states in which the radial stress is increasing as much as the circumferential stress is decreasing (i.e., $\sigma_r = -\sigma_\theta$), and in addition, if plane strain conditions are assumed, the vertical stress remains unchanged and the typical stress path in stress invariant space will be depicted by a straight line perpendicular to the I (i.e., first invariant of the stress tensor) axis. Figure 6.13, on the other hand, shows the stress path obtained from a bounding surface plasticity analysis. It will be noted that the stress path is not, as

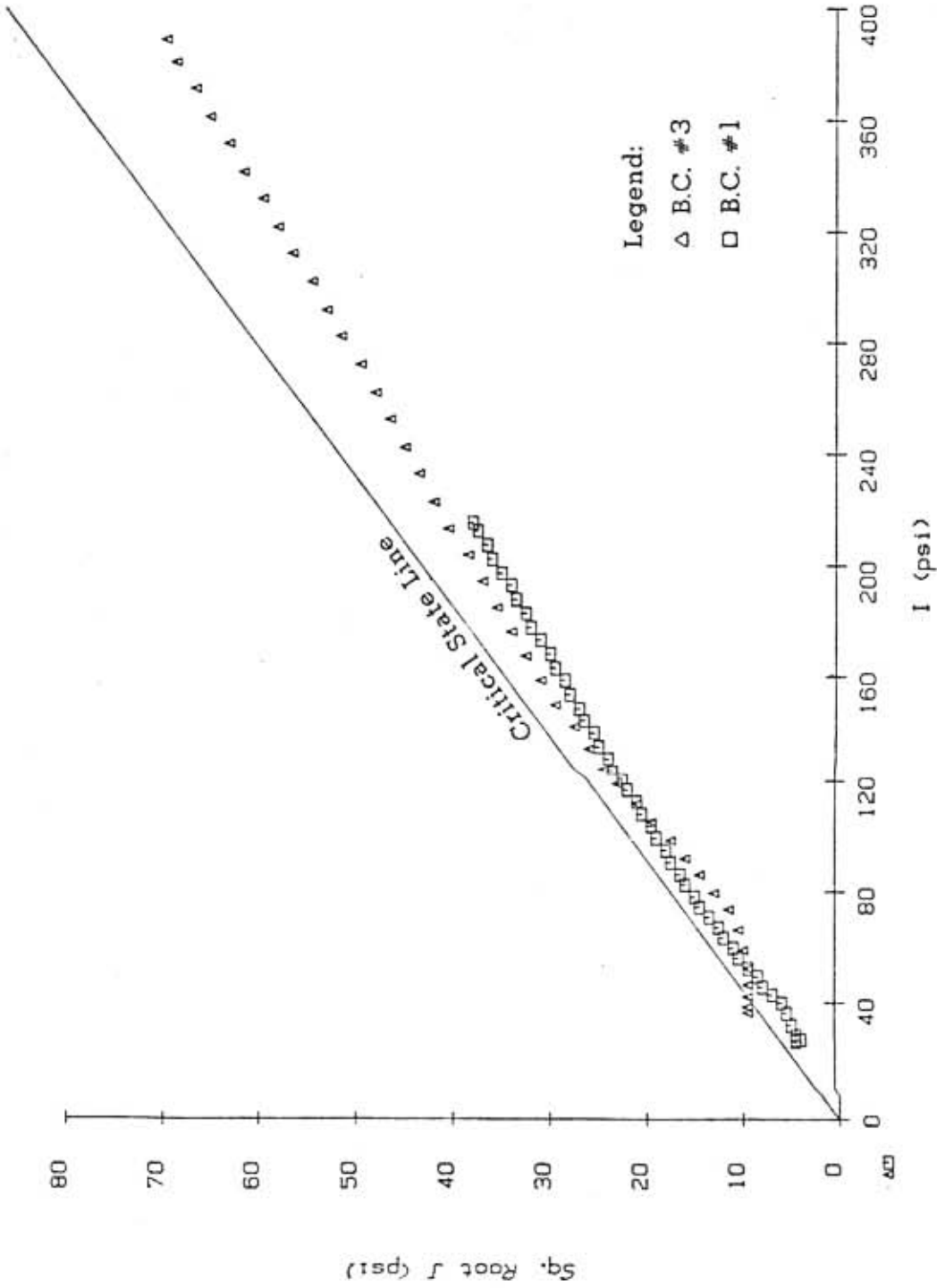


Figure 6.13 Stress Paths Followed by Critical Soil Element Adjacent to Cavity Membrane for B.C. #1 and B.C. #3

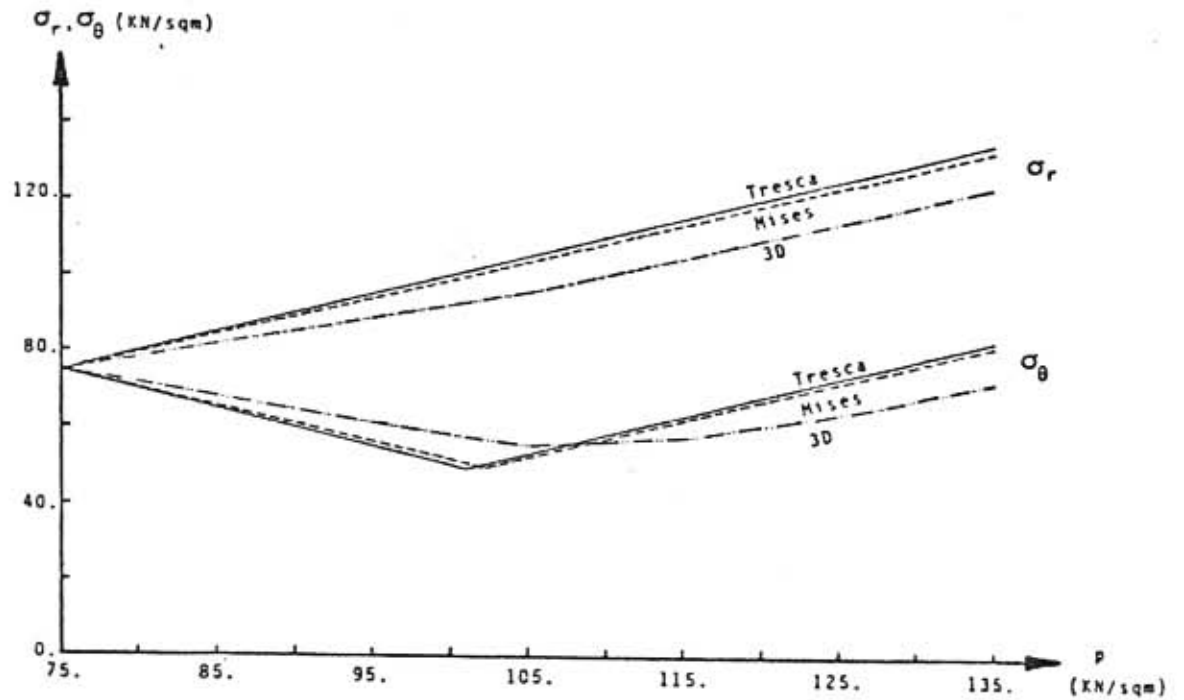
predicted by an elastic relationship, normal to the I axis, but moves along an approximate straight line trajectory between the triaxial stress path and the isotropic compression loading path. It must be reiterated that this stress path is only for dense sands, and has not been confirmed for loose sands or clays.

Another important comment that can be made upon visually inspecting this stress path is its movement away from the critical state line which suggests that the dense sand elements are not undergoing sufficient shear to initiate dilation. It is also apparent that the ratio of the deviatoric component of the stress tensor to its hydrostatic conjugate is decreasing, and this furthermore implies that the homogenous, isotropic soil elements are undergoing more of a volume strain than a shear strain as the cavity pressure increases. Based on this observation, it can be deduced that the model parameters which control hardening along the hydrostatic axis, D and W , become progressively more influential in the solution to the cylindrical cavity stress-strain problem at higher internal pressure levels. These stress paths, however, differ from those computed by Aboim (1981) using Lade's elasto-plastic model in a finite element simulation of the pressuremeter tests in dense crushed Napa basalt. His theoretical study produced stress paths which were initially vertical and then advanced along a slope very close to that of the triaxial stress path.

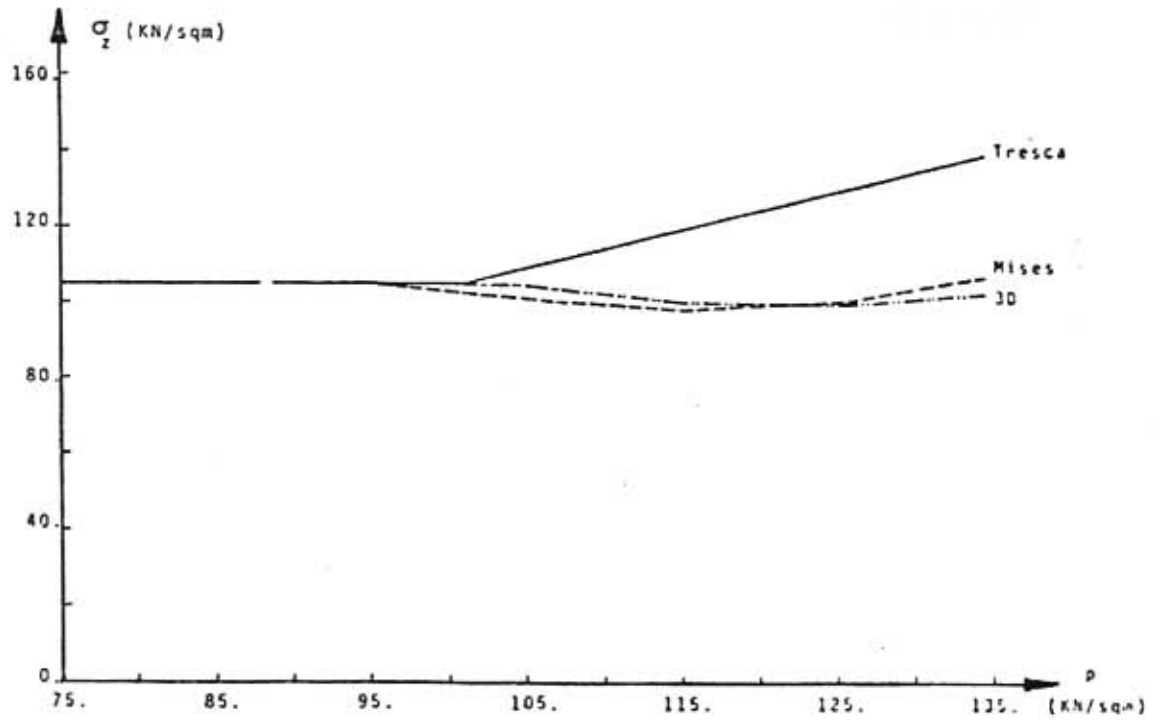
6.4.4 Variation of principal stresses with cavity pressure.

Aboim (1981) also examined the change in magnitude of each of the principal stresses (σ_r , σ_z , σ_θ) with increasing *cylindrical cavity pressure in media characterized by* Von-Mises and Tresca yield criteria; these results are presented in figure 6.14. A similar set of data, extracted from the bounding surface analysis in this thesis, is presented in figures 6.15a and 6.15b for the B.C. #1 element mesh shown in figure 6.9. Since the stress gradients are extraordinarily high in element #1 (which can be seen later in figure 6.16), it was not possible to distinguish clearly, the points at which the incremental circumferential and vertical stress changed signs; consequentially, it was necessary to include analysis of another element (see figure 6.15b) where the effect of the cavity pressure was attenuated sufficiently enough to allow a more distinct observation of the variation in principal stresses; element #6 of B.C. #1 was chosen for this purpose.

A comparison of figures 6.14 and 6.15 reveals that the trend in the radial stress with cavity pressure is analogous for all three constitutive models (i.e. bounding surface elasto-plastic, Von-Mises elastic-perfectly plastic, and the Tresca elastic-perfectly plastic). Note that in figure 6.14, the variation of the principal stresses is exactly as predicted by elastic analysis up to a cavity pressure slightly greater than 100 psi.



(a)



(b)

Figure 6.14 Predicted Principal Stresses as a Function of the Pressuremeter Pressure - Mises and Tresca Materials (from Aboim, 1981)

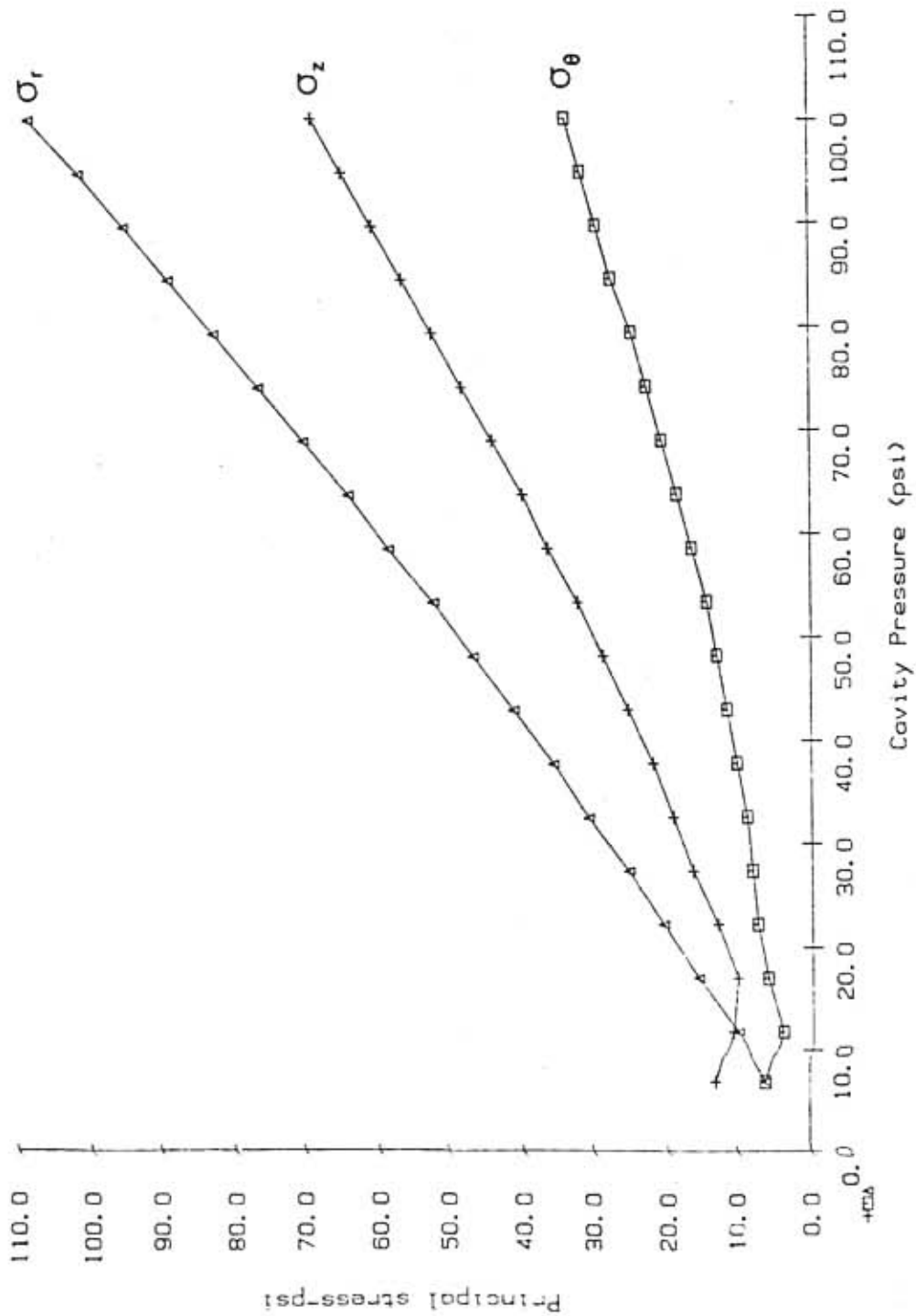


Figure 6.15a Predicted Principal Stresses as a Function of Pressuremeter Pressure for Element #1 of B.C. #1

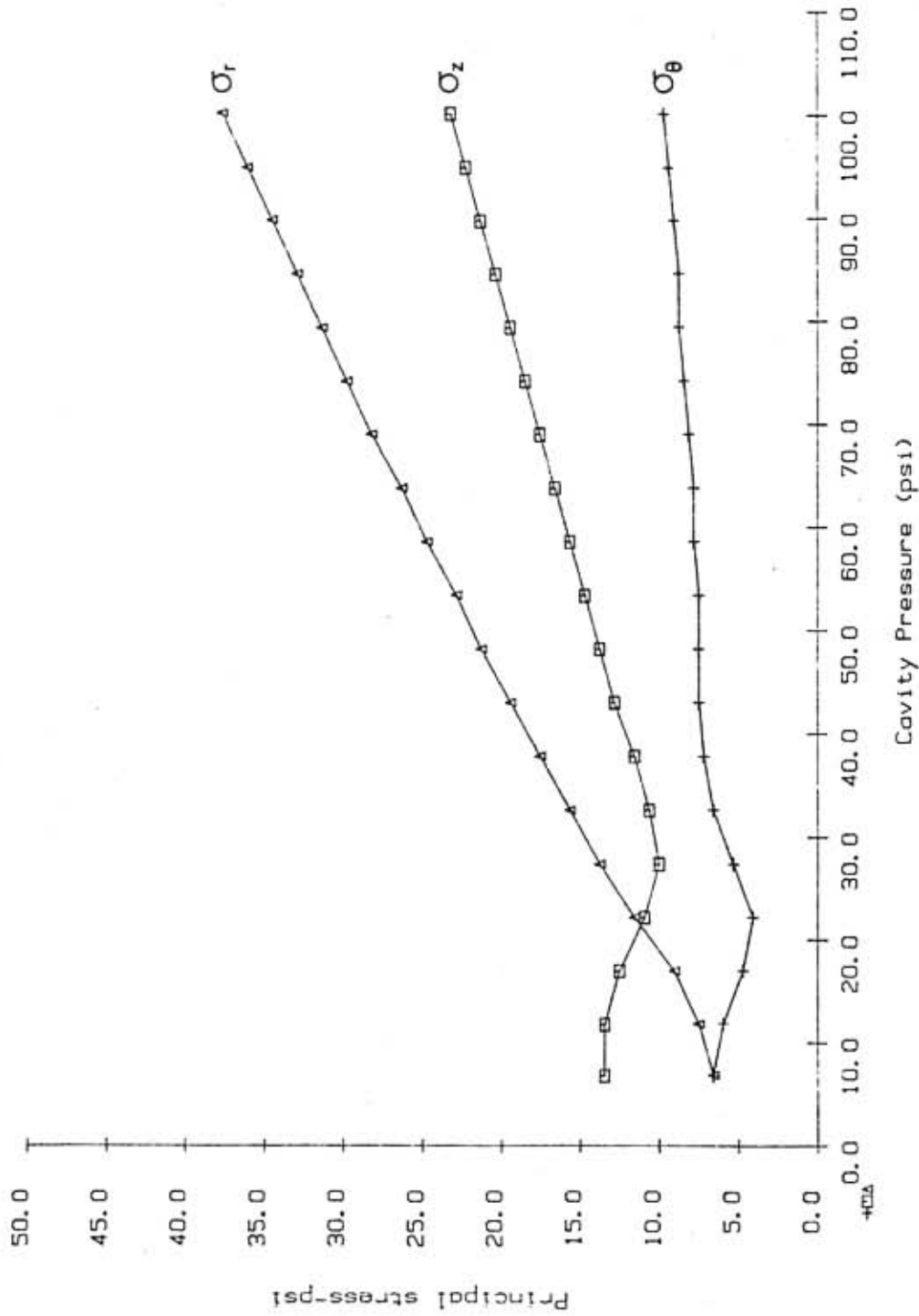


Figure 6.15b Predicted Principal Stresses as a Function of Pressuremeter Pressure for Element #6 of B.C. #1

Qualitatively, the circumferential stress undergoes the same changes for the three models considered, and the key difference is the magnitude of the cavity pressure at which the increase in hoop stress starts. A logical comparison cannot be made among all three cases since the material considered for the Mises and Tresca criteria (Napa basalt) is different from the material (Reid-Bedford sand) used in the B.S. analysis, and also, it has not been ascertained at what distance from the pressuremeter axis the results shown in figure 6.14 apply. Nevertheless, according to B.S. theory, it can be concluded that the circumferential stress, although it never becomes a tension stress in dense sands, does undergo an initial decrease until some point at which this stress starts increasing at a rate somewhat lower than that of the radial stress.

Figure 6.15 also indicates that the vertical principal stress very rapidly becomes the intermediate principal stress and assumes this role for the remainder of the cavity expansion phase. Wood and Wroth (1977) have confirmed this postulated behavior of σ_z in their true triaxial tests which were used to study failure modes related to pressuremeter tests. This response, which shows σ_z increasing at a rate between that of q_r and σ_θ , effectively ensures that the vertical stress always remains the intermediate principal stress and is hence consistent with the whole method of analysis of the results of pressuremeter tests which assume that this stress (σ_z) does not influence the behavior and

that all deformation, and ultimate failure, occurs on vertical $r:\theta$ planes.

6.4.5. Stress distribution with distance from PMT axis.

When a pressuremeter probe is inserted into the subsurface, it is important to know the radius of the cylindrical soil zone which is going to influence the pressuremeter stress-strain curve. Figure 6.16 represents a typical distribution of stress as a function of radial distance from the pressuremeter axis. Evidently, the constitutive properties of the soil elements within an approximate distance of 15 inches from the probe's axis exert a major portion of the influence on the predicted stress-strain response. It is also obvious that the elements of soil within about three inches from the expanding membrane are subjected to the largest stress gradients, and this manifests the importance of not disturbing these soil elements during self-boring operations.

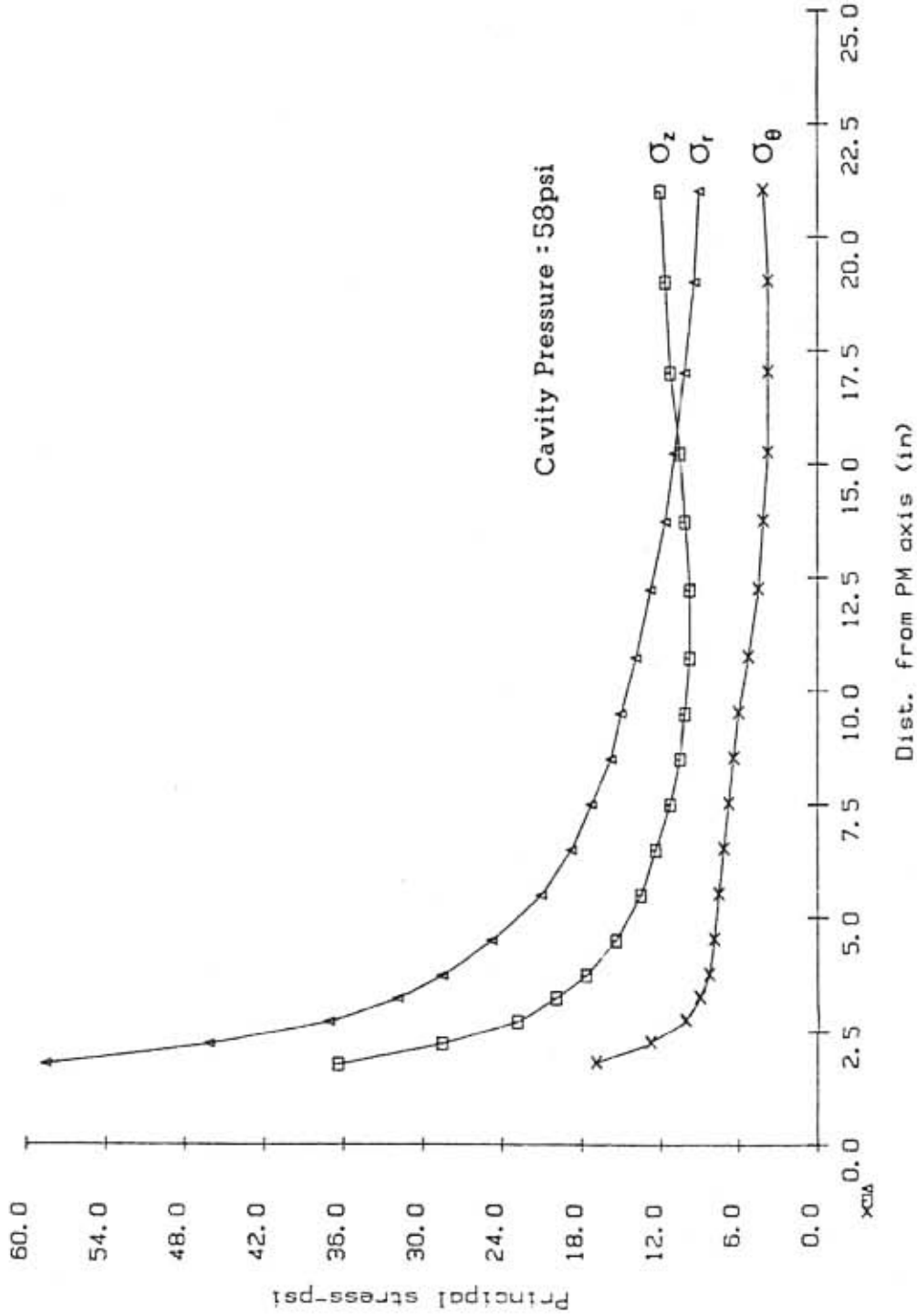


Figure 6.16 Typical Distribution of Principal Stresses with Distance from Axis of Self-Boring Pressuremeter

CHAPTER 7
CONCLUSIONS AND RECOMMENDATIONS

The primary goal of this thesis was to critically examine the practicality of the bounding surface elasto-plastic constitutive model along stress paths other than the triaxial and the isotropic consolidation loading paths which were used to standardize the model parameters. The outcome of this investigation indicate that the model performed with mixed success along the designated impartial stress paths, i.e. the pressuremeter stress path and the K_0 consolidation path. First, the simulation of the soil response when subjected to the cylindrical cavity finite element representation generated a "pressuremeter curve" which agreed closely with the experimentally observed stress-strain behavior. This statement is however only valid for one of the laboratory boundary conditions reproduced (i.e. B.C. #1), and it is perhaps appropriate not to include the results of the B.C. #3 simulation in an appraisal of the utility of the model since the results of this test may have been alternatively biased by the representation of the boundary state used in numerical analysis. The second "general" loading path scrutinized, K_0 consolidation, afforded less impressive results; the magnitude of the coefficient of lateral earth pressure was

much higher than the observed value, and, more interestingly, it was found that the bounding surface theory mathematically modeled the value of K_0 as a decreasing function of the level of bulk stress.

We can therefore conclude that the bounding surface constitutive equations functioned rationally along the pressuremeter stress path, but failed to provide credible results in its application to simulate the magnitude of K_0 .

These problems that arose in the course of research suggest a host of possible arenas in which to concentrate subsequent research efforts. The following is a list of recommendations which may be categorized under three general headings: 1) the bounding surface elasto-plastic model, 2) the finite element computer program, and 3) the controlled-environment pressuremeter tests.

Conclusions and Recommendations on B.S. Model

1a. A comparison of the B.S. model to other commonly used elasto-plastic theories with the intention of identifying the key differences which lead to the erroneous K_0 predictions should be of foremost importance. The Lade model (presented in Chapter 2) has been used successfully to model this loading path (Aboim, 1981), and it will be illuminating to comparatively explore the elements of both these constitutive laws in order to recognize and correct the existing problems in the mathematical modelling of K_0 by the bounding surface theory.

1b. The three-dimensional shape of the bounding surface in principal stress space can be visualized by imagining cross-sections cut through the \sqrt{J} vs. I plane and the octahedral plane. The form of the surface in each of these planes plays an integral role in determining the path of the plastic strain rate tensor since its direction is uniquely defined by the normal to the bounding surface at the image stress coordinate. For the present bounding surface model, the shape in \sqrt{J} vs. I space is shown in figure #3.1 while the shape of the surface is circular when viewed on the octahedral plane. The significance of the functional form on the octahedral plane becomes evident when one realizes that the soil response is indifferent to the shape of the surface on the octahedral plane whenever two of the three principal stresses are equal. This happens to be exactly the case for the triaxial test and the hydrostatic compression stress paths, both of which are used to calibrate the model. However, under general loading conditions, such as in the pressuremeter stress path, where the three principal stresses are changing simultaneously, there is movement of the stress path around the surface on the octahedral plane, and as has been mentioned, none of the experiments used to calibrate the model offer any indication of the performance of the constitutive law when the stress path moves along such a three-dimensional course.

Since the conventional laboratory experiments presently used in calibration procedures do not provide any grounds

for justifying the use of a circular bounding surface section on the octahedral plane, the author urges the initiation of a laboratory study at the University of Florida to inspect the suitability of the surface in predicting soil response when all three principal stresses are permitted to vary; such an investigation was carried out by Dr. Lade, who is now at UCLA, using a cubical triaxial device, and his results suggest the trace of the yield/failure surface on the octahedral plane should be as exhibited in figure 2.3. The writer therefore also recommends a feasibility study into possible replacement of the current functional form of the bounding surface by the equation of the yield criteria (eqns. 2.7.9 and 2.7.12) as proposed by Lade.

1c. Another important aspect of general loading paths, which is not taken into account by the existing bounding surface theory, is the influence of rotation of the principal planes on the stress-strain properties of the soil medium. If we use standard triaxial test data as the source of information for proposing the shape of a bounding surface, we cannot generalize this shape for arbitrary loading conditions unless we assume that the material is always isotropic or the principal planes undergo no rotation as a result of the applied general loading. Geotechnical engineers do encounter many practical situations where the coordinate reference axes of the principal planes are not fixed; for instance, such a situation would have emerged in

this thesis if we had considered an axi-symmetric expansion of the pressuremeter without the constraint of plane strain. Based on these arguments, it is advocated that a controlled study be performed to investigate the effect of principal plane rotation on the constitutive nature of the material; the ideal apparatus for achieving this objective would be a triaxial test on a hollow cylindrical specimen subjected to axial and torsional stresses (Saada and Townsend, 1981).

1d. Presently, stress-induced or native anisotropy is modelled by using a non-associated flow law in which normality is associated to a plastic potential rather than to the bounding surface. The approach involves finding an appropriate potential function to simulate the anisotropic qualities of the material; in the opinion of the author, this approach has no rational basis since it is merely a curve-fitting scheme used to recreate the laboratory test data. Although an in-depth strategy has not been fully ruminated, the author proposes a concept for modelling anisotropy which combines the use of an ellipsoid as a density function (similar to that used by Chang, 1983) to devise an anisotropy index which can then be introduced into the framework of the continuum mechanics approach. The shape of the density function (see figure 2.4 c) will be controlled by the magnitudes of the principal stresses which bears greater physical significance than the plastic potential function in manifesting the degree of particle

packing (or number of inter-particle contacts) in the principal stress directions.

1e. The wide variation in the computed model parameters R and S demonstrate the necessity for a reassessment of the method used to normalize triaxial stress-strain data. Some sort of statistical analysis will be useful in seeking an improved function of the confining pressure which could be used to produce a consistent set of model parameters from a single triaxial test. The data suggests that the confining pressure should be expressed in exponent form with the exponent being greater than one; an additional model parameter can be included by making this exponent a variable to be determined by trial and error.

1f. The deficiency of good triaxial dilatation predictions lends credence to two conceivable modifications: i) the logarithmic portion of the bounding surface should be substituted with a more suitable continuous function such as a hyperbola, and ii) the parameter Q, which control the major and minor axes of the ellipse, can be experimented with as being a function of the hardening parameter rather than fixing it as a constant value for all ranges of stress-strain behavior.

1g. From a more fundamental standpoint, Malvern (personal communication 11/2/83) expresses some uncertainty regarding the use of the plastic strain tensor as the sole substate variable to describe the contemporaneous constitutive equations of many materials including soils.

He argues that it is possible to arrive at the same state of plastic strain in a soil mass by following very dissimilar loading stages, but we would expect the soil response to be somewhat dependent on the detailed history of its loading in order to truly characterize its constitution. Therefore, using the plastic strain tensor does not afford a means of completely defining the current stress-strain characteristics of the material, but he goes on to add that we are yet to detect a suitable replacement or complement to the plastic strain tensor as a state variable. Finally, Malvern concludes that we should in no way expect to precisely model general behavior from a simple phenomenological model since we do not reckon into these equations the microscopic factors affecting soil response such as the texture, size, shape, angularity, etc.

Conclusions and Recommendations on Computer Program

2a. The most crucial limitation of the computer program was the lack of routines to permit simulation of a constant stress boundary condition. The author feels that the results of B.C. #3 pressuremeter simulation may have been more closely modelled if this boundary condition could have been imposed. If this program is to be used in the future for similar applications, the writer strongly recommends incorporation of the constant stress boundary condition capability.

2b. The [CL] matrix (i.e. the constitutive relationship) which is used to determine the element

stiffness matrix in the finite element program is assumed to be symmetric; this matrix is only symmetric however when associative flow is implemented in the bounding surface analysis. It is possible that in some eventual research situations, a non-associative flow rule with a corresponding asymmetric [CL] matrix will be appropriate for analysis so it is important to consider modifying the program to solve for the nodal displacements in the terms of the nodal forces when the element stiffness matrices (which are stored in the global stiffness matrix) are not symmetric; in matrix notation, this is represented as $[Q] = [K][u]$ where Q are the nodal forces, K is the global stiffness matrix, and u are the nodal displacements. This would require the replacement of the present solution technique in the subroutine BANSOL by a more general Gauss-Jordan or Gauss-Seidel method for solving the system of simultaneous linear equations.

2c. In elasticity, the strain definition is based on an initial state against which the current configuration is compared; it is assumed that the detailed process by which the material has moved from the initial state to the current configuration does not affect the final state, provided the process is elastic. Even with this assumption the characterization of the state of strain is not so simple unless the displacements and displacement gradients are small; in fact, only when they are infinitesimal is the so called small strain theory rigorously true.

Nevertheless, in metals, where elastic strains usually are not much greater than 0.002, the infinitesimal strain theory gives good results for practical purposes (Malvern, 1969), and since this computer program was originally developed for linear elastic analysis of metals, it was therefore appropriate to use the Lagrangian description of strain. When the displacement-gradients are not small compared to unity, as may be the case in elasto-plastic analysis of soil stress-strain response, it will be necessary to improve the precision of the numerical analysis by introducing a different characterization of strain. Before going on to suggest a better option for describing the strains during elasto-plastic analysis of soils, it is instructive to explain the relevant description of motion of a continuum (based on classical non-relativistic kinematics): the referential description has as its independent variables a) the position of the particle in an arbitrarily chosen reference configuration and b) the time t . However, for elastic analysis, the reference configuration is usually chosen to be the natural or unstressed state at time $t = 0$, and this is the so-called Lagrangian description which is presently used in the finite element program. It is advised then that we replace this strain description by a referential description which is updated after application of each load increment (this is commonly referred to in literature as an updated Lagrangian description). The basic difference between the Lagrangian description and this

proposed updated Lagrangian description would be that the computation of the element strains will not be based on the unstressed configuration, but more realistically on the continuously revised geometry of the finite element.

Conclusions and Recommendations on SPBM Lab Tests

3a. An attempt should be made to perform at least two pressuremeter tests under identical conditions in order to judge the degree of variability in the prepared samples introduced by the sand rain technique. This will also indicate the level of reliability of the observed cavity expansion data so that these tests may be able to serve unquestionably as a reference data base by which the predictive capability of constitutive relationships can be validated.

3b. Since the computer program in its present form can only model known displacement conditions at the boundary, it is advisable, if a similar study is ever done in the future, to subject the expanding pressuremeter to the boundary condition combination in the calibration chamber which permits no lateral or vertical displacement of the sand specimen. In modelling such a boundary condition, it will not be necessary to make adjustments to the finite element meshes, which proved to be an awkward demand in this research, to compensate for the constant stress boundary conditions which could not be represented exactly.

REFERENCES

- Aboim, Carlos A. "A Study of the Self-Boring Pressuremeter on Stiff Clay." Doctoral Dissertation, Stanford University, 1981.
- Aboim, C.A., and W.H. Roth. "Bounding-Surface Plasticity Theory Applied to Cyclic Loading of Sand." In International Symposium on Numerical Models in Geomechanics. Zurich, Switzerland: N.P., 1982.
- Al Hussaini, Mosaid M., and Frank C. Townsend. Investigation of K_0 Testing in Cohesionless Soils. Vicksburg, Miss.: U.S. Army Engineer Waterways Experiment Station, 1985.
- Ansal, A.M., R.J. Krizek and Z.P. Bazant. "Prediction of Soil Behavior by Endochronic Theory." In Limit Equilibrium, Plasticity and Generalized Stress-Strain in Geotechnical Engineering, ed. Raymond K. Yong and Hon Yim Ko. New York, N.Y.: ASCE, 1980.
- Baguelin, F., J.F. Jezequel and D.H. Shields. The Pressuremeter and Foundation Engineering. Clausthal, Germany: Trans Tech. Publications, 1978.
- Baladi, G.Y., and I.S. Sandler. "Examples of the Use of the Cap Model for Simulating the Stress-Strain Behavior of Soils." In Limit Equilibrium, Plasticity and Generalized Stress-Strain in Geo-Technical Engineering, ed. Raymond K. Yong and Hon Yim Ko. New York, N.Y.: ASCE, 1980.
- Chang, Ching S. "Constitutive Modeling for Sand - A Particulate Mechanics Approach." In Proceedings of the International Conference on Constitutive Laws for Engineering Materials, ed. C.S. Desai and R.H. Gallagher. Tuscon, Arizona: Department of Civil Engineering, University of Arizona, 1983.
- Christian, J.T. "User Needs: A View from Industry." In Limit Equilibrium, Plasticity and Generalized Stress-Strain in Geotechnical Engineering, ed. Raymond K. Yong and Hon Yim Ko. New York, N.Y.: ASCE, 1980.

- Clough, R.W., and R.T. Woodward. "Analysis of Embankment Stresses and Deformations." Journal of the Soil Mechanics and Foundation Division. ASCE, Vol. 93, No. SM4 (July, 1967): 529-549.
- Dafalias, Y.F., L.R. Hermann and J.S. DeNatale. "Description of Natural Clay Behavior by a Simple Bounding Surface Plasticity Formulation." In Limit Equilibrium Plasticity and Generalized Stress-Strain in Geotechnical Engineering, ed. Raymond K. Yong and Hon Yim Ko. New York, N.Y.: ASCE, 1980.
- Dafalias, Y.F., and E.P. Popov. "Plastic Internal Variables Formalism on Cyclic Plasticity." Journal of Applied Mechanics. ASME, Vol. 43, No. 4 (December 1976): 645-651.
- Davidson, J.L., K. Heidbrecht and J. Shoucair. Self-Boring Pressuremeter Testing in the University of Florida Calibration Chamber. Gainesville, Florida: Civil Engineering Department, University of Florida, 1983.
- Desai, C.S., and John T. Christian. Numerical Methods in Geotechnical Engineering. New York, N.Y.: McGraw-Hill Book Co., 1977.
- Drucker, D.C., and W. Prager. "Soil Mechanics and Plastic Analysis or Limit Design." Quarterly of Applied Mathematics. Vol. 10, No. 2 (July, 1952): 157-175.
- Duncan, J.M. and C.Y. Chang. "Non-Linear Analysis of Stress and Strain in Soils." Journal of Soil Mechanics and Foundation Division. ASCE Vol. 96, No. SM5 (September, 1970): 1629-1653.
- Hill, R. The Mathematical Theory of Plasticity. London: Oxford University Press, 1950.
- Hodge, Jr., P., and G.H. White, Jr. "A Quantitative Comparison of Flow and Deformation Theories of Plasticity." Journal of Applied Mechanics. ASME, Vol. 17, No. 2 (1950): 180-184.
- Hughes, J.M. "An Instrument for the Insitu Measurement of the Properties of Soft Clay," Doctoral Dissertation, University of Cambridge, 1973.
- Hughes, J.M., C.P. Wroth and D. Windle. "Pressuremeter Tests in Sands." Geotechnique. Vol. 30, No. 4 (1977): 455-477.
- Jain, S.K. Fundamental Aspects of the Normality Rule. Blacksburg, Virginia: Engineering Publications, 1980.

- Jewell, R.J., M. Fahey and C.P. Wroth. "Laboratory Study of the Pressuremeter Test in Sand." Geotechnique. Vol. 30, No. 4 (1980): 507-531.
- Koiter, W.T. "On Partially Plastic Thick-Walled Tubes." Biezano Anniversary Volume in Applied Mechanics. Stan Harlem: N.P., 1953.
- Kondner, R.L. "Hyperbolic Stress-Strain Response: Cohesive Soils." Journal of the Soil Mechanics and Foundation Division. ASCE, Vol. 89, No. SMI (January, 1963): 115-143.
- Lade, Poul V. "Elasto-Plastic Stress-Strain Model for Sand." In Limit-Equilibrium, Plasticity and Generalized Stress-Strain in Geotechnical Engineering, ed. Raymond K. Yong and Hon Yim Ko. New York, N.Y.: ASCE, 1980.
- Laier, J.E., J.H. Schmertmann and J.H. Schaub. "Effect of Finite Pressuremeter Length in Dry Sand." Proc. Spec. Conf. on Insitu Testing. ASCE, Vol. 1 (1975): 241-259.
- Lheur, J.M. "An Experimental Study on Quasi-Static Cone Penetration Tests on Saturated Sands," Master's Thesis, University of Florida, 1976.
- Little, R.W. Elasticity, Englewood Cliffs, New Jersey: Prentice-Hall Inc., 1973.
- Malvern, L.E. Introduction to the Mechanics of a Continuous Medium. Englewood Cliffs, New Jersey: Prentice-Hall Inc., 1969.
- Mana, A.I. "Finite Element Analysis of Deep Excavation Behavior in Soft Clay," Doctoral Dissertation, Stanford University, 1978.
- Mendelson, A. Plasticity: Theory and Application. New York: N.Y.: Macmillan Publishing Co., 1978.
- Mizuno, E., and W.F. Chen. "Plasticity Models for Soils - Theory and Calibration." In Limit Equilibrium, Plasticity and Generalized Stress-Strain in Geotechnical Engineering, ed. Raymond K. Yong and Hon Yim Ko. New York, N.Y.: ASCE, 1980.
- Poorooshasb, H.B., and B. Lelievre. "Expansion of Cavities in Sand." In Application of Plasticity and Generalized Stress-Strain in Geotechnical Engineering, ed. R.N. Yong and E.T. Selig. New York, N.Y.: ASCE, 1980.

- Prager, W. "Recent Developments in Mathematical Theory of Plasticity." Journal of Applied Physics. Vol. 20 (1949): 235-241.
- Prevost, J.H., and B.E. Hjorth. "Plastic-Limit Equilibrium States in Soil Media." In Application of Plasticity and Generalized Stress-Strain in Geotechnical Engineering, ed. R.N. Yong and E.T. Selig. New York, N.Y.: ASCE, 1980.
- Saada, A.S. and F.C. Townsend. State of the Art: Laboratory Strength Testing of Soils. Special Technical Publication 740, Philadelphia, Pa.: ASTM, 1981.
- Schofield, A., and Peter Wroth. Critical State Soil Mechanics. New York, N.Y.: McGraw-Hill Book Co., 1968.
- Taesiri, Y., M.C. McVay and F.C. Townsend. Evaluation and Development of Constitutive Models to Characterize Moving Wheel Stress Paths. Project No. 244*W17. Gainesville, Florida: Civil Engineering Department, University of Florida, 1983.
- Timoshenko, S.P., and J.N. Goodier. Theory of Elasticity. New York, N.Y.: McGraw-Hill Book Co., 1970.
- Wilson, Edward L. "Structural Analysis of Axisymmetric Solids." AIAA Journal. Vol. 3, No. 12 (December, 1965): 2269-2274.
- Wood, D.M., and C.P. Wroth. "Some Laboratory Experiments Related to the Results of Pressuremeter Tests." Geotechnique. Vol. 27, No. 2 (1977): 181-201.
- Wroth, C.P. "British Experience with the Self-Boring Pressuremeter." In Symposium on the Application of the Pressuremeter organized by the French Petroleum Institute, April 1982 at Ponts et Chaussees.
- Yong, R.N., and H.Y. Ko. "Soil Constitutive Relationships and Modelling of Soil Behavior." In Limit Equilibrium, Plasticity and Generalized Stress-Strain in Geotechnical Engineering, ed. Raymond K. Yong and Hon Yim Ko. New York, N.Y.: ASCE, 1980.
- Zienkiewicz, O.C. The Finite Element Method. London, England: McGraw-Hill Book Co., 1982.

APPENDIX A
TRIAxIAL TEST DATA

TRIAxIAL COMPRESSIOn TEST RESULTS

Effective Confining pressure (psf) = 50
 Estimate of Young's Modulus (psi) = 4000
 Estimate of Poisson's Ratio = .25
 Unit weight (pcf) = 102.6
 Performed by Townsend & Devo

Results of regression analysis:
 Model parameter, R = .09
 Model parameter, S = .16
 Correlation coefficient = .93

Slope of critical state line = .249

Deviatoric Stress (psi)	Total Axial Strain (%)	Total Volumetric Strain (%)	Major Principal Stress (psi)	Elastic Axial Strain (%)	Elastic Volumetric Strain (%)	Plastic Axial Strain (%)	Plastic Volumetric Strain (%)	Elastic Shear Strain (%)	Plastic Shear Strain (%)	2nd Inv. of Stress Tensor (psi)	Sig. Coefficient	Root J
0.00	0	0	50.00	0.462952953	1.988888889							
40.16	.11	.07	99.16	0.910707070	0.855185185	0.189239390	0.244614615	0.033552137	70.38293923	0.164859574		
61.19	.07	.12	111.19	1.135148148	0.966574074	0.068518521	0.152439396	0.019328655	76.37067756	0.07467116		
62.60	.13	.08	112.56	1.150370370	0.980185185	0.135829520	0.215914615	0.037467753	66.11617754	0.093486208		
67.93	.15	.05	117.93	1.237962963	0.620311431	0.242070370	0.171018519	0.160221429	59.31940765	0.284288496		
73.02	.18	.08	123.02	1.352222222	0.675111111	0.447777778	0.175308659	0.352035269	42.15811679	0.417505516		
75.41	.13	.09	128.44	1.372929293	0.726596596	0.447407407	0.175703704	0.37322241	40.39745110	0.372424311		
81.19	.22	.11	133.19	1.510555556	0.770777778	0.653444444	0.257122272	0.504700548	48.02976802	0.25448711		
85.20	.24	.11	138.28	1.654814615	0.817407407	0.765185185	0.182582593	0.609393883	50.92848129	0.28463650		
93.95	.26	.11	143.95	1.728793704	0.864251052	0.771395735	0.252682183	0.686526366	57.02247472	0.362911035		
95.42	.29	.11	148.42	1.822327273	0.911266266	1.077407407	0.183707704	0.783881118	56.22231348	0.372098523		
102.5	.32	.12	153.50	1.916656567	0.958302939	1.283539393	0.241656567	1.041626111	59.75575283	0.871528100		
108.56	.34	.12	158.56	2.01030370	1.005185185	1.399295740	0.174814815	1.147213368	67.87714421	0.915791821		
112.95	.38	.12	163.95	2.110185185	1.051970393	1.629614615	0.144937407	1.42151292	57.18365718	1.000485009		
119.39	.44	.11	169.39	2.209318918	1.101735293	2.196481481	1.75376574	1.923716616	60.8380951	1.94827039		
124.21	.47	.11	174.21	2.300185185	1.150002593	2.939814615	0.005092729	2.62718180	71.127692	1.49129104		
127.38	.55	.11	179.38	2.395252525	1.197362263	3.104074074	0.34625650	2.745795236	74.677777	1.83759974		
134.0	.58	.09	184.60	2.492929293	1.246286286	3.207407407	0.34625650	2.964265849	77.1184671	1.597228521		
132.44	.7	.07	189.44	2.582227272	1.291111111	4.417777778	0.991111111	3.936546662	80.60572132	2.482198826		
141.24	.9	.04	194.24	2.670555556	1.339371718	6.294444444	1.0357178	5.00938653	83.3996250	3.41123121		
147.24	1.11	.04	199.24	2.76666667	1.383232323	8.973539394	1.45353939	7.073947379	85.0090351	4.513601906		
152.92	1.18	.04	204.24	2.86666667	1.427362363	1.665240741	1.897362363	8.92584919	87.1487930	4.92993339		
157.01	1.36	.11	209.01	2.96952939	1.47378296	1.882407407	2.348362363	9.927113939	90.1491574	5.54142172		
161.89	1.55	.12	213.89	3.06851852	1.49942526	1.250914615	3.49825393	1.18512526	92.4729304	6.28027372		
166.35	1.78	.15	218.90	3.091666667	1.498232323	1.470333333	4.645232323	1.40352688	96.2862742	7.60203946		
171.86	2.07	.18	224.90	3.18252939	1.51296206	1.75140741	6.39129630	1.70152814	99.7294173	8.574551009		
176.48	2.40	.17	226.48	3.268148148	1.534074074	2.15385185	8.63407407	2.11330713	101.890775	1.037564827		
180.07	3.01	.15	230.87	3.334444444	1.574222222	2.675055556	1.17717272	2.6567232	104.473543	1.771906308		
185.4	3.5	.13	235.40	3.432929393	1.616666667	3.156666667	1.47166667	3.18557099	107.0107993	1.475413521		

TAXIAL COMPRESSION TEST RESULTS

Effective confining pressure (psf) * 42
 Estimate of Young's Modulus (psf) * 54000
 Estimate of Poisson's Ratio * .25
 Unit Weight (pcf) * 104.02
 Performed by Heidebrecht

Results of regression analysis :
 Model parameter, R * .153
 Model parameter, S * .406
 Correlation coefficient * .9333

Slope of critical state line * .237

Reviatoric Stress (psi)	Total Axial Strain (%)	Total Volumetric Strain (%)	Major Principal Stress (psi)	Elastic Axial Strain (%)	Elastic Volumetric Strain (%)	Plastic Axial Strain (%)	Plastic Volumetric Strain (%)	Plastic Shear Strain (%)	Plastic Equivalent Strain (%)	2nd Inv. of Deviator	Sig Co	Elev Root J
0.00	0	0	45.00	.0416565667	.125							
1.76	.052	0	45.75	.052352533	.001626226	.007407407	-.001626226	.0426811532	1.016196474	1.890151316		
4.4	.125	.007	45.40	.061451461	.004074074	.1175518519	-.002929293	.1017183555	2.346341184	1.752992425		
21.9	.479	.028	66.30	.040535556	.020271778	.128444444	.007327272	.1176571924	12.64355009	.183703289		
44.7	.866	.076	80.70	.082777778	.041588889	.152327272	.034011111	.1485833318	28.90759003	.593561522		
61.7	.954	.111	102.10	.115814814	.0533004074	.2441851852	.050092926	.1371010077	37.9846241	.273225606		
81.2	.949	.131	125.20	.150797979	.071831852	.257639296	.0593148148	.2416424710	46.68684185	.2314718634		
94.2	.886	.131	139.20	.174444444	.087222222	.411555556	.043777778	.343280103	54.34835534	.284473031		
104.0	.711	.124	143.60	.193707073	.0368518519	.3167962969	.0271481481	.4332887132	60.31028514	.3275342934		
170.9	.96	.069	165.90	.223988889	.111944444	.756111111	-.042944444	.6498873155	69.06164753	.412372919		
131.1	1.205	-.014	175.10	.243777778	.121208889	.962727273	-.152569339	.8725922943	75.63062027	.5183594205		
136.6	1.454	-.111	151.60	.2585105105	.123252793	1.139481482	-.232529293	1.104385532	80.59804756	.6166618725		
146.8	1.698	-.234	131.80	.2718918519	.159329293	1.426148148	-.36292926	1.341869342	84.75501950	.7124545870		
152.2	1.95	-.366	131.20	.2818518519	.140929293	1.663148148	-.50692926	1.539333334	87.8721050	.8147558040		
157.2	2.207	-.51	202.20	.291111111	.145555556	1.915888889	-.652555556	1.84841037	76.7734629	.9164917505		
161.8	2.459	-.662	286.40	.299676296	.1430148148	2.163370270	-.811814815	2.107984450	93.41521753	1.015409371		
167.0	2.715	-.828	210.30	.304814815	.152401407	2.409510519	-.90240741	2.363093026	95.50146953	1.11572793		
163.0	2.93	-.933	213.80	.315792926	.152362963	2.669407408	-.114929630	2.630753667	97.4952912	1.217041864		
171.9	3.251	-1.263	217.30	.321891852	.160959293	2.60014815	-.143303293	3.03200120	99.510512	1.360193441		
173.4	3.413	-1.358	220.10	.324252529	.161206296	3.289740741	-.50012963	3.281183151	101.824021	1.465533494		
174.4	3.784	-1.379	221.40	.3243148148	.1624074074	3.411818185	-.51440741	3.40666222	101.2672972	1.519359331		
176.4	3.803	-1.476	221.00	.326456667	.153933333	3.535933333	-.635933333	3.537521322	101.8449875	1.56495272		
175.8	4.371	-1.939	224.80	.330959293	.164914815	4.02037037	-.90140140	4.07230532	103.007844	1.764431754		
181.1	5.009	-2.927	227.10	.332222222	.168611111	4.67177778	-.24636111	4.757130556	103.135340	2.036360917		
184.5	5.303	-2.366	225.30	.341686667	.170933333	5.56133333	-.31683333	5.721281701	106.5781246	2.41114798		
184.9	5.294	-3.552	229.30	.342074074	.172057037	5.59159293	-.52520570	6.177291602	101.7506447	2.60430054		
184.4	6.408	-3.448	223.40	.3414814815	.1737407407	6.66519519	-.61814074	6.298593620	106.459394	2.62210774		
183.6	6.935	-5.834	226.60	.340000000			-.5334	6.861513274	106.0015094	2.81261648		
181.7	6.22	-4.507	224.70	.3364814815	.1624074074	7.365510519	-.86524074	8.213393411	104.491133	3.52234939		
180.3	9.592	-5.007	225.20	.339896009	.1669444444	9.26011111	-.51754444	9.514050573	104.0942035	4.112450573		

TRIAL COMPRESSION TEST RESULTS

Effective confining pressure (psi) = 35
 Estimate of Young's Modulus (psi) = 5400
 Estimate of Poisson's Ratio = .25
 Unit Weight (pcf) = 103.6
 Performed by Heidebrecht

Results of regression analysis 1
 Model parameter, R = .12
 Model parameter, S = .4
 Correlation coefficient = .9371
 Slope of critical state line = .262

Deviatoric Stress (psi)	Total Axial Strain (%)	Total Volumetric Strain (%)	Major Principal Stress (psi)	Elastic Axial Strain (%)	Elastic Volumetric Strain (%)	Plastic Axial Strain (%)	Plastic Volumetric Strain (%)	Plastic Equivalent Shear Strain (%)	Sq. Root of Deviator Stress (psi)	Sig C ₁ Root J	Sig C ₂ Root J
0.00	0	0	35.00	.0324074074	.0372222222						
23.9	.081	0	58.90	.0442592593	.021236298	.0367487407	-.022129030	.0367066886	13.78857143	.0562103518	
40.7	.139	.014	75.70	.0737037037	.0376831852	.0636236296	-.073693185	.0619421697	23.44815345	.0727614798	
55.7	.23	.042	90.70	.1031481481	.0519740741	.1268518519	-.009574074	.1126202737	32.17940909	.1223721458	
68	.342	.07	103.00	.1232239239	.0623629650	.2160740741	.007670370	.1859343195	39.23001830	.1550198933	
70.4	.354	.097	105.40	.1307037037	.0691831852	.3236296296	.0731814814	.2719673947	46.61544094	.2234366065	
87.2	.559	.105	122.20	.1618148148	.0874740741	.3973185185	.024292593	.3712580206	50.34333346	.2344831323	
97.3	.683	.097	123.30	.1727777778	.0863688889	.5102222222	-.016111111	.428022421	53.35678010	.2831122425	
107.8	.917	.042	137.60	.1937037037	.095181032	.7266236296	-.137183185	.6688816702	58.3168766	.3344435438	
107.2	1.05	-.084	142.20	.1905185185	.092525293	.8514314815	-.182525293	.7903063852	61.89134284	.4403193144	
111	1.107	-.139	146.00	.2057555556	.107777778	.9294444445	-.24177778	.9009383050	64.01587306	.4310094096	
116.6	1.416	-.265	151.60	.219239239	.105663650	1.200074074	-.37236363	1.14659768	67.3190137	.5913185314	
121.7	1.666	-.404	156.70	.2237037037	.1126831852	1.4406236296	-.516603185	1.336776822	70.2352771	.6957636693	
126.4	1.916	-.543	161.40	.2340740741	.1176575370	1.681923926	-.650837037	1.547126860	72.9707401	.8330664501	
129.8	2.167	-.773	161.60	.2407037037	.1218181852	1.921623630	-.893163185	1.927359557	74.24006432	.836823603	
137.6	2.418	-.877	169.60	.2474074074	.1237037037	2.170525993	-.00070370	2.162666603	77.13599305	.9816451845	
136.1	2.603	-1.009	171.10	.2530370370	.126105185	2.41692363	-.18970370	2.43276706	78.57737167	1.014703214	
137.8	2.925	-1.253	172.80	.25181852	.12739296	2.66884819	-.18905759	2.710670205	79.53886708	1.194998019	
140.3	3.193	-1.434	175.30	.258143148	.127974074	2.92393185	-.36390741	2.93013212	81.02227275	1.40832097	
140.6	3.439	-1.617	175.60	.2607037037	.130181852	3.178623630	-.78718513	3.268689593	81.17544285	1.40344219	
141.7	3.566	-1.735	176.70	.2624074074	.1320703703	3.376923630	-.85620370	3.404975717	81.81053312	1.56937376	
143.5	3.818	-1.925	179.30	.2657407407	.1328703704	3.52729296	-.00707037	3.67209317	82.84976361	1.551766360	
146.5	4.07	-2.145	181.20	.2712962963	.1356481481	3.788703704	-.275064815	3.948140320	84.58151442	1.637142374	
147.2	4.191	-2.396	182.20	.273939296	.1362362963	4.428407408	-.252723630	4.565124288	84.389595960	1.880479444	

TRIAXIAL COMPRESSION TEST RESULTS

Effective confining pressure (psf) = 25
 Estimate of Young's Modulus (psi) = 34000
 Estimate of Poisson's Ratio = .25
 Unit Weight (pcf) = 102.58
 Performed by Handbracht

Results of regression analysis:
 Model parameter, P = .132
 Model parameter, S = .343
 Correlation coefficient = .9932

Slope of critical state line = .26

Deviatoric Stress (psi)	Total Axial Strain (%)	Total Volumetric Strain (%)	Major Principal Stress (psi)	Elastic		Plastic		Plastic		Plastic Equivalent Shear Strain (%)	2nd Inv. of Deviator Stress (psi)	Sig. Cr. Est. Root J
				Axial Strain (%)	Volumetric Strain (%)	Axial Strain (%)	Volumetric Strain (%)	Shear Strain (%)				
0.00	0	0	25.00	.0231481481	.0694444444							
35.74	.503	-.055	60.74	.0651851852	.0320255276	.2985148148	.0218074074	.7507280461	20.63449867	30.97692492		
60	.543	-.082	85.00	.1111111111	.0555555556	.4938888889	.0744444444	.3631232486	34.84101614	20.95712364		
67.8	.606	-.069	92.00	.1535555556	.0627777778	.4934444444	.0662222222	.4128889922	39.14431824	26.15055819		
79.8	.723	-.077	98.80	.1366666667	.0693333333	.5805555556	.0406333333	.5195039347	42.60344586	29.83153441		
78.1	.899	-.014	103.10	.1446296236	.0723148148	.6343705784	.0863348183	.6762532212	45.03185601	24.72322594		
85.3	1.071	-.11	110.80	.1588888889	.0794444444	.9121111112	.1934444444	.8445929299	49.35653368	42.62446764		
90.3	1.304	-.261	115.90	.1633333333	.0416666667	1.135666667	.2451666667	1.003157218	52.48113946	51.93745142		
95.1	1.556	-.412	121.10	.1779629630	.088814815	1.593378037	.500981481	1.32015137	53.6838086	39.00927396		
94.6	1.629	-.376	124.10	.1844444444	.0722222222	1.443555556	.608222222	1.403970748	51.36406660	62.74709397		
104.7	1.373	-.824	129.70	.1938888889	.0963444444	1.779111111	.928944444	1.806609169	60.44673317	71.17678342		
107.2	2.532	-1.123	132.20	.1985185185	.0922922222	2.153481482	1.22725926	2.218362876	61.09194084	69.60708612		
110.4	2.856	-1.386	135.40	.2044444444	.1022222222	2.651555556	1.43822222	2.75927223	63.73546970	1.063167673		
112.9	3.224	-1.69	137.90	.2090740741	.1045370370	3.01435926	1.79453704	3.129040603	65.18274528	1.206101286		
114.3	3.612	-2.005	139.50	.2120370370	.1080185185	3.39962303	2.11101852	3.455887853	66.10660581	1.31345525		
117	4.116	-2.431	142.00	.2166666667	.1083333333	3.839333333	2.53333333	4.103584116	67.34938148	1.521026222		

ISOTROPIC COMPRESSION TEST DATA

Diameter of specimen (in.) * 2.7189
 Height of specimen (in.) * 7.289
 Volume of specimen (cc) * 724.12105
 Weight of specimen (gm) * 107.45303
 Density of sample (lb/cu ft) * 81
 Estimated relative density * 81
 -P- value (k) * 32.6
 Estimated bulk modulus (psi) * 36000
 Estimated β (psi) * .0005
 Estimated β (k) * 7.8
 Test performed by Townsend & Devo

Increment No.	Chamber Pressure (psi)	Back Pressure (psi)	Effective Confining Stress (psi)	Volume Change (cc)	Increment Volume Strain (%)	Total Volume Strain (%)	First Invariant (psi)	First Invariant (psi)	Change in First Invariant (psi)	Increment		Increment	
										Elastic Volume Strain (%)	Plastic Volume Strain (%)	Elastic Volume Strain (%)	Plastic Volume Strain (%)
START	70	60.73	9.27	START	0	0	27.81	27.81	0	0	0	0	
1	75	60.78	14.22	.15	.0433379	.0433379	42.66	42.66	14.95	.01375	.01375	.0261111	.0261111
2	80	60.79	19.21	.3	.04142037	.08475827	51.69	51.69	14.97	.01386111	.01375	.02713165	.02713165
3	85	60.79	24.21	.29	.04004800	.12480627	71.63	71.63	15	.01389889	.04158000	.0291076	.0291076
4	90	60.73	29.21	.23	.03452414	.15933041	81.63	81.63	15	.01388889	.07538889	.02934801	.02934801
5	95	60.78	34.22	.13	.0262283	.18555871	72.66	72.66	-14.97	.01386111	.04157773	.02626577	.02626577
6	100	60.73	39.21	-.1	.0290003	.18355868	51.63	51.63	-15.03	.0139167	.0261111	.02140516	.02140516
7	105	60.75	44.2	.3	.0414203	.0266731	47.73	47.73	-14.98	.0137778	.01389333	.0293338	.0293338
8	110	60.74	49.2	.28	.0324767	.0159662	27.78	27.78	-14.97	.0138511	.0138511	.01521040	.01521040
9	115	60.78	14.22	.26	.04371476	.06490758	42.66	42.66	14.88	.0137778	.01375000	.01133593	.01133593
10	120	60.79	19.21	.27	.03728607	.10219345	51.63	51.63	14.37	.01386111	.0261111	.07438054	.07438054
11	125	60.78	24.22	.23	.03432414	.13651759	72.65	72.65	13.03	.01391667	.0413778	.0333181	.0333181
12	130	60.78	29.22	.24	.0314517	.16796976	82.66	82.66	13	.01388889	.0541667	.11444702	.11444702
13	135	60.8	34.2	.27	.03726007	.20523003	102.0	102.0	14.34	.01383333	.06325000	.13703483	.13703483
14	140	60.8	39.2	.26	.03590310	.24113313	117.0	117.0	13	.01388889	.06315803	.15911104	.15911104
15	145	60.8	44.2	.24	.03314317	.27427620	132.0	132.0	13	.01388889	.0530778	.17916532	.17916532
16	150	60.8	49.2	.26	.03530310	.31257931	147.0	147.0	13	.01388889	.11031667	.20118154	.20118154

APPENDIX B
SOURCE LISTING OF COMPUTER PROGRAM

APPENDIX B
SOURCE LISTING OF COMPUTER PROGRAM

```

C*****
C ANALYSIS OF AXISYMMETRIC SOLIDS BY THE FINITE ELEMENT METHOD
C CONSTITUTIVE LAW 13 BOUNDING SURFACE PLASTICITY MODEL
C PROGRAMMED BY DEVO SEEREERAM
C THIS PROGRAM IS A COMBINATION OF ORIGINAL PROGRAMS WRITTEN
C BY WILSON (I.E. AXSYN) & TAESIRI (ELASTO-PLASTIC CONSTITUTIVE LAW)
C*****
      IMPLICIT REAL*8 (A-H,O-Z)
      REAL*4 HED(20)
      COMMON/INTGR/NUMNP, NUMEL, NUMMAT, NUMPC, NP, IBC(20), JBC(20), NPLATE,
1 NUMCOL, NUMROW, IX(550,5), NPP1, NPP2, NPP, MTYPE, NSTEP, NDUMMY(550), N,
1 ICHANGE, MAXPRIN1, IPRINT, ISOTROP, NCRIT
      COMMON/PROP/RO(50), AKO(50), EE(7), ET(10), MATYP(34)
      COMMON/PARM/EG, EK, XR, XS, XT, XU, XW, XD, BN, RIO, GAMMA, HBU, HBL
      COMMON/LOAD/CODE(500), T(500), TEMP, PR(20), ACELZ, ANCFG, ANGLE(4)
      COMMON/GEOM/R(500), Z(500), UR(500), UZ(500), RADIST(25), ELEV(34)
1 ROWTMP(34), DISP(500,2)
      COMMON/STRESS/SIGMA(4,550), G, PZERO, RZERO, GSTRSS(550),
1 PATM, AIO(550), AHARD(550), XAHARD(550), ETA(550), SIGDOT(4,550),
1 PHYDM, BKS(550), ZETA(550)
      COMMON/ARG/S(10,10), P(10), TT(4), DD(3,3), HH(6,10),
1 RR(4), RRE(4,550), RRP(4,550), RRT(4,550), ZZ(4), C(4,4), CL(4,4,550),
1 H(6,10), D(6,6), F(6,10), TP(6), XI(10), LM(4), DADZETA(550),
1 DADZETA(550), DXADZETA(550), DXADZETA(550), VN(4,550), BETA(550),
1 VNSIG(550), ISIGN(550), DZETA(550), DETA(550), RRR(5,550),
1 ZZ(5,550)
      COMMON /BANARG/ B(116), A(116,58), MBAND, NUMBLK
C*****
C CALL TSKTME
C*****
C INITIALIZE
      ACELZ=0.0
      ANCFG=0.0
      DO 9990 I=1,20
1 IBC(I)=0
1 JBC(I)=0
9990 PR(I)=0
      DO 9991 I=1,4
1 ANGLE(I)=0
1 TT(I)=0
1 LM(I)=0
1 RR(I)=0
9991 ZZ(I)=0
      DO 9992 I=1,550
      DO 9992 J=1,5
9992 IX(I,J)=0
      DO 9993 I=1,20
9993 HED(I)=0
      DO 9994 I=1,34
1 MATYP(I)=0
1 ELEV(I)=0
9994 ROWTMP(I)=0
      DO 9995 J=1,10
9995 P(J)=0
      DO 9996 I=1,50
1 RO(I)=0
1 AKO(I)=0
1 ET(I)=0
9996 XI(I)=0
      DO 9997 I=1,500
1 CODE(I)=0
1 T(I)=0
1 R(I)=0
1 Z(I)=0
1 UR(I)=0
9997 UZ(I)=0
      DO 9998 I=1,25
9998 RADIST(I)=0
      DO 9999 I=1,500
1 VN(I)=0
      DO 9999 J=1,2
9999 DISP(I,J)=0

```

15
16
17
18
19
20
21
22
23
24
25
26
27
28
29
30
32
33
35
36
37
38
39
44
45
46
49
51
52
53
54
55
56
57
58
60
61

OCTOBER 28, 1983 15:13 NERDC -- SYSTEM SUPPORT UTILITIES -- CARDLI

```

DO 9989 I=1,4
DO 9989 J=1,550
9989 SIGMA(I,J)=0
DO 9988 I=1,550
NDUMMY(I)=1
9988 GSTRSS(I)=0
DO 9987 I=1,5
DO 9987 J=1,550
RRR(I,J)=0
9987 ZZZ(I,J)=0
DO 9986 I=1,10
DO 9986 J=1,10
9986 S(I,J)=0
DO 9985 I=1,3
DO 9985 J=1,3

9985 DD(I,J)=0
DO 9984 I=1,6
DO 9984 J=1,10
HH(I,J)=0
H(I,J)=0
9984 F(I,J)=0
DO 9983 I=1,4
DO 9983 J=1,4
9983 C(I,J)=0
DO 9982 I=1,6
DO 9982 J=1,6
9982 D(I,J)=0
DO 9981 I=1,6
9981 TP(I)=0
DO 9980 I=1,116
9980 B(I)=0
DO 9979 I=1,116
DO 9979 J=1,50
9979 A(I,J)=0
C*****
C READ AND PRINT OF CONTROL INFORMATION AND MATERIAL PROPERTIES
C*****
C 50 READ (5,1000) HEID, NUMNP, NUMEL, NUMMAT, NP, NBC, NEC
WRITE (6,2000) HEID, NUMNP, NUMEL, NUMMAT, NP, NBC, NEC
APP=NP
NPP=0
WRITE(6,2030)
C*****
C READ AND PRINT FIRST CYCLE LOAD APPROXIMATIONS AND ATM PRESSURE
C*****
C WRITE (6,2032)
READ(5,1005)RZERO,PZERO,PATM
WRITE(6,2012)RZERO,PZERO,PATM
C*****
C READ AND PRINT OF MATERIAL PROPERTY VALUES
C THIS DATA REQUIRES TWO CARDS PER MATERIAL TYPE
C*****
C 56 DO 59 MM=1, NUMMAT
READ (5,1001) N, R0(M), AKO(M), EG, EK, XR, XS, XT, XU, XW, XD, BN, RIO,
$GAMMA, HBU, HBL
59 WRITE(6,2015) N, R0(M), AKO(M), EG, EK, XR, XS, XT, XU, XW, XD, BN, RIO,
$GAMMA, HBU, HBL
2015 FORMAT(1X, 'MATERIAL # =', I5/
$1X, 'DENSITY =', F9.4/
$1X, 'COEFFICIENT OF LATERAL EARTH PRESSURE =', F10.2/
$1X, 'SHEAR MODULUS =', F10.0/
$1X, 'DULK MODULUS =', F10.0/
$1X, 'R =', E10.5, 10X, 'S =', E10.5/
$1X, 'T =', E10.5, 10X, 'U =', E10.5/
$1X, 'W =', E10.5, 10X, 'D =', E10.5/

```

62
64
66
67
70
71
72
73
74
75
76
77
78
79
80
81
82
83
84
85
86
87
88
90
93
94
95
96
97
98
101
102
103
105
107
108
109
110
111
112
113
114
115
117

```

$IX, 'SLOPE OF THE CSL =',E10. 5/
$IX, 'RATIO OF MAJOR TO MINOR AXES OF ELLIPSE =',E10. 5/
$IX, 'GAMMA - USED IN MAPPING RULE =',E10. 5/
$IX, 'CONSTANT USED IN COMPUTING UNLOAD PLASTIC MODULUS =',E10. 5/
$IX, 'CONSTANT USED IN COMPUTING RELOAD PLASTIC MODULUS =',E10. 5/
C*****
C
C READ POSITIONS OF BOUNDARIES BETWEEN ELEMENTS
C*****
      READ (5,1003) NPLATE, NUMCOL, NUMROW, NLHFRE, NRHFRE
      L=0
101  READ(5,1002) N, RADIST(N)
      IF(N.EQ.1) GO TO 102
      DELTN=N-L
      DELTR=(RADIST(N)-RADIST(L))/DELTN
102  L=L+1
      IF(L.EQ.NUMCOL+1) GO TO 103
      IF(L.EQ.N) GO TO 101
      RADIST(L)=RADIST(L-1)+DELTR
      GO TO 102
103  L=0
104  READ (5,1007) N, MATYP(N), ELEV(N)
      IF(N.EQ.1) GO TO 105
      DELTN=N-L
      DELTEL=(ELEV(N)-ELEV(L))/DELTN
105  L=L+1
      IF(L.EQ.NUMROW+1) GO TO 106
      IF(L.EQ.N) GO TO 104
      ELEV(L)=ELEV(L-1)+DELTEL
      MATYP(L)=MATYP(L-1)
      GO TO 105
C*****
C
C GENERATE NODAL POINT DATA
C*****
106  NCP1=NUMCOL+1
      NRP1=NUMROW+1
      NPP1=NPLATE+1
      NPP2=NPP1+1
      NCOL=0
      NROW=0
      DO 107 N=1, NUMNP
      NCOL=NCOL+1
      NROW=NROW+1
      CODE(N)=0.0
      IF(NCOL.EQ.NCP1.AND.NRHFRE.EQ.0) CODE(N)=1.0
      IF(NCOL.EQ.1.AND.NLHFRE.EQ.0) CODE(N)=1.0
      IF(NROW.EQ.NRP1) CODE(N)=3.0
      R(N)=RADIST(NCOL)
      Z(N)=ELEV(NROW)
      UR(N)=0.0
      UZ(N)=0.0
      IF(NCOL.LT.NCP1) NROW=NROW-1
      IF (N.EQ.NPP1.AND) N.GT.1) NROW=NROW+1
      IF(NCOL.EQ.NCP1) NCOL=0
      IF (N.EQ.NPP1.AND) N.GT.1) NCOL=0
107  CONTINUE
      IF(NBC.EQ.0) GO TO 5000
      DO 108 N=1, N1C
      READ(5,1006) N1N, CODE(NPN), UR(NPN), UZ(NPN)
108  CONTINUE
5000  CONTINUE
      MPRINT=0
      DO 109 N=1, NUMNP
      IF(MPRINT.GT.0) GO TO 3109
      WRITE (6,2004)
      MPRINT=75
3109  MPRINT=MPRINT-1
      WRITE(6,2002) N, CODE(N), R(N), Z(N), UR(N), UZ(N)
109  CONTINUE

```

133
134
135
136
137
140
141
142
143
144
145
146
147
148
149
150
151
152
153
154
155
156
157
158
159
160
161
162
163
164
165
166
167
168
169
170
171
172
173
175
176
177
178
179
180
181
182
183
184
186
187
188
189
190
191

OCTOBER 28, 1983 15:13 NERDC -- SYSTEM SUPPORT UTILITIES -- CARDLI

```

C*****
C      DETERMINE BAND WIDTH
C*****
      J=0
      DO 340 N=1, NUMEL
      DO 340 I=1, 4
      DO 325 L=1, 4
      KK=IABS(IX(N, I)-IX(N, L))
      IF (KK-J) 325, 325, 320
320  J=KK
325  CONTINUE
340  CONTINUE
      MBAND=2*J+2
      IF (MBAND.GT.54) WRITE(6,2017)
      IF (MBAND.GT.54) GO TO 550
C*****
C      INITIALIZE DISPLACEMENTS AND STRESSES IN PLATE
C*****
      DO 3 N=1, NUMNP
      DO 3 I=1, 2
      DISP(N, I)=0.0
3    CONTINUE
      IF (NPLATE.EQ.0) GO TO 5002
      DO 4 N=1, NPLATE
      GSTRSS(N)=0.0
      DO 4 I=1, 4
      SIGMA(I, N)=0.0
4    CONTINUE
5002 CONTINUE
C*****
C      CALCULATE GRAVITY STRESSES          (MODIFIED 4/8/82 PJB)
C*****
      NLMAX=NUMEL-NUMCOL+1
      DO 6 NR=NPP1, NLMAX, NUMCOL
      DO 5 NRP=1, NUMCOL
      N=NR+NRP-1
      MTYPE=IX(N, 5)
      IL=IX(N, 1)
      JL=IX(N, 2)
      GSTRSS(N)=0.5*RO(MTYPE)*(Z(IL)-Z(JL))
      IF (NR.EQ.NPP1) GO TO 5
      NBFOR=N-NUMCOL
      MTYPE=IX(NBFOR, 5)
      IL=IX(NBFOR, 1)
      JL=IX(NBFOR, 2)
      GSTRSS(N)=GSTRSS(N)+GSTRSS(NBFOR)+0.5*RO(MTYPE)*(Z(IL)-Z(JL))
5    CONTINUE
6    CONTINUE
      MPRINT=0
      DO 20 N=NPP1, NUMEL
      MTYPE=IX(N, 5)
      GSZ=GSTRSS(N)
      GSR=GSZ*AKO(MTYPE)
      GST=GSR
      GSRZ=0.0
      IF (MPRINT.GT.0) GO TO 7
      WRITE(6,1997)
      WRITE(6,1998)
      MPRINT=76
7    MPRINT=MPRINT-1
      WRITE(6,1999) N, GSR, GSZ, GST, GSRZ
20  CONTINUE
C*****
C      CALCULATE APPROXIMATE LOAD STRESSES
C*****

```

246
247
248
249
250
251
252
253
254
255
256
257
258
259
260
261
263
264
265
266
267
268
269
270
271
274
275
276
277
278
279
280
281
282
283
306
307
308
309
310
311
312
313
314
315
316
317

OCTOBER 28, 1983 15:13 NERDC -- SYSTEM SUPPORT UTILITIES -- CARDLI

```

C*****
DO 10 N=NPP1,NUMEL
IK=IX(N,1)
KK=IX(N,3)
MTYPE=IX(N,5)
ZDIST=Z(NPP2)-((Z(IK)+Z(KK))/2.0)
RDIST=(R(IK)+R(KK))/2.0
SFACTR=(RZERO**2)/((RZERO+ZDIST)**2)
C BEGIN MODIFICATION FOR PRESSUREMETER B.C.
SFACTR=1.0
C END OF MODIFICATION
IF(ZDIST.LT.(RDIST-RZERO)) SFACTR=0.0
SIGMA(2,N)=PZPRO*SFACTR
SIGMA(1,N)=SIGMA(2,N)*AKO(MTYPE)
SIGMA(3,N)=SIGMA(1,N)
SIGMA(4,N)=0.0
10 CONTINUE
29 MPRINT=0
DO 11 N=NPP1,NUMEL
IF(MPRINT.GT.0) GO TO 9
WRITE(6,1996)
WRITE(6,1998)
MPRINT=76
9 MPRINT=MPRINT-1
WRITE(6,1999) N,(SIGMA(I,N),I=1,4)
11 CONTINUE
C*****
C
C ADD GRAVITY STRESSES TO LOAD STRESSES
C*****
DO 30 N=NPP1,NUMEL
MTYPE=IX(N,5)
SIGMA(2,N)=SIGMA(2,N)+GSTRSS(N)
SIGMA(1,N)=SIGMA(1,N)+GSTRSS(N)*AKO(MTYPE)
SIGMA(3,N)=SIGMA(1,N)
MTYPE=IX(N,5)
AIO(N)=AKO(MTYPE)*GSTRSS(N)*2.0+SIGMA(1,N)
30 CONTINUE
C
C TIME=TIME(0)
C WRITE(6,2021) TIME
C*****
C COMPUTE ELASTIC STIFFNESS MATRIX BASED ON BULK MODULUS
C AND SHEAR MODULUS VALUES. C(4,4)
C*****
C(1,1)=EK-(2.0*EG/3.0)+2*EG
C(2,2)=C(1,1)
C(3,3)=C(1,1)
C(1,2)=EK-2.0*EG/3.0
C(2,1)=C(1,2)
C(1,3)=C(1,2)
C(2,3)=C(1,2)
C(3,1)=C(1,2)
C(3,2)=C(1,2)
C(1,4)=0.0
C(2,4)=0.0
C(3,4)=0.0
C(4,1)=0.0
C(4,2)=0.0
C(4,3)=0.0
C(4,4)=2.0*EG
CALL SYMINV(C,4)
C
C*****
C SOLVE NON-LINEAR STRUCTURE BY SUCCESSIVE APPROXIMATIONS
C*****
C
C NSTEP=1

```

318
319
320
321
322
323
324
325
326
327
328
329
330
331
334
335
336
337
338
339
340
341
342
343
344
345
346
347
348
349
350
351
352
353
354
355
356

OCTOBER 28, 1983 15:13 NERDC -- SYSTEM SUPPORT UTILITIES -- CARDLI

```

      PRESSURE=0.0
      READ (5,1008) MAXPRINT
      WRITE(6,1009) MAXPRINT
      READ (5,1008) ISOTROP
      IF (ISOTROP.EQ.1) WRITE (6,7933)
7933  FORMAT(1X,'THIS IS AN ISOTROPIC CONSOLIDATION TEST')
      IF (ISOTROP.EQ.2) WRITE (6,7934)
7934  FORMAT(1X,'THIS IS A STANDARD TRIAXIAL TEST')
      READ(5,1008) NCRIT
      WRITE(6,9314) NCRIT
9314  FORMAT(1X,'ELEMENT UNDER SCRUTINY=',I4)
      IPRINT=0
C
      DO 500 NNN=1,NP
      ISAND=0
      IPRINT=IPRINT+1
C
      READ AND PRINT OF PRESSURE BOUNDARY CONDITIONS
C
      READ (5,1007) NUMPC
      IF (NUMPC) 290,310,290
290  IF (IPRINT.NE.MAXPRINT) GO TO 295
      WRITE (6,2014) NSTEP
      WRITE (6,2034) NUMPC
      WRITE (6,2005)
295  DO 300 L=1,NUMPC
      READ (5,1007) IDC(L),JBC(L),PR(L)
      IF (IPRINT.NE.MAXPRINT) GO TO 296
      WRITE (6,2007) IDC(L),JBC(L),PR(L)
296  PRESSURE=PRESSURE+PR(L)
300  CONTINUE
310  CONTINUE
      IF (IPRINT.NE.MAXPRINT) GO TO 321
      WRITE(6,2050) PRESSURE
C
C*****
C FORM STRESS-STRAIN RELATIONSHIP FOR EACH ELEMENT
C BY CALLING SUBR SAND TO COMPUTE THE CL(4,4,N) MATRIX
C FOR ELEMENT #N
C NDUMMY(N) HAS BEEN INITIALIZED TO 1 FOR STEP # 1
C NDUMMY(N) VARIABLE INSTRUCTS THE USE OF THE APPROPRIATE
C PLASTIC MODULUS EQUATION
C*****
C
321  DO 330 N=1,NUMEL
      CALL SAND
330  CONTINUE
C
C
C FORM STIFFNESS MATRIX
C
343  CALL STIFF
C
C SOLVE FOR DISPLACEMENTS
C
      CALL BANSOL
C
C
C TIME=TTIME(0)
C WRITE (6,2021) TIME
C
C COMPUTE STRESSES
C
      CALL STRESS
C
C*****
C CHECK TO SEE IF VNSIG IS CORRECT FOR EVERY ELEMENT
C IF NOT, REFORM CL MATRIX USING THE CORRECT VALUE
C OF NDUMMY
C*****
C
      IF (ICHANGE.EQ.1) GO TO 321

```

357
358

359

360
361363
364
365
366
367
376
377
378
379
380
381
382

383

```

C*****
C IF NDUMMIES ARE O.K. ADD INCREMENTAL
C DISPLACEMENTS & PROCEED TO NEXT PRESSURE INCREMENT
C*****
MPRINT=0
DO 31 N=1,NUMNP
DISP(N,1)=DISP(N,1)+B(2*N-1)
DISP(N,2)=DISP(N,2)+B(2*N)
IF (IPRINT.NE.MAXPRINT) GO TO 31
IF(MPRINT.GT.0) GO TO 32
MPRINT=75
IF (IPRINT.NE.MAXPRINT) GO TO 31
WRITE (6,2014) NGTEP
WRITE (6,2022)
32 MPRINT=MPRINT-1
WRITE (6,2005) N,R(N),Z(N),DISP(N,1),DISP(N,2)
31 CONTINUE
C
C NSTEP=NSTEP+1
C
C IF (IPRINT.GT.MAXPRINT) IPRINT=0
500 CONTINUE
C*****
550 STOP
C*****
1000 FORMAT (20A4/B110)
1001 FORMAT(I10,F10.0,F10.1,2F10.0,3E10.5/BE10.5)
1002 FORMAT(I10,7F10.0)
1003 FORMAT(B110)
1004 FORMAT(BF10.0/BF10.0)
1005 FORMAT(BF10.0)
1006 FORMAT(I10,7F10.0)
1007 FORMAT (2I10,F10.0)
1008 FORMAT(I10)
1009 FORMAT(1X,'PRINTS AFTER',I10,' STEPS')
1996 FORMAT(38H1APPROXIMATE FIRST CYCLE LOAD STRESSES)
1997 FORMAT (17H1GRAVITY STRESSES)
1998 FORMAT (7H0EL NO.,11X,4HSIGR,11X,4HSIGZ,7X,8HSIGTHETA,10X,
1 5HTAURZ/)
1999 FORMAT (17,4F15.2)
2000 FORMAT (1H1 20A4/
1 30HO NUMBER OF NODAL POINTS-----,I10 /
2 30HO NUMBER OF ELEMENTS-----,I10 /
3 30HO NUMBER OF DIFF. MATERIALS---,I10 /
4 30HO NUMBER OF LOAD STEPS-----,I10 /
5 30HO NUM SPEC BOUND DISP-----,I10 /
6 30HO NUM SPEC ELEM MATS-----,I10 )
2001 FORMAT (49H1ELEMENT NO. I J K L MATERIAL )
2002 FORMAT (112,3F12.2,2E24.4,F12.2)
2003 FORMAT (1113,416,1113)
2004 FORMAT ( 97H1NODAL POINT TYPE R-ORDINATE Z-ORDINATE R LD
1AD OR DISPLACEMENT Z LOAD OR DISPLACEMENT )
2005 FORMAT (1H0, I J PRESSURE '/')
2006 FORMAT (1X,I12,2F12.2,1P2E20.7)
2007 FORMAT (216,F12.4)
2008 FORMAT (23HOPLANE STRESS STRUCTURE )
2009 FORMAT (26HONDDAL POINT CARD ERROR N=,I5)
2012 FORMAT(30HO RADIUS OF LOADED AREA -----,F10.2/
130HO SURFACE PRESSURE -----,F10.4/
230HO ATMOSPHERIC PRESSURE-----,F10.4)
2013 FORMAT (1H1,5X,7HELEMENT,5X,1HI,5X,1HJ,5X,1HK,5X,1HL,5X,
1 8HMATERIAL/)
2014 FORMAT (12H1STEP NUMBER ,I3)
2017 FORMAT (29HOBAND WIDTH EXCEEDS ALLOWABLE )
2018 FORMAT (1H0,2216)
2019 FORMAT (1H0,117,2116)
2020 FORMAT (1H1,25HNDAL POINTS AND ELEMENTS )
2021 FORMAT (22H0TIME SINCE BEGINNING=,F10.3,2X,3HSEC )
2022 FORMAT (1H0,124IN.P. NUMBER ,12H R-ORDINATE ,12H Z-ORDINATE ,
1 6X,14HR-DISPLACEMENT,6X,14HZ-DISPLACEMENT/)
2030 FORMAT (1H0,' MINOR PRINCIPAL STRESSES')

```

371
372
373

375
386
387
388

389
390
394

397
398
399
400
401
402

403
404

406

408
409
410

415
416
417
418
419

424
425
430

434
437
438
439
440
441

OCTOBER 28, 1983 15:13 NERDC -- SYSTEM SUPPORT UTILITIES -- CARDLI

2031 FORMAT (1H0, ' OCTAHEDRAL STRESSES')
 2032 FORMAT (1H0, ' FIRST CYCLE STRESSES ARE A FOOTING LOAD')
 2033 FORMAT (1H0, ' FIRST CYCLE STRESSES ARE FOR PILE LOADING')
 2034 FORMAT (1H0, 13, ' BOUNDARY PRESSURE LOADS APPLIED')
 2035 FORMAT (1H0, ' NUMBER OF PILES-----', I10/
 1 1H0, ' DEG ANGLE OF LOAD SPREAD-----', F10. 2/
 2 1H0, ' ATMOSPHERIC PRESSURE-----', F10. 4)
 2036 FORMAT (1H0, ' PILE NUMBER-----', I10/
 1 1H0, ' FIRST ELEMENT-----', I10/
 2 1H0, ' ND. PILE ELEMENTS-----', I10/
 3 1H0, ' PILE LOAD-----', F10. 4)
 2048 FORMAT (1H0, 3314)
 2049 FORMAT (1H0, 16, 3114)
 2050 FORMAT (1X, 'CAVITY PRESSURE =', F12. 5)

C

END

443
444

OCTOBER 28, 1983

15:13

NERDC -- SYSTEM SUPPORT UTILITIES -- CARDLI

```

C
C
C          SUBROUTINE STRESS
C
C          IMPLICIT REAL*8 (A-H, O-Z)
C          COMMON/INTGR/NUMNP, NUMEL, NUMMAT, NUMPC, NP, IBC(20), JBC(20), NPLATE,
1 NUMCOL, NUMROW, IX(550, 5), NPP1, NPP2, NPP, MTYPE, NSTEP, NDUMMY(550), N,
1 ICHANGE, MAXPRINT, IPRINT, ISOTROP, NCRIT
C          COMMON/PROP/RO(50), AKO(50), EE(7), ET(10), MATYP(34)
C          COMMON/LOAD/CODE(600), T(600), TEMP, PR(20), ACELZ, ANGFQ, ANGLE(4)
C          COMMON/GEOM/R(600), Z(600), UR(600), RADIST(25), ELEV(34)
1 ROWTMP(34), DISP(600, 2)
C          COMMON/STRSS/SIGMA(4, 550), Q, PZERO, RZERO, OSTRSS(550),
1 PATH, AIO(550), AHARD(550), XAHARD(550), ETA(550), SIGDOT(4, 550),
1 PHYDM, BKS(550), ZETA(550)
C          COMMON/ARG/S(10, 10), P(10), TT(4), DD(3, 3), HH(6, 10),
1 RR(4), RRE(4, 550), RRP(4, 550), RRT(4, 550), ZZ(4), C(4, 4), CL(4, 4, 550),
1 H(6, 10), D(6, 6), F(6, 10), TP(6), XI(10), LM(4), DADETA(550),
1 DADZETA(550), DXADETA(550), DXADZETA(550), VN(4, 550), BETA(550),
1 VNDSIG(550), ISIGN(550), DZETA(550), DETA(550), RRR(5, 550),
1 ZZZ(5, 550)
C          COMMON /BANARG/ B(116), A(116, 58), MBAND, NUMBLK
C*****
C          IF (NPLATE.EQ.0) GO TO 2
C          DO 1 N=1, NPP1
C          IX(N, 5)=IABS(IX(N, 5))
C          1 CONTINUE
C          COMPUTE ELEMENT STRESSES
C*****
C          2 XXE=0.0
C          XPE=0.0
C          MPRINT=0
C
C          DO 300 M=NPP1, NUMEL
C
C          N=M
C          IX(N, 5)=IABS(IX(N, 5))
C          MTYPE=IX(N, 5)
C
C          CALL GUAD(VOL)
C          IX(N, 5)=MTYPE
C
C          DO 120 I=1, 4
C          II=2*I
C          JJ=2*IX(N, I)
C          P(II-1)=B(JJ-1)
C          120 P(II)=B(JJ)
C
C          DO 150 I=1, 2
C          RR(I)=P(I+B)
C          DO 150 K=1, B
C          150 RR(I)=RR(I)-S(I+B, K)*P(K)
C
C          COMM=S(9, 9)*S(10, 10)-S(9, 10)*S(10, 9)
C          IF (COMM) 155, 160, 155
C          155 P(9)=(S(10, 10)*RR(1)-S(9, 10)*RR(2))/COMM
C          P(10)=(-S(10, 9)*RR(1)+S(9, 9)*RR(2))/COMM
C
C          160 DO 170 I=1, 6
C          TP(I)=0.0
C          DO 170 K=1, 10
C          170 TP(I)=TP(I)+H(1, K)*P(K)
C
C          171 RR(1)=TP(2)
C          RR(2)=TP(6)
C          RR(3)=(TP(1)+TP(2)*RRR(5, N)+TP(3)*ZZZ(5, N))/RRR(5, N)
C          RR(4)=TP(3)+TP(5)
C*****
C          CHANGE SIGNS OF STRAIN MATRIX SO THAT COMPRESSION IS +VE
C          RRT(I, N) IS TOTAL STRAIN MATRIX TO BE USED LATER ON OUT

```

445
446
447
448459
460
461
462
463
464
465
466
467
468
469
470
471
472
473
474
475
476
477
478
479
480
481
482
483
484
485
486
487
488
489
490
491
492
493
494
495
496
497
498
499
500
501
502
504

OCTOBER 28, 1983 15:13 NERDC -- SYSTEM SUPPORT UTILITIES -- CARDLI

```

C OF THIS LOOP
C*****
C      DO 175 I=1,4
      RRT(I,N)=-RR(I)
      IF (I.EQ.4) RRT(I,N)=-RR(I)/2.0
175 RR(I)=-RR(I)
C*****
C      CALCULATE INCREMENTAL STRESSES DUE TO STRAINS
C*****
C      DO 5 K=1,4
5 SIGDOT(K,N)=0.0
      DO 6 I=1,4
      DO 6 K=1,4
6 SIGDOT(I,N)=SIGDOT(I,N)+CL(I,K,N)*RR(K)
C*****
C      RESET STRESSES TO GRAVITY STRESSES AT END OF FIRST CYCLE ONLY
      THIS IS NOT USED AT PRESENT!!!!!!!!!!!!!!
      IF (NSTEP.GT.1) GO TO 7
      SIGMA(2,N)=GSTRSS(N)
      SIGMA(3,N)=AKO(MTYPE)*GSTRSS(N)
      SIGMA(1,N)=AKO(MTYPE)*GSTRSS(N)
C*****
C      COMPUTE VECTOR N : VECTOR SIGDOT, THIS INDICATES
      WHETHER WE HAVE A VIRGIN LOADING, UNLOADING OR
      RELOADING CONDITION
      THIS VARIABLE IS CALLED VNDSIG(N) FOR ELEMENT #N
C*****
C      7 CONTINUE
      VNDSIG(N)=SIGDOT(1,N)*VN(1,N)+SIGDOT(2,N)*VN(2,N)+SIGDOT(3,N)*
      *VN(3,N)+SIGDOT(4,N)*2.0*VN(4,N)
C*****
C      COMPUTE THE EXPECTED VALUE OF NDUMMY(N) & STORE IN
      A VARIABLE ISIGN(N)
C*****
C      IF (VNDSIG(N).GT.0.0 .AND. BETA(N).GT.1.0) ISIGN(N)=0
      IF (VNDSIG(N).GT.0.0 .AND. BETA(N).EQ.1.0) ISIGN(N)=1
      IF (VNDSIG(N).LT.0.0 .AND. BETA(N).GE.1.0) ISIGN(N)=-1
C*****
C      300 CONTINUE
C*****
C      TEST TO SEE IF THE ASSUMED VALUE OF NDUMMY(N) IS
      ACTUALLY EQUAL TO ISIGN(N). IF NOT, SET NDUMMY(N)
      EQUAL TO ISIGN(N). ALSO, SET ICHANGE EQUAL TO 1
      TO INSTRUCT PROGRAM TO RE-COMPUTE THE CL MATRIX
      WITH THE CORRECT SIGN OF NDUMMY(N)
C*****
C      ICHANGE = 0
C*****
C      DO 656 I= 1,NUMEL
      IF (NDUMMY(I) .NE. ISIGN(I)) ICHANGE =1
      IF (NDUMMY(I) .NE. ISIGN(I)) NDUMMY(I)=ISIGN(I)
656 CONTINUE
C*****
C      THIS RETURNS SUBR STRESS TO THE MAIN PROGRAM FOR
      RECOMPUTATION IF NDUMMY(N) DOES NOT HAVE THE PROPER VALUE
C*****
C      IF (ICHANGE.EQ.1) GO TO 320
C*****
C      IF ALL THE NDUMMY(N) VALUES WERE CORRECT,
      THE PROGRAM

```

505

507

509

510

514

525

OCTOBER 28, 1983 15:13 NERDC -- SYSTEM SUPPORT UTILITIES -- CARDLI

```

C      CONTINUES NORMALLY TO COMPUTE THE FOLLOWING:
C      A. UPDATED STRESSES
C      B. UPDATED HARDENING PARAMETERS
C      C. PRINCIPAL STRESSES
C*****
C      ADD STRESS INCREMENTS TO PREVIOUS STRESSES
C      NOTE : SIGDOT(I,N) IS NOW ADDED TO SIGMA(I,N)
C
C      DO 91 J=1,NUMEL
C      DO 91 I=1,4
C      SIGMA(I,J)=SIGMA(I,J)+SIGDOT(I,J)
C      91 CONTINUE
C*****
C      COMPUTE INCREMENTAL ELASTIC STRAINS RRE(I)
C*****
C      DO 11 J = 1,NUMEL
C      DO 11 I = 1,4
C      11 RRE(I,J)=C(I,1)*SIGDOT(1,J)+C(I,2)*SIGDOT(2,J)+C(I,3)*SIGDOT(3,J)+
C      *C(I,4)*SIGDOT(4,J)
C*****
C      COMPUTE INCREMENTAL PLASTIC STRAINS RRP(I)
C*****
C      DO 13 J=1,NUMEL
C      DO 13 I=1,4
C      13 RRP(I,J)=RRT(I,J)-RRE(I,J)
C*****
C      COMPUTE DZETA, I.E. CHANGE IN PLASTIC VOLUMETRIC STRAIN
C*****
C      DO 141 I=1,NUMEL
C      DZETA(I) = RRP(1,I) + RRP(2,I) + RRP(3,I)
C      141 ZETA(I) = ZETA(I) + DZETA(I)
C*****
C      COMPUTE FICTITIOUS INCREMENTAL PLASTIC EQUIVALENT SHEAR STRAIN, DETA1
C*****
C      DO 25 I=1,NUMEL
C      XX = (DZETA(I)**2)/3.0
C      YY = RRP(1,I)*RRP(1,I) + RRP(2,I)*RRP(2,I) + RRP(3,I)*RRP(3,I)
C      YY = YY + 2.0*RRP(4,I)*RRP(4,I)
C      DETA(I) = DSQRT((YY-XX)*0.5)
C*****
C      UPDATE FICTITIOUS PLASTIC EQUIVALENT SHEAR STRAIN, ETA FOR EACH ELEMENT
C*****
C      ETA(I) = ETA(I) + DETA(I)
C*****
C      UPDATE HARDENING PARAMETERS AHARD(N) & XAHARD(N) FOR ELEMENT N
C*****
C      IF (ATHETA.GT.BN) GO TO 191
C      AHARD(I) = AHARD(I) + DADETA(I)*DETA(I) + DADZETA(I)*DZETA(I)
C      XAHARD(I) = PHYOM*AHARD(I)*PATM
C      GO TO 88
C      191 XAHARD(I) = XAHARD(I) +DXADETA(I)*DETA(I)+DXADZETA(I)*DZETA(I)
C      AHARD(I) = XAHARD(I)*RIO*(EXP(1.0)-1.0)/PATM/EXP(1.0)
C*****
C      OUTPUT STRESSES
C*****

```

524

528

533

534

537

538

539

OCTOBER 28, 1963 15:13 NERDC -- SYSTEM SUPPORT UTILITIES -- CARDLI

C	CALCULATE PRINCIPAL STRESSES	540
C		541
	88 CC=(SIGMA(1,1)+SIGMA(2,1))/2.0	784
	BB=(SIGMA(1,1)-SIGMA(2,1))/2.0	785
	CR=DSGRT(SIGMA(4,1)*SIGMA(4,1)+BB*BB)	786
	SIG3=CC-CR	787
	SIG1=CC+CR	788
	IF(SIGMA(3,1).GE.SIG3) GO TO 10	
	SIG2=SIG3	
	SIG3=SIGMA(3,1)	
	GO TO 15	
	10 IF(SIGMA(3,1).LE.SIG1) GO TO 12	
	SIG2=SIG1	
	SIG1=SIGMA(3,1)	
	GO TO 15	
	12 SIG2=SIGMA(3,1)	
	15 SIGT=(SIG1+SIG2+SIG3)/3.0	
C		551
C		553
	IF (MPRINT) 105,105,110	
	105 IF (IPRINT.NE.MAXPRINT) GO TO 25	
	WRITE (6,2014) NSTEP	555
	WRITE (6,2001)	557
	MPRINT=40	558
	110 MPRINT=MPRINT-1	559
	WRITE(6,2002)I,RRR(5,1),ZZZ(5,1),SIGMA(1,1),SIGMA(2,1),	
	1 SIGMA(3,1),SIGMA(4,1),SIG1,SIG2,SIG3	
	SIGRD=SIGMA(1,1)-AKQ(MTYPE)*GSTRSS(I)	
	SIGZD=SIGMA(2,1)-GSTRSS(I)	
	SIGTD=SIGMA(3,1)-AKQ(MTYPE)*GSTRSS(I)	
	WRITE (6,2005) SIGRD,SIGZD,SIGTD	
	25 CONTINUE	
C		571
C	TIME=TIME(0)	573
C	WRITE (6,2021) TIME	574
C		572
C	320 RETURN	575
C		576
	2000 FORMAT (45HOFIRST LINE WITH GRAVITY, SECOND LINE WITHOUT)	577
	2001 FORMAT (1H0,'ELFM',T9,'R',T16,'Z',T21,'SIGR',T27,'SIGZ',	
	\$T34,'SIGT',T41,'TAURZ',T48,'SIG1',T55,'SIG2',	
	\$T62,'SIG3//')	
	2002 FORMAT(1X,13,2F7.2,1PE10.3,1PE10.3,1P4E10.3,1P4E10.3,	
	1 OPF6.1,OPF6.2,1X,OPF6.3)	
	2003 FORMAT(1H)	582
	2004 FORMAT (1H+,T127,'*')	
	2005 FORMAT (34X,1P5E10.3)	
	2014 FORMAT (12H1STEP NUMBER ,13)	583
	2021 FORMAT (22H0TIME SINCE BEGINNING=,F10.3,2X,3HSEC)	584
C		585
	END	586

OCTOBER 28, 1983 15:13 NERDC -- SYSTEM SUPPORT UTILITIES -- CARDLI

```

C
C      SUBROUTINE STIFF
C
C      IMPLICIT REAL*8 (A-H,O-Z)
COMMON/INTOR/NUMNP, NUMEL, NUMMAT, NUMPC, NP, IBC(20), JBC(20), NPLATE,
1 NUMCOL, NUMROW, IX(550,5), NPP1, NPP2, NPP, MTYPE, NSTEP, NDUMMY(550), N,
1 ICHANGE, MAXPRINT, IPRINT, ISOTROP, NCRIT
COMMON/PROP/RO(50), AK0(50), EE(7), ET(10), MATYP(34)
COMMON/LOAD/CODE(600), T(600), TEMP, PR(20), ACELZ, ANGFQ, ANGLE(4)
COMMON/GEOM/R(600), Z(600), UR(600), UZ(600), RADIST(25), ELEV(34)
1, ROWTMP(34), DISP(600,2)
COMMON/STRSS/SIGMA(4,550), G, PZERO, RZERO, GSTRSS(550),
1 PATM, AIO(550), AHARD(550), XAHARD(550), ETA(550), SIGDOT(4,550),
1 PHYOM, BKS(550), ZETA(550)
COMMON/ARG/S(10,10), F(10), TT(4), DD(3,3), HH(6,10),
1 RR(4), RRE(4,550), RRP(4,550), RRT(4,550), ZZ(4), C(4,4), CL(4,4,550),
1 H(6,10), D(6,6), F(6,10), TP(6), XI(10), LM(4), DADETA(550),
1 DADZETA(550), DXADETA(550), DXADZETA(550), VN(4,550), BETA(550),
1 VNDSIG(550), ISIGN(550), DZETA(550), DETA(550), RRR(5,550),
1 ZZZ(5,550)
COMMON /BANARG/ B(116), A(116,58), MBAND, NUMBLK
C
C*****
C      INITIALIZATION
C*****
      REWIND 2
      NR=29
      ND=2*NB
      ND2=2*ND
      STOP=0.0
      NUMBLK=0
C
      DO 50 N=1,ND2
      B(N)=0.0
      DO 50 M=1,ND
      50 A(N,M)=0.0
C*****
C      FORM STIFFNESS MATRIX IN BLOCKS
C*****
      60 NUMBLK=NUMBLK+1
      NH=NB*(NUMBLK+1)
      NM=NH-NB
      NL=NM-NB+1
      KSHIFT=2*NL-2
C
      DO 210 N=1,NUMEL
C
      IF (IX(N,5)) 210,210,65
      65 DO 80 I=1,4
      IF (IX(N,I)-NL) 60,70,70
      70 IF (IX(N,I)-NM) 90,90,80
      80 CONTINUE
      GO TO 210
C
      90 CALL QUAD(VOL)
C
      IF (VOL) 142,142,144
      142 WRITE (6,2003) N
      STOP=1.0
      144 IF (IX(N,3)-IX(N,4)) 145,145,145
      145 DO 150 II=1,9
      CC=S(II,10)/S(10,10)
      P(II)=P(II)-CC*P(10)
      DO 150 JJ=1,9
      150 S(II,JJ)=S(II,JJ)-CC*S(10,JJ)
C
      DO 160 II=1,8
      CC=S(II,9)/S(9,9)
      P(II)=P(II)-CC*P(9)
      DO 160 JJ=1,8
      160 S(II,JJ)=S(II,JJ)-CC*S(9,JJ)
C

```

587
588
589600
601
602
603
604606
607
608
609
610611
612
613
614
615616
617
618
619
620621
622
623
624
625626
627
628
629
630
631
632633
634
635
636
637638
639
640
641
642643
644
645
646
647648
649
650

OCTOBER 28, 1983 15:13 NERDC -- SYSTEM SUPPORT UTILITIES -- CARDLI

		651
C	ADD ELEMENT STIFFNESS TO TOTAL STIFFNESS	652
C	165 DO 166 I=1,4	653
C	166 LM(I)=2*IX(N,I)-2	654
		655
		656
	DO 200 I=1,4	657
	DO 200 K=1,2	658
	II=LM(I)+K-KSHIFT	659
	KK=2*I-2+K	660
	B(II)=B(II)+P(KK)	661
	DO 200 J=1,4	662
	DO 200 L=1,2	663
	JJ=LM(J)+L-II+J-KSHIFT	664
	LL=2*J-2+L	665
	IF(JJ) 200,200,175	666
175	IF(ND-JJ) 180,175,195	667
180	WRITE (6,2004) N	668
	STOP=1.0	669
	GO TO 210	670
195	A(II,JJ)=A(II,JJ)+S(KK,LL)	671
200	CONTINUE	672
210	CONTINUE	673
		674
C	ADD CONCENTRATED FORCES WITHIN BLOCK	675
		676
	DO 250 N=NL,NM	677
	K=2*N-KSHIFT	678
	B(K)=B(K)+UZ(N)	679
250	B(K-1)=B(K-1)+UR(N)	680
		681
	BOUNDARY CONDITIONS	682
		683
	1. PRESSURE B. C.	684
		685
	IF (NUMPC) 260,310,260	686
260	DO 300 L=1,NUMPC	687
	I=JBC(L)	688
	J=JBC(L)	689
	PP=PR(L)/6.	690
	DZ=(Z(I)-Z(J))*PP	691
	DR=(R(J)-R(I))*PP	692
	RX=2.0*R(I)+R(J)	693
	ZX=R(I)+2.0*K(J)	694
	IF (NPP) 262,264,262	695
262	RX=3.0	696
	ZX=3.0	697
264	II=2*I-KSHIFT	698
	JJ=2*J-KSHIFT	699
	IF (II) 280,280,265	700
265	IF (II-ND) 270,270,280	701
270	SINA=0.0	702
	COSA=1.0	703
	IF (CODE(I)) 271,272,272	704
271	SINA=DSIN(CODE(I)/57.3)	705
	COSA=DCOS(CODE(I)/57.3)	706
272	B(II-1)=B(II-1)+RX*(COSA*DZ+SINA*DR)	707
	B(II)=B(II)-RX*(SINA*DZ-COSA*DR)	708
280	IF (JJ) 300,300,285	709
285	IF (JJ-ND) 290,290,300	710
290	SINA=0.0	711
	COSA=1.0	712
	IF (CODE(J)) 291,292,292	713
291	SINA=DSIN(CODE(J)/57.3)	714
	COSA=DCOS(CODE(J)/57.3)	715
292	B(JJ-1)=B(JJ-1)+ZX*(COSA*DZ+SINA*DR)	716
	B(JJ)=B(JJ)-ZX*(SINA*DZ-COSA*DR)	717
300	CONTINUE	718
		719
		720
	2. DISPLACEMENT B. C.	721
		722
310	DO 400 M=NL,NM	
	IF (M-NUMNP) 315,315,400	

OCTOBER 28, 1983 15:13 NERDC -- SYSTEM SUPPORT UTILITIES -- CARDLI

315	U=UR(M)	723
	N=2*M-1-KSHIFT	724
	IF (CODE(M)) 390,400,316	725
316	IF (CODE(M)-1.) 317,370,317	726
317	IF (CODE(M)-2.) 318,390,318	727
318	IF (CODE(M)-3.) 390,380,370	728
370	CALL MODIFY(A,B,ND2,MBAND,N,U)	729
	GO TO 400	730
380	CALL MODIFY(A,B,ND2,MBAND,N,U)	731
390	U=UZ(M)	732
	N=N+1	733
	CALL MODIFY(A,B,ND2,MBAND,N,U)	734
400	CONTINUE	735
C		736
C	WRITE BLOCK OF EQUATIONS ON TAPE AND SHIFT UP LOWER BLOCK	737
C	WRITE (2) (B(N), (A(N,M), M=1, MBAND), N=1, ND)	738
C		739
	DO 420 N=1,ND	740
	K=N+ND	741
	B(N)=B(K)	742
	B(K)=0.0	743
	DO 420 M=1,ND	744
	A(N,M)=A(K,M)	745
420	A(K,M)=0.0	746
C		747
C	CHECK FOR LAST BLOCK	748
C		749
	IF (NM-NUMNP) 50,480,480	750
480	CONTINUE	751
C*****		752
	IF (STOP) 490,500,490	753
490	CALL EXIT	754
500	RETURN	755
C		756
2003	FORMAT (26HNEGATIVE AREA ELEMENT NO. ,I4)	757
2004	FORMAT (29HOBAND WIDTH EXCEEDS ALLOWABLE, I4)	758
	END	759
		760

OCTOBER 28, 1983 15:13 NERDC -- SYSTEM SUPPORT UTILITIES -- CARDLI

```

C*****
C
C      SUBROUTINE QUAD(VOL)
C*****
C      IMPLICIT REAL*8 (A-H,O-Z)
C      COMMON/INTGR/NUMNP, NUMEL, NUMMAT, NUMPC, NP, IBC(20), JBC(20), NPLATE,
1 NUMCOL, NUMROW, IX(550,5), NPP1, NPP2, NPP, MTYPE, NSTEP, NDUMMY(550), N,
1 ICHANGE, MAXPRINT, IPRINT, ISOTROP, NCRIT
C      COMMON/PROP/RO(50), AKO(50), EE(7), ET(10), MATYP(34)
C      COMMON/LOAD/CODE(600), T(600), TEMP, PR(20), ACELZ, ANGFG, ANGLE(4)
C      COMMON/GEOM/R(600), Z(600), UR(600), RADIST(25), ELEV(34)
1, ROWTMP(34), DISP(600,2)
C      COMMON/STRSS/SIGMA(4,550), G, PZERO, RZERO, GSTRSS(550),
1 PATM, AIO(550), AHARD(550), XAHARD(550), ETA(550), SIGDOT(4,550),
1 PHYDM, BKS(550), ZETA(550)
C      COMMON/ARG/S(10,10), P(10), TT(4), DD(3,3), HH(6,10),
1 RR(4), RRE(4,550), RRP(4,550), RRT(4,550), ZZ(4), C(4,4), CL(4,4,550),
1 H(6,10), D(6,6), F(6,10), TP(6), X1(10), LM(4), DADZETA(550),
1 DADZETA(550), DXADZETA(550), DXADZETA(550), VN(4,550), BETA(550),
1 VNDSIG(550), ISIGN(550), DZETA(550), DETA(550), RRR(5,550),
1 ZZZ(5,550)
C      COMMON /BANARG/ B(116), A(116,58), MBAND, NUMBLK
C*****
90 I=IX(N,1)
   J=IX(N,2)
   K=IX(N,3)
   L=IX(N,4)
   MTYPE=IX(N,5)
   IX(N,5)=-IX(N,5)
C*****
C      FORM STRESS-STRAIN RELATIONSHIP
C*****
C      THE CL MATRIX FOR EACH ELEMENT HAS BEEN FORMED PREVIOUSLY
C      IN SUBR SAND
C*****
C      THE MATRIX IS INVERTED IN SUBROUTINE SYMINV
C*****
C      FORM QUADRILATERAL STIFFNESS MATRIX
C*****
RRR(5,N)=(R(I)+R(J)+R(K)+R(L))/4.0
ZZZ(5,N)=(Z(I)+Z(J)+Z(K)+Z(L))/4.0
DO 94 M=1,4
  MM=IX(N,M)
  IF(R(MM)) 93,91,93
91 R(MM)=0.01+RRR(5,N)
  IF(CODE(MM)) 93,92,93
92 CODE(MM)=1.0
93 RRR(M,N)=R(MM)
94 ZZZ(M,N)=Z(MM)
C*****
DO 96 II=1,10
  P(II)=0.0
DO 95 JJ=1,6
95 HH(JJ,II)=0.0
DO 96 JJ=1,10
96 S(II,JJ)=0.0
DO 119 II=1,4
  JJ=IX(N,II)
119 ANGLE(II)=CODE(JJ)/57.3
C*****
IF (K-L) 125,120,125
120 CALL TRISTF(1,2,3)
RRR(5,N)=(RRR(1,N)+RRR(2,N)+RRR(3,N))/3.0
ZZZ(5,N)=(ZZZ(1,N)+ZZZ(2,N)+ZZZ(3,N))/3.0
VOL=XI(1)
GO TO 130
125 VOL=0.0

```

761
762
763

775
776
777
778
779
780

781
782
783

835
836
837

8
8
840
841
842
8
844
845
8
8

849
850
851
852
853
854
855
856
857

859
860

863
864
865

OCTOBER 28, 1983

15:13

NERDC -- SYSTEM SUPPORT UTILITIES -- CARDLI

CALL TRISTF(4,1,5)	866
VOL=VOL+XI(1)	867
CALL TRISTF(1,2,5)	868
VOL=VOL+XI(1)	869
CALL TRISTF(2,3,5)	870
VOL=VOL+XI(1)	871
CALL TRISTF(3,4,5)	872
VOL=VOL+XI(1)	873
C*****	875
DO 140 II=1,6	876
DO 140 JJ=1,10	877
140 HH(II, JJ)=HH(II, JJ)/4.0	
C*****	879
130 RETURN	
C*****	881
END	

OCTOBER 28, 1983

15:13

NERDC -- SYSTEM SUPPORT UTILITIES -- CARDLI

```

D(5,2)=XI(1)*(CL(4,1,N)+CL(4,3,N))
D(5,3)=XI(4)*CL(4,3,N)+XI(1)*CL(4,4,N)
D(5,6)=XI(1)*CL(4,2,N)
D(6,3)=XI(4)*CL(2,3,N)+XI(1)*CL(2,4,N)
D(6,5)=XI(1)*CL(2,4,N)
C
C
C      4. FORM COEFFICIENT-DISPLACEMENT TRANSFORMATION MATRIX
C
COMM=RR(2)*(ZZ(3)-ZZ(1))+RR(1)*(ZZ(2)-ZZ(3))+RR(3)*(ZZ(1)-ZZ(2))
DD(1,1)=(RR(2)*ZZ(3)-RR(3)*ZZ(2))/COMM
DD(1,2)=(RR(3)*ZZ(1)-RR(1)*ZZ(3))/COMM
DD(1,3)=(RR(1)*ZZ(2)-RR(2)*ZZ(1))/COMM
DD(2,1)=(ZZ(2)-ZZ(3))/COMM
DD(2,2)=(ZZ(3)-ZZ(1))/COMM
DD(2,3)=(ZZ(1)-ZZ(2))/COMM
DD(3,1)=(RR(3)-RR(2))/COMM
DD(3,2)=(RR(1)-RR(3))/COMM
DD(3,3)=(RR(2)-RR(1))/COMM
C
DO 120 I=1,3
J=2*LM(I)-1
H(1,J)=DD(1,I)
H(2,J)=DD(2,I)
H(3,J)=DD(3,I)
H(4,J)=DD(1,I)
H(5,J+1)=DD(2,I)
120 H(6,J+1)=DD(3,I)
C
C      ROTATE UNKNOWNNS IF REQUIRED
C
DO 125 J=1,2
I=LM(J)
IF (ANGLE(I)) 122,125,125
122 SINA=DSIN(ANGLE(I))
COSEA=DCOS(ANGLE(I))
IJ=2*I
DO 124 K=1,6
TEM=H(K,IJ-1)
H(K,IJ-1)=TEM*COSEA+H(K,IJ)*SINA
124 H(K,IJ)= -TEM*SINA+H(K,IJ)*COSEA
125 CONTINUE
C
C      5. FORM ELEMENT STIFFNESS MATRIX (H)T*(D)*(H)
C
DO 130 J=1,10
DO 130 K=1,6
IF (H(K,J)) 129,130,129
128 DO 129 I=1,6
129 F(I,J)=F(I,J)+D(I,K)*H(K,J)
130 CONTINUE
C
DO 140 I=1,10
DO 140 K=1,6
IF (H(K,I)) 138,140,138
138 DO 139 J=1,10
139 S(I,J)=S(I,J)+H(K,I)*F(K,J)
140 CONTINUE
C
C      6. FORM THERMAL LOAD MATRIX
C
150 COMM=RO(MTYPE)*ANGFG**2
TP(1)=COMM*X1(7)
TP(2)=COMM*X1(7)
TP(3)=-RO(MTYPE)*ACELZ
TP(4)=COMM*X1(1)
TP(5)=COMM*X1(7)
TP(6)=COMM*X1(8)
C
DO 160 I=1,10
DO 160 K=1,6
160 P(I)=P(I)+H(K,I)*TP(K)
C

```

938
939
940
941
942
943
944
945
946
947
948
949
950
951
952
953
954
955
956
958
959
960
961
962
963
964
965
966
967
968
969
970
971
972
973
974
975
976
977
978
979
980
981
982
983
984
985
986
987
988
989
990
991
992
993
994
995
996
997
998
999
1000
1001
1002
1003
1004

OCTOBER 28, 1983 15:13 NERDC -- SYSTEM SUPPORT UTILITIES -- CARDLI

C		1005
C	FORM STRAIN TRANSFORMATION MATRIX	1006
C		1007
	400 DO 410 I=1,6	1008
	DO 410 J=1,10	1009
	410 HH(I,J)=HH(I,J)+H(I,J)	1010
C	RETURN	1011
C	END	1012
		1013
		1014

OCTOBER 28, 1983 15:13 NERDC -- SYSTEM SUPPORT UTILITIES -- CARDLI

C	SUBROUTINE MODIFY(A, B, NEG, MBAND, N, U)	1015
		1016
C	IMPLICIT REAL*8 (A-H, O-Z)	1017
	DIMENSION A(116, 58), B(116)	
C	DO 250 M=2, MBAND	1019
	K=N-M+1	1020
	IF(K) 235, 235, 230	1021
230	B(K)=B(K)-A(K, M)*U	1022
	A(K, M)=0.0	1023
235	K=N+M-1	1024
	IF(NEG-K) 250, 240, 240	1025
240	B(K)=B(K)-A(N, M)*U	1026
	A(N, M)=0.0	1027
250	CONTINUE	1028
	B(N)=U	1029
	RETURN	1030
C	END	1031
		1032
		1033

OCTOBER 28, 1983 15:13 NERDC -- SYSTEM SUPPORT UTILITIES -- CARDLI

C		1034
	SUBROUTINE INTER(XI,RR,ZZ)	1035
C		1036
	IMPLICIT REAL*8 (A-H,O-Z)	1037
	DIMENSION RR(4), ZZ(4), XI(10), XM(6), R(6), Z(6), XX(6)	1038
	DATA XX /3*1.0,3*3.0/	1039
C		1040
	COMM=RR(2)*{ZZ(3)-ZZ(1)}+RR(1)*{ZZ(2)-ZZ(3)}+RR(3)*{ZZ(1)-ZZ(2)}	1041
	COMM=COMM/24.0	1042
	R(1)=RR(1)	1043
	R(2)=RR(2)	1044
	R(3)=RR(3)	1045
	R(4)=(R(1)+R(2))/2.	1046
	R(5)=(R(2)+R(3))/2.	1047
	R(6)=(R(3)+R(1))/2.	1048
C		1049
	Z(1)=ZZ(1)	1050
	Z(2)=ZZ(2)	1051
	Z(3)=ZZ(3)	1052
	Z(4)=(Z(1)+Z(2))/2.	1053
	Z(5)=(Z(2)+Z(3))/2.	1054
	Z(6)=(Z(3)+Z(1))/2.	1055
C		1056
	30 DO 35 I=1,6	1057
	35 XM(I)=XX(I)*R(I)	1058
C		1059
	40 DO 50 I=1,10	1060
	50 XI(I)=0.0	1061
C		1062
	DO 100 I=1,6	1063
	XI(1)=XI(1)+XM(I)	1064
	XI(2)=XI(2)+XM(I)/R(I)	1065
	XI(3)=XI(3)+XM(I)/(R(I)**2)	1066
	XI(4)=XI(4)+XM(I)*Z(I)/R(I)	1067
	XI(5)=XI(5)+XM(I)*Z(I)/(R(I)**2)	1068
	XI(6)=XI(6)+XM(I)*Z(I)**2/(R(I)**2)	1069
	XI(7)=XI(7)+XM(I)*R(I)	1070
	XI(8)=XI(8)+XM(I)*Z(I)	1071
	XI(9)=XI(9)+XM(I)*R(I)**2	1072
	XI(10)=XI(10)+XM(I)*R(I)*Z(I)	1073
100	CONTINUE	1074
C		1075
	DO 150 I=1,10	1076
150	XI(I)=XI(I)*COMM	1077
C		1078
	RETURN	1079
C		1080
	END	

OCTOBER 28, 1983 15:13 NERDC -- SYSTEM SUPPORT UTILITIES -- CARDLI

C		1081
	SUBROUTINE SYMINV(A, NMAX)	1082
C		1083
	IMPLICIT REAL*8 (A-H, O-Z)	
	DIMENSION A(4, 4)	1084
C		1085
	DO 200 N=1, NMAX	1086
C		1087
	D=A(N, N)	1088
	DO 100 J=1, NMAX	1089
100	A(N, J)=-A(N, J)/D	1090
C		1091
	DO 150 I=1, NMAX	1092
	IF (N-I) 110, 150, 110	1093
110	DO 140 J=1, NMAX	1094
	IF (N-J) 120, 140, 120	1095
120	A(I, J)=A(I, J)+A(I, N)*A(N, J)	1096
140	CONTINUE	1097
150	A(I, N)=A(I, N)/D	1098
C		1099
	A(N, N)=1.0/D	1100
C		1101
200	CONTINUE	1102
C		1103
	RETURN	1104
C		1105
	END	1106

```

C          SUBROUTINE BANSOL                                1107
C                                                    1108
C          IMPLICIT REAL*8 (A-H,O-Z)                    1109
C          COMMON /BANARC/ B(116),A(116,58),MM,NUMBLK
C                                                    1111
C          NN=58                                          1113
C          NL=NN+1                                        1114
C          NH=NN+NN                                       1115
C          REWIND 1                                       1116
C          REWIND 2                                       1117
C          NB=0                                           1118
C          GO TO 150                                       1119
C*****
C          REDUCE EQUATIONS BY BLOCKS                    1120
C*****
C          1. SHIFT BLOCK OF EQUATIONS
C          100 NR=NB+1                                     1123
C              DO 125 N=1,NN                               1124
C              NM=NN+N                                     1125
C              B(N)=B(NM)                                  1126
C              B(NM)=0.0                                   1127
C              DO 125 M=1,MM                               1128
C              A(N,M)=A(NM,M)                             1129
C          125 A(NM,M)=0.0                                  1130
C
C          2. READ NEXT BLOCK OF EQUATIONS INTO CORE
C          150 IF (NUMBLK-NB) 150,200,150                1131
C              READ (2) (B(N), (A(N,M), M=1,MM), N=NL, NH) 1132
C              IF (NB) 200,100,200                        1133
C
C          3. REDUCE BLOCK OF EQUATIONS
C          200 DO 300 N=1,NN                               1134
C              IF (A(N,1)) 225,300,225                   1135
C          225 B(N)=B(N)/A(N,1)                            1136
C              DO 275 L=2,MM                              1137
C              IF (A(N,L)) 230,275,230                   1138
C          230 C=A(N,L)/A(N,1)                             1139
C              I=N+L-1                                    1140
C              J=0                                         1141
C              DO 250 K=L,MM                              1142
C              J=J+1                                       1143
C          250 A(I,J)=A(I,J)-C*A(N,K)                     1144
C              B(I)=B(I)-A(N,L)*B(N)                    1145
C              A(N,L)=C                                    1146
C          275 CONTINUE                                    1147
C          300 CONTINUE                                    1148
C
C          4. WRITE BLOCK OF REDUCED EQUATIONS ON TAPE 2
C          375 IF (NUMBLK-NB) 375,400,375                1149
C              WRITE (1) (B(N), (A(N,M), M=2,MM), N=1,NN) 1150
C              GO TO 100                                   1151
C*****
C          BACK-SUBSTITUTION
C*****
C          400 DO 450 M=1,NN                              1152
C              N=NN+1-M                                    1153
C              DO 425 K=2,MM                              1154
C              L=N+K-1                                    1155
C          425 B(N)=B(N)-A(N,K)*B(L)                     1156
C              NM=N+NN                                    1157
C              B(NM)=B(N)                                 1158
C          450 A(NM,NB)=B(N)                              1159
C              NR=NB-1                                    1160
C              IF (NB) 475,500,475                       1161
C          475 BACKSPACE 1                                1162
C              READ (1) (B(N), (A(N,M), M=2,MM), N=1,NN) 1163

```

OCTOBER 28, 1983

15:13

NERDC -- SYSTEM SUPPORT UTILITIES -- CARDLI

	BACKSPACE 1	1178
	GO TO 400	1179
C	*****	1180
C	ORDER UNKNOWN IN B ARRAY	1181
C	*****	1182
	500 K=0	1183
	DO 600 NB=1, NUMBLK	1184
	DO 600 N=1, NN	1185
	NM=N+NN	1186
	K=K+1	1187
	600 B(K)=A(NM, NB)	1188
C		1189
	RETURN	1190
C		1191
	END	1192

OCTOBER 28, 1983

15:13

NERDC -- SYSTEM SUPPORT UTILITIES -- CARDLI

C
C
C
C

SUBROUTINE SAND

```

IMPLICIT REAL*(A-H,O-Z)
EXTERNAL FF,FBETA,FBETA1
COMMON/INTGR/NUMNP, NUMEL, NUMMAT, NUMPC, NP, IBC(20), JBC(20), NPLATE,
1 NUMCOL, NUMROW, IX(550,5), NPP1, NPP2, NPP, MTYPE, NSTEP, NDUMMY(550), N,
1 ICHANGE, MAXPRINT, IPRINT, ISOTROP, NCRIT
COMMON/PAARM/EG, EK, XR, XS, XT, XU, XW, XD, BN, RIO, GAMMA, HBU, HBL
COMMON /BLK3/ SI, SJ, OMEGA, AP, RIO1, ALPHA, BN1, XA, GAMMA1
COMMON/STRSS/SIGMA(4,550), G, PZERO, RZERO, GSTRSS(550),
1 PATM, AIO(550), AHARD(550), XAHARD(550), ETA(550), SIGDOT(4,550),
1 PHYDM, BKS(550), ZETA(550)
COMMON/ARG/S(10,10), P(10), TT(4), DD(3,3), HH(6,10),
1 RR(4), RRE(4,550), RRP(4,550), RRT(4,550), ZZ(4), C(4,4), CL(4,4,550),
1 H(6,10), D(6,6), F(6,10), TP(6), XI(10), LM(4), DADETA(550),
1 DADZETA(550), DXADETA(550), DXADZETA(550), VN(4,550), BETA(550),
1 VNDSIG(550), ISIGN(550), DZETA(550), DETA(550), RRR(5,550),
1 ZZ(5,550)
DIMENSION SS(4), VN(4)
DATA ZERO, HALF, ONE, TWO, THREE, FOUR, FIVE, SIX, HUNDRED
$ /0. EO, .5EO, 1. EO, 2. EO, 3. EO, 4. EO, 5. EO, 6. EO, 100. EO/

```

```

C*****
C RENAME SOME SOIL PARAMETERS FOR COMMON/BLK3/
C*****
RIO1=RIO
BN1=BN
GAMMA1=GAMMA
XA = XAHARD(N)

```

```

C*****
C COMPUTE STRESS INVARIANTS I1 & ROOT J2
C SI = I1 & SJ = J2
C SIGC = NORMALIZING PRESSURE
C SET SIGC EQUAL TO THE INITIAL VALUE OF I1
C SIGC1 IS FOR THE LOG SURFACE
C SS(I) = DEVIATORIC COMPONENTS

```

```

SI=SIGMA(1,N)+SIGMA(2,N)+SIGMA(3,N)
DO 3 I=1,3
3 SS(I) = SIGMA(1,N) - SI/THREE
SS(4) = SIGMA(4,N)
SJ = (((SIGMA(1,N)-SIGMA(2,N))**2+(SIGMA(2,N)-SIGMA(3,N))
**2+(SIGMA(1,N)-SIGMA(3,N))**2)/6.0)+(SIGMA(4,N))**2
SJKY =DSGRT(SJ)
SIGC = SIGMA(3,N)
SIGC1= SIGC
SG3=DSGRT(THREE)
IF (N.EQ.NCRIT) PRINT *, 'ROOT J=' , SJKY, 'SI=' , SI, 'NSTEP=' , NSTEP
IF (NSTEP.EQ.1) ETA(N)= XR*DSGRT(SJ)/(SIGC-XS*DSGRT(SJ))
IF (NSTEP.EQ.1) ZETA(N)=XW*(1-EXP(-XD*SI))
IF (N.EQ.NCRIT) PRINT *, 'ETA=' , ETA(N)
IF (N.EQ.NCRIT) PRINT *, 'ZETA=' , ZETA(N)

```

C
C
C
C
C
C
C
C
C
C
C
C

```

COMPUTE HARDENING FUNCTIONS: Q(ETA) AND H(ETA)
AND THEIR DERIVATIVES: DHDETA AND DQDETA.

```

```

AUX=XR+XS*ETA(N)
Q=ETA(N)/AUX
SGJ = DSGRT(SJ)
DQDETA =XR/(AUX*AUX)
AUX=XT+XU*ETA(N)
ALPHA=ETA(N)/AUX

```

OCTOBER 28, 1983 15:13 NERDC -- SYSTEM SUPPORT UTILITIES -- CARDLI

```

HHH=DTAN(ALPHA)
DHDETA=(XT/(AUX*AUX))/(DCOS(ALPHA)*DCOS(ALPHA))

CCCCC
COMPUTE FUNCTIONS: THETA(ETA) AND OMEGA(ETA)
AND THEIR DERIVATIVES: DTTDETA AND DOMDETA.

EXPMD=EXP(ONE)/(EXP(ONE)-ONE)
PHYOM=EXPMD/RIO
ATHETA=DSGRT(SJ)/SI
IF (N.EQ.NCRIT) PRINT *, 'ATHETA=', ATHETA, 'NSTEP=', NSTEP
THETA=SG3+THREI/G
OMEGA=ONE/(THREE*HHH)
DTTDETA=-THREI*DGDDETA/G/G
DOMDETA=-OMEGA*DHDETA/HHH

CCCCC
COMPUTE A=A(ETA, ZETA) AND B=B(ETA, ZETA) INITIALLY

SQJ=DSGRT(SJ)
IF(NSTEP.NE.1) GO TO 12345
B=BN
CALL SOLVE (7,FF)
AHARD(N)=Z/PATM
XAHARD(N)=PHYOM*AHARD(N)*PATM
XA=XAHARD(N)

CCCCC
COMPUTE DADETA(N) AND DADZETA(N)

12345 AP=AHARD(N)*PATM
IF (NSTEP.EQ.1) SI=1.000001*SI
BRAJI=ONE-SG3*DSGRT(SJ)/(SI-AIO(N))
IF (N.EQ.NCRIT) PRINT *, 'BRAJI=', BRAJI
IF (NSTEP.EQ.1) SI=SI/1.000001
IF (ISOTROP.EQ.1) BRAJI = ONE
IF (ISOTROP.EQ.2) BRAJI=ZERO
IF (BRAJI.LT.ZERO) BRAJI=ZERO
IF (ATHETA.GT.BN) GO TO 8888
DFDSJ=(RIO-ONE)/BN
AXKP= SIGC*(SQJ*G+THREE)
BXKP= SG3*(AXKP-AP/RIO)
CXKP= G*SIGC*DFDSJ*DFDSJ
DFDETATX = -TWO*SI*G*DGDDETA*(BXKP+CXKP)
GERT=THETA*G*SIGC/AP-ONE/RIO
DGHJ=DFDSJ**4
DFTX=DSGRT(12.0*AP*AP*GERT*GERT+TWO*DCHJ*G*G*SIGC*SIGC)
DFDATX=-TWO*THETA*G*SIGC/RIO*PATM+(TWO-RIO)/RIO*PATM*PATM
**TWO*AHARD(N)
DADETA(N)= DFDETATX/DFDATX
DADZETA(N)= BRAJI/((XD*PATM)*(XW-ZETA(N)))
GO TO 765

8888 BNEX=BN*(EXP(ONE)-ONE)
DXADZETA(N)=(PHYOM*BRAJI)/((XW-ZETA(N))*XD)
YLOGA1=ONE+DLOG(ONE-THETA*G*SIGC1/XAHARD(N))
DFTX1=DSGRT(HALF+THREE*BNEX*BNEX*YLOGA1*YLOGA1)
CX12=DLOG(ONE-THETA*G*SIGC1/XAHARD(N))
DFDXATX=BNEX*(CX12+THETA*G*SIGC1/XAHARD(N))
DFDETATX = SIGC*DGDDETA*(BNEX*YLOGA1*SG3-1)
DXADETA(N)= DFDETATX/DFDXATX
GO TO 7777

```


OCTOBER 28, 1983

15:13

NERDC -- SYSTEM SUPPORT UTILITIES -- CARDLI

```

C
C
C      COMPUTE BOUNDING PLASTIC MODULUS BKS
C
C 456 CONTINUE
      TRVN=VN(1,N)+VN(2,N)+VN(3,N)
      TRVM=VM(1)+VM(2)+VM(3)
      S123=DFDETA*DSQRT(HALF-ONE/SIX*TRVM*TRVM)
      BKP=-S123/DF-DFDZETA*TRVM/DF
      IF (NDUMMY(N).EQ.1) BKS(N)=BKP
      IF (NDUMMY(N).EQ.-1.AND.BETA(N).EQ.1.0) BKS(N)=100*EG
      IF (NDUMMY(N).EQ.-1.AND.BETA(N).EQ.1.0) GO TO 917
      IF (NDUMMY(N).EQ.-1) BKS(N)=HBU*BETA(N)/(BETA(N)-ONE)
917  IF (NDUMMY(N).EQ.0) BKS(N)=BKP+HBL*(ONE-ONE/BETA(N))
C
C      THE VARIABLE PHY IS GOING TO BE USED TO COMPUTE THE CL MATRIX
C      COMPUTE PHY
C
C      EL=EK-EG*TWO/THREE
C      VNEVN=ZERO
C      DO 51 I=1,3
51  VNEVN=VNEVN+VN(I,N)*VN(I,N)
      VNEVN=VNEVN+TWO*VN(4,N)*VN(4,N)
      VNEVN=VNEVN+TWO*EG+EL*TRVN*TRVN
      PHY=-ONE/(BKS(N)+VNEVN)
C
C      COMPUTE CONSTITUTIVE LAW
C
C      AUX1=TWO*EG*PHY
C      AUX2=EL*TRVN*PHY
C      CL(1,1,N)=EL+TWO*EG+((AUX1*VN(1,N)+AUX2)*(EL*TRVN+TWO*EG*VN(1,
C      *N)))
C      CL(1,2,N)=EL+((AUX1*VN(2,N)+AUX2)*(EL*TRVN+TWO*EG*VN(1,N)))
C      CL(1,3,N)=EL+((AUX1*VN(3,N)+AUX2)*(EL*TRVN+TWO*EG*VN(1,N)))
C      CL(1,4,N)=AUX1*VN(4,N)*(EL*TRVN+TWO*EG*VN(1,N))
C      CL(2,1,N)=EL+((EL*TRVN+TWO*EG*VN(2,N))*(AUX1*VN(1,N)+AUX2))
C      CL(2,2,N)=EL+TWO*EG+((EL*TRVN+TWO*EG*VN(2,N))*(AUX1*VN(2,N)+AUX2))
C      CL(2,3,N)=EL+((EL*TRVN+TWO*EG*VN(2,N))*(AUX1*VN(3,N)+AUX2))
C      CL(2,4,N)=AUX1*VN(4,N)*(EL*TRVN+TWO*EG*VN(2,N))
C      CL(3,1,N)=EL+((EL*TRVN+TWO*EG*VN(3,N))*(AUX1*VN(1,N)+AUX2))
C      CL(3,2,N)=EL+((EL*TRVN+TWO*EG*VN(3,N))*(AUX1*VN(2,N)+AUX2))
C      CL(3,3,N)=EL+TWO*EG+((EL*TRVN+TWO*EG*VN(3,N))*(AUX1*VN(3,N)+AUX2))
C      CL(3,4,N)=AUX1*VN(4,N)*(EL*TRVN+TWO*EG*VN(3,N))
C      CL(4,1,N)=TWO*EG*VN(4,N)*(AUX1*VN(1,N)+AUX2)
C      CL(4,2,N)=TWO*EG*VN(4,N)*(AUX1*VN(2,N)+AUX2)
C      CL(4,3,N)=TWO*EG*VN(4,N)*(AUX1*VN(3,N)+AUX2)
C      CL(4,4,N)=EG+(4.0*EG*EG*VN(4,N)*VN(4,N)*PHY)
C
C      RETURN
C      END

```

OCTOBER 28, 1983

15:13

NERDC -- SYSTEM SUPPORT UTILITIES -- CARDLI

000000

```
FUNCTION FF(X)
  IMPLICIT REAL*8 (A-H, O-Z)
  COMMON /BLK3/ SI, SJ, OMEGA, AP, RIO1, ALPHA, BN1, XA, GAMMA1
  WER=(RIO1-1.0)/RN1
  FF=SI*SI+WER*WER*SJ-2.0*SI*X/RIO1+(2.0-RIO1)/RIO1*X*X
  RETURN
END
```

OCTOBER 29, 1983

15:13

NERDC -- SYSTEM SUPPORT UTILITIES -- CARDLI

CCCC

```
FUNCTION FBETA(X)
  IMPLICIT REAL*8 (A-H, O-Z)
  COMMON /BLK3/ SI, SJ, OMEGA, AP, RIO1, ALPHA, BN1, XA, GAMMA1
  GTX=(RIO1-1.0)/BN1
  GTY=(2.0-RIO1)/RIO1
  GTZ=X*SI-3.0*GAMMA1*(X-1.0)
  FBETA=GTZ+GTX+GTX*X*X*5J-2.0*GTZ*AP/RIO1+GTY*AP*AP
  RETURN
END
```

OCTOBER 28, 1983

15:13

NERDC -- SYSTEM SUPPORT UTILITIES -- CARDLI

C
C
C
C
C

```
FUNCTION FBETA1(X)
  IMPLICIT REAL*8 (A-H,O-Z)
  COMMON /BLK3/ SJ, SJ, OMEGA, AP, RIO1, ALPHA, BN1, XA, GAMMA1
  CVB=EXP(1,0)-1.0
  CVB1=(XA-3.0*GAMMA1-X)/(SI-3.0*GAMMA1)
  FBETA1=CVB1*DSORT(SJ)+BN1*CVB*X*(DLOG(X)-DLOG(XA))
  RETURN
END
```

OCTOBER 28, 1983

15:13

NERDC -- SYSTEM SUPPORT UTILITIES -- CARDLI

C
C
C
C
C

```
SUBROUTINE SOLVE(Z, FUNC)
  IMPLICIT REAL*8 (A-H, O-Z)
  EXTERNAL FUNC
  COMMON /BLK3/ SJ, SJ, OMEGA, AP, RIO1, ALPHA, BN1, XA, GAMMA1
  A=1.0E-10
  B=1.0
110  F1=FUNC(A)
     FJ=FUNC(B)
     IF (F1*FJ. LE. 0.0) GO TO 111
     A=B
     B=B+1.0
     GO TO 110
111  TOL=1.0E-10
     Z=ZERDIN(A, B, FUNC, TOL)
     RETURN
     END
```

OCTOBER 28, 1983

15:13

NERDC -- SYSTEM SUPPORT UTILITIES -- CARDLI

C
C
C
C
C

```
SUBROUTINE SOLVE(Z, FUNC)
  IMPLICIT REAL*8 (A-H, O-Z)
  EXTERNAL FUNC
  COMMON /BLK3/ SI, SJ, OMEGA, AP, RIO1, ALPHA, BN1, XA, GAMMA1
  A=1.0E-10
  B=1.0
110  F1=FUNC(A)
     FJ=FUNC(B)
     IF(FI*FJ.LE.0.0) GO TO 111
     A=B
     B=B+1.0
     GO TO 110
111  TOL=1.0E-10
     Z=ZEROIN(A, B, FUNC, TOL)
     RETURN
     END
```


OCTOBER 28, 1983

15:13

NERDC -- SYSTEM SUPPORT UTILITIES -- CA

```

CCCCC
CONVERGENCE TEST
CCCCC
40 TOL1=2.0*EPS*ABS(B)+0.5*TOL
   XM=0.5*(C-B)
   IF(ABS(XM).LE.TOL1) GO TO 90
   IF(FB.EQ.0.0) GO TO 90
   IS BISECTION NECESSARY
   IF(ABS(E).LT.TOL1) GOTO 70
   IF(ABS(FA).LE.ABS(FB)) GO TO 70
   IS QUADRATIC INTERPOLATION POSSIBLE
   IF(A.NE.C) GO TO 50
   LINEAR INTERPOLATION
   S=FB/FA
   P=2.0*XM*S
   G=1.0-S
   GO TO 60
CCCCC
   INVERSE QUADRATIC INTERPOLATION
50 G=FA/FC
   R=FB/FC
   S=FB/FA
   P=S*(2.0*XM*G*(G-R)-(B-A)*(R-1.0))
   G=(G-1.0)*(R-1.0)*(S-1.0)
   ADJUST SIGNS
60 IF(P.GT.0.0) G=-G
   P=ABS(P)
   IS INTERPOLATION ACCEPTABLE
   IF((2.0*P).GE.(3.0*XM*G-ABS(TOL1*G))) GO TO 70
   IF(P.GE.ABS(0.5*E*G)) GO TO 70
   E=D
   D=P/G
   GO TO 80
   BISECTION
70 D=XM
   E=D
   COMPLETE STEP
80 A=B
   FA=FB
   IF(ABS(D).GT.TOL1) B=B+D
   IF(ABS(D).LE.TOL1) B=B+SIGN(TOL1, XM)
   FR=FF(B)
   IF((FB*(FC/ABS(FC))).GT.0.0) GO TO 20
   GO TO 30
CCCCC
   DONE
90 ZEROIN=B
   RETURN
   END

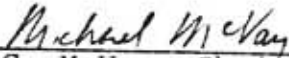
```


BIOGRAPHICAL SKETCH

Devo Seereeram was born on July 4th, 1958, in Chaguanas, Trinidad, where he attended Montrose Vedic primary school until the age of 12. His secondary education continued at Presentation College over the next seven years of his life culminated by a first place high school ranking in the University of Cambridge's General Certificate of Examination "Ordinary Level" and "Advanced Level."

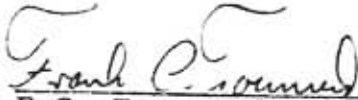
After high school, Devo spent two years working for his father's highway construction company before deciding to further his education at the University of Florida. He graduated in Spring 1982 with a BSCE (high honors) degree, and proceeded immediately into the U.F. Master of Engineering program where an anticipated graduation is expected in Fall of 1983. Devo plans to seek a research assistantship at his alma mater so that he may continue uninterruptedly toward a doctoral degree. Upon completion of the Ph.D program, he intends to return home to take control of his patriarch's business enterprise, and, if possible, lecture on a part-time basis at the local branch of the engineering college of the University of the West Indies.

I certify that I have read this study and that in my opinion it conforms to acceptable standards of scholarly presentation and is fully adequate, in scope and quality, as a thesis for the degree of Master of Engineering.




M.C. McVay, Chairman
Assistant Professor of Civil
Engineering

I certify that I have read this study and that in my opinion it conforms to acceptable standards of scholarly presentation and is fully adequate, in scope and quality, as a thesis for the degree of Master of Engineering.



F.C. Townsend
Professor of Civil Engineering

I certify that I have read this study and that in my opinion it conforms to acceptable standards of scholarly presentation and is fully adequate, in scope and quality, as a thesis for the degree of Master of Engineering.



J.L. Davidson
Associate Professor of Civil
Engineering

This this was submitted to the Graduate Faculty of the College of Engineering and to the Graduate School, and was accepted as partial fulfillment of the requirements for the degree of Master of Engineering.

December 1983

Dean, College of Engineering

Dean for Graduate Studies and
Research